People's Democratic Republic of Algeria
Ministry of Higher Education and Scientific Research
University of 8 Mai 1945Guelma

Faculty of Sciences and Technology
Department of Mechanical Engineering
Domiciliation laboratory: Laboratory of Mechanics and Structures (LMS)

Thesis

Submitted in Candidacy for the Degree of *Doctorate in Third Cycle*

Field: Sciences and technologies Stream: Mechanical Engineering
Speciality: Mechanical Construction

Presented by:
MRABTI Ammar

Title

Application of Variational Mode Decomposition for Fault Diagnosis in Rotating Machines

Defended on: *July 8th 2025* Before the jury composed of:

Full name	Rank	University	
Mr. FATMI Louendi	Pr.	Univ. of 8 Mai 1945 Guelma	President
Mr. YOUNES Ramdane	MC/A	Univ. of Larbi Tebessi Tebessa	Supervisor
Mr. OUELAA Nouredine	Pr.	Univ. of 8 Mai 1945 Guelma	Co-supervisor
Mr. DJEBALA Abderrazek	Pr.	Univ. of 8 Mai 1945 Guelma	Examiner
Mr. BABOURI Mohamed Khemissi	Pr.	Univ. of Sciences and Technology Houari Boumediene, Algiers	Examiner
Mr. KEBABSA Tarek	MC/A	National Higher School of Technology and Engineering, Annaba,	Guest

Academic year: 2024/2025

الأهم هو ألا تتوقف عن طرح الأسئلة، فالفضول له سبب

وجوده الخاص

L'important est de ne jamais cesser de poser des questions, La curiosité a sa propre raison d'exister

The important thing is not to stop questioning, Curiosity has its own reason for existing

Albert Einstein

Dedication

I dedicate this thesis:

For my dear parents, whose unwavering commitment, continuous support, and tremendous sacrifices have accompanied me throughout my academic journey. Your love and encouragement have been my greatest sources of strength.

To my brothers and sisters, for their inspiration, love, and unwavering support.

To my friends, for their loyalty and encouragement during the most challenging moments.

Finally, to all those who believed in me, who offered their help and support, whether openly or discreetly, I extend my deepest gratitude.

Acknowledgments & Gratitude

« الحمد لله »

First and foremost, I would like to express my deep gratitude to my thesis advisors, **Dr. Younes Ramdane** and **Pr. Ouelaa Nouredine**, for their guidance, expertise, and support. Working alongside them, both professionally and personally, has been a valuable and enriching experience. Their availability, scientific rigor, commitment to excellence, and supportive approach have been instrumental in my growth throughout this journey.

I would also like to extend my thanks to **Pr. Djamaa Mohamed Chrif** for his invaluable assistance, as well as to all the members of the Laboratory of Mechanics and Structures (LMS) for their support, with special recognition to **Mr. Ouerfellah Rabeh** for his technical expertise and valuable advice. My gratitude also goes to all the faculty members of the Mechanical Engineering Department at the University of Guelma.

A heartfelt thank you to my colleagues for their support and camaraderie during these years of research. I have been fortunate to work alongside passionate researchers with an exceptional level of scientific expertise.

I would like to express my sincere gratitude to the CFD and its chairman, **Pr. Bezzazi Abderrezak**, for their time and constructive evaluation of my work. I would like to thank **Pr. Fatmi Louendi** for accepting to chair my thesis defense jury, as well as **Pr. Djebala Abderrazek** and **Pr. Babouri Mohamed Khemissi**, the examiners of my thesis, for their presence and constructive feedback, which significantly contributed to improving the quality of this work. Also, I would like to express my gratitude for **Dr. Kebabsa Tariq** for accepting to be present as a guest among the defense jury.

I am also deeply grateful to my family and friends for their emotional support and unwavering presence throughout this journey.

I sincerely thank all those who contributed, directly or indirectly, to the completion of this work. Their support, trust, and presence throughout this journey have been truly invaluable. To all of you, I extend my deepest and most sincere gratitude.

Résumé

Cette thèse propose une approche innovante pour le diagnostic des défauts dans les machines tournantes, en exploitant la Décomposition en Mode Variationnelle (VMD) pour améliorer la précision et la robustesse de la détection dans des environnements complexes. Elle débute par une revue des stratégies de maintenance conditionnelle, mettant en avant les limites des méthodes traditionnelles et l'intérêt des techniques avancées de traitement du signal.

La VMD est comparée à la Décomposition en Mode Empirique (EMD) pour démontrer sa supériorité dans l'isolement des signatures de défauts issues de signaux bruités. Un critère basé sur l'entropie de Shannon est proposé pour optimiser le nombre de fonctions de mode intrinsèque (IMF). En complément, des méthodes avancées, comme l'Analyse Multi-Résolution par Ondelettes (WMRA) est intégrée à la VMD pour affiner la détection des défauts subtils.

Une contribution majeure de cette recherche réside dans le développement d'un cadre hybride combinant la VMD et les réseaux LSTM (Mémoire Longue et Court Terme) pour la classification des défauts et l'évaluation de leur gravité. Cette combinaison exploite efficacement la décomposition de signal et l'apprentissage séquentiel, démontrant une grande précision, même avec des données limitées, et un fort potentiel pour les applications industrielles.

En conclusion, la méthode VMD se révèle particulièrement efficace pour diagnostiquer les défauts des machines tournantes dans des conditions de fonctionnement difficiles, ouvrant de nouvelles perspectives pour la maintenance conditionnelle.

Mots-clés : Décomposition en Mode Variationnelle (VMD), Détection de défauts, Machines tournantes, Analyse vibratoire, Traitement du signal, Maintenance conditionnelle, Décomposition du signal, Signaux vibratoires.

Abstract

This thesis proposes an innovative approach for diagnosing faults in rotating machinery by utilizing Variational Mode Decomposition (VMD) to enhance detection accuracy and robustness in complex environments. It begins with a review of condition-based maintenance strategies, highlighting the limitations of traditional methods and the potential of advanced signal processing techniques.

VMD is compared to Empirical Mode Decomposition (EMD) to demonstrate its superiority in isolating fault signatures from noisy signals. A criterion based on Shannon entropy is proposed to optimize the number of Intrinsic Mode Functions (IMFs). Additionally, advanced methods such as Wavelet Multi-Resolution Analysis (WMRA) is integrated with VMD to refine the detection of subtle faults.

A major contribution of this research lies in developing a hybrid framework combining VMD and Long Short-Term Memory (LSTM) networks for fault classification and severity assessment. This combination effectively leverages signal decomposition and sequential learning, achieving high accuracy even with limited data and demonstrating strong potential for industrial applications.

In conclusion, the VMD method proves particularly effective for diagnosing faults in rotating machinery under challenging operating conditions, opening new avenues for condition-based maintenance.

Keywords: Variational Mode Decomposition (VMD), Fault detection, Rotating machinery, Vibration analysis, Signal processing, Condition-based maintenance, Signal decomposition, Vibration signals.

ملخص

تقترح هذه الأطروحة نهجًا مبتكرًا لتشخيص الأعطال في الآلات الدوارة من خلال استخدام التحليل باستخدام طريقة التفكيك في الوضع التباييني (VMD) لتحسين دقة وموثوقية الكشف عن الأعطال في البيئات المعقدة. تبدأ الدراسة بمراجعة استراتيجيات الصيانة القائمة على الحالة، مع تسليط الضوء على حدود الأساليب التقليدية وأهمية تقنيات معالجة الإشارات المتقدمة.

تمت مقارنة VMD مع التحليل باستخدام طريقة التفكيك في الوضع التجريبي (EMD) لإثبات تفوق VMD في عزل إشارات الأعطال الناتجة عن الإشارات الملوثة بالضوضاء. وتم اقتراح معيار يعتمد على إنتروبيا شانون لتحسين عدد الوظائف الوضعية الجوهرية .(IMFs) بالإضافة إلى ذلك، تم دمج أساليب متقدمة مثل التحليل متعدد الدقة باستخدام المويجات (WMRA) مع VMD لتحسين اكتشاف الأعطال الدقيقة.

تتمثل إحدى المساهمات الرئيسية لهذا البحث في تطوير إطار عمل هجين يجمع بين VMD وشبكات الذاكرة طويلة وقصيرة المدى (LSTM) لتصنيف الأعطال وتقييم حدتها. هذا الدمج يستفيد بفعالية من تحليل الإشارات والتعلم التسلسلي، مما يحقق دقة عالية حتى مع البيانات المحدودة، ويظهر إمكانيات قوية للتطبيقات الصناعية.

في الختام، أثبتت طريقة VMD فعاليتها بشكل خاص في تشخيص أعطال الآلات الدوارة تحت ظروف تشغيل صعبة، مما يفتح آفاقًا جديدة للصيانة القائمة على الحالة

الكلمات المفتاحية: التفكيك في الوضع التباييني (VMD)، كشف العيوب، الآلات الدوارة، تحليل الاهتزازات، معالجة الإشارات، الصيانة المستندة إلى الحالة، تفكيك الإشارة، الإشارات الاهتزازية.

List of abbreviations

Symbol	Signification
AD	Average Defect
AI	Artificial intelligence
BPFI	Ball Pass Frequency Inner
BPFO	Ball Pass Frequency Outer
BPF	Ball Pass Frequency
CF	Cage defect Frequency
CD	Critical Defect
CGS	Spectral Center of Gravity
C_e	Input torque
CEEMDAN	Complete Ensemble Empirical Mode Decomposition with Adaptive Noise
CWT	Continuous Wavelet Transform
DWT	Discrete Wavelet Transform
E	Energy
EMD	Empirical Mode D Decomposition
EEMD	Ensemble Empirical Mode Decomposition Improved
F_{Br}	Belt Resonance Frequency
FC	Crest Factor
FFT	Fast Fourier Transform
FK	K Factor
F_r	Rotation Frequency
F_m	Meshing Frequency
HFRT	High Frequency Resonance Technique
HHT	Hilbert-Huang Transform
IMF	Intrinsic Mode Functions
IMID	Integration of Modulation Intensity Distribution
LMSDS	Mechanics and Structures Laboratory Database
LOWESS	Locally Weighted Point Cloud Smoothing Method
LSTM	Long Short-Term Memory
MCSA	Motor Current Signature Analysis

MID	Modulation Intensity Distribution
OWMRA	Optimized Wavelet Multi-Resolution Analysis
P2P	Peak to Peak
P	Power
PSD	Power Spectral Density
RMS	Root Mean Square
RNN	Recurrent Neural Networks
Rpm	Rotations per minute
SD	Small Defect
SE	Shannon Entropy
SE_{imf}	Shannon Entropy for each IMF
STFT	Short-Term Fourier Transform
T	Belt Tension
VC	Crest Value
VMD	Variational Mode Decomposition
WMRA	Wavelet Multiresolution Analysis
WT	Wavelet Transform

List of figures

Chapter 1

Chapter 2

Chapter 3

Chapter 4

List of tables

Chapter 1

Chapter 2

Chapter 3

Chapter 4

Tables of contents

Chapter 01: Fundamental Notions and Bibliography

Chapter 02: Comparative study between VMD and EMD for the diagnosis of rotating machine faults

Chapter 03: Fault diagnosis by a new VMD-WMRA approach, optimized by a new criterion

Chapter 04: Automated diagnosis of rotating machine faults using the VMD-LSTM approach

General Introduction

In an industrial context where global competition imposes increasing demands on performance, reliability, and cost reduction, companies must optimize the operation of their production equipment. Rotating machinery, which plays a central role in various industrial sectors such as energy, transportation, and manufacturing, is subjected to intensive operating conditions, both in terms of running time and rotational speed. These operating conditions, while necessary to meet production requirements, increase the risk of failures and equipment degradation. The resulting unplanned production shutdowns often generate costs that far exceed those of direct repairs.

To address these challenges, industrial maintenance plays a crucial role in preventing failures, extending equipment lifespan, and reducing operating costs. Among modern strategies, condition-based maintenance has emerged as a key approach. Unlike corrective maintenance, which intervenes after failures occur, or systematic preventive maintenance, which follows fixed schedules, condition-based maintenance relies on real-time monitoring of equipment. This strategy allows for the early detection of potential failures, enabling timely interventions before critical defects develop. As a result, resources are optimized, equipment availability is improved, and industrial operations benefit from a proactive maintenance approach.

Among the tools used in condition-based maintenance, vibration analysis is one of the most effective for monitoring the health of rotating machinery [1]. This technique relies on capturing vibration signals generated by machines in operation, followed by their analysis to detect the onset and progression of mechanical faults. Although vibration signals contain valuable information, they are often complex, nonlinear, and non-stationary, making their processing particularly challenging. Traditional approaches, such as spectral analysis or simple indicators (kurtosis, RMS, crest factor), quickly reach their limitations when dealing with subtle defects or noisy environments.

These limitations have led to the emergence of advanced signal processing techniques that leverage the adaptive and multi-scale properties of vibration signals. Among these techniques, Empirical Mode Decomposition (EMD) [2] marked a significant advancement by decomposing signals into intrinsic mode functions that reflect local dynamic phenomena. However, EMD presents drawbacks such as mode mixing and increased sensitivity to noise.

To overcome these challenges, Variational Mode Decomposition (VMD) [3] offers a robust and precise alternative. VMD enables optimal separation of signal components while minimizing mode interference. This method has proven particularly effective in isolating fault signatures in complex vibration signals, even in the presence of noise.

Beyond these decomposition techniques, integrating complementary methods provides additional tools for processing the complex signals of rotating machinery. These approaches exploit the time-frequency characteristics of signals, facilitating the detection of subtle modulations associated with mechanical defects. Moreover, the rise of artificial intelligence, particularly deep learning models such as Long Short-Term Memory (LSTM) networks, opens new perspectives. These algorithms, capable of modeling sequential relationships in signals, enable automatic fault classification and precise severity assessment.

This thesis is positioned within this framework by exploring and developing hybrid approaches that combine VMD with advanced signal processing techniques and artificial intelligence methods. The primary objective is to enhance the sensitivity and robustness of fault diagnosis in rotating machinery, with a particular focus on gears and bearings, which are critical components in many industrial systems. More specifically, the contributions of this research include:

- The development of optimization criteria to improve the selection of intrinsic mode functions in VMD.
- The integration of VMD with complementary techniques, such as Wavelet Multi-Resolution Analysis (WMRA) to enhance diagnostic accuracy, particularly in noisy environments.
- The implementation of LSTM networks for automatic fault classification and severity assessment, even with limited datasets.

To achieve these objectives, this thesis follows a structured and progressive approach, organized as follows:

- Chapter 1 presents a literature review on maintenance strategies and fault detection techniques in rotating machinery, with a particular focus on condition-based methods and vibration analysis.
- Chapter 2 provides an in-depth comparison between EMD and VMD in the context of vibration-based fault diagnosis, highlighting their respective advantages in identifying gear defects.

- Chapter 3 introduces an innovative approach that combines VMD with WMRA, optimized by an entropy-based criterion, to overcome the challenges posed by noisy signals and ensure robust fault detection.
- Chapter 4 presents the development of an automated diagnostic framework that integrates VMD and LSTM networks to autonomously and accurately classify and detect faults, relying on experimental datasets covering various fault scenarios.

By leveraging the capabilities of VMD and integrating it with modern artificial intelligence tools, this research makes a significant contribution to the field of condition-based maintenance. It aims to provide robust solutions tailored to the increasing demands of modern industrial environments while improving the reliability and availability of critical equipment.

The work presented in this thesis aligns with a research initiative aimed at strengthening Algeria's expertise in condition-based maintenance and industrial diagnostics. By proposing robust and efficient approaches, this research contributes to the development of predictive maintenance systems, enhancing the reliability of rotating machinery while addressing the challenges of modern industrial operations.

Chapter 01

Fundamental Notions and Bibliography

In this chapter, we provide an overview of industrial maintenance with a particular focus on current methods for detecting faults in rotating machinery. Through a comprehensive literature review, we highlight vibration analysis as a key method for fault detection. We examine its practices, the techniques for processing vibrational signals, and its specific applications in condition-based preventive maintenance. Emphasis is placed on the utilization of signals associated with common failures in industrial machines. This work illustrates the growing importance of vibration analysis, underscoring the need for a detailed understanding of the dynamic behavior of structures to enable early fault diagnosis and better anticipation of machine malfunctions.

1. Introduction

In modern industry, machine monitoring and diagnostics play a crucial role in ensuring operational reliability. Among the various available methods, vibration analysis stands out as a particularly effective technique, capable of identifying anomalies at an early stage before they lead to major failures.

This introductory chapter presents the fundamentals of industrial maintenance, with a focus on condition-based monitoring. It then explores the main methodologies of vibration analysis, covering time-domain, frequency-domain, and time-frequency approaches. These techniques enable the identification of common faults in rotating machinery, including defective bearings, shaft misalignment, gear anomalies, and belt issues. Recent advancements in artificial intelligence have further enhanced these traditional methods, providing increased fault detection capabilities.

This overview synthesizes major theoretical developments and their practical applications in predictive maintenance. By integrating these vibration analysis tools, industries can detect early signs of failure and optimally plan maintenance interventions. This proactive approach, which underpins the research presented in this thesis, represents a major challenge for modern industry.

2. Generalities on maintenance

Maintenance is a comprehensive discipline that encompasses proactive and reactive measures to ensure the optimal functionality, reliability, and longevity of equipment and systems [4]. It involves a systematic approach that includes preventive actions to avoid failures, corrective interventions to quickly resolve defects, predictive methodologies that use data analysis for preventive maintenance, and condition-based strategies tailored to the equipment's state.

Fundamentally, maintenance refers to the processes and activities performed on machines to ensure their continuous operation, enhance their durability, and maximize their efficiency. Its primary objectives are to minimize downtime, extend equipment lifespan, optimize performance, and maintain profitability.

2.1 Importance of maintenance

The significance of maintenance lies in ensuring the operational reliability, longevity, and cost-effectiveness of machinery [5]. It serves to guarantee the uninterrupted functionality and durability of equipment, machines, and assets. By systematically implementing maintenance strategies, industries can minimize unplanned downtime, mitigate failure risks, and extend the operational lifespan of critical systems. Its central role in performance optimization, maximizing uptime, and controlling operational costs highlights its importance in improving productivity, ensuring safety, and meeting production requirements. Furthermore, effective maintenance practices contribute to a safer work environment, increased asset value, and sustainable operations.

2.2 Types of maintenance

Maintenance encompasses a variety of methods, each designed to align with specific conceptual frameworks. As illustrated in Figure 1.1, the choice of a maintenance method depends on the presence or absence of a failure. Maintenance strategies are classified into three main categories: corrective maintenance, preventive maintenance, and predictive maintenance [6].

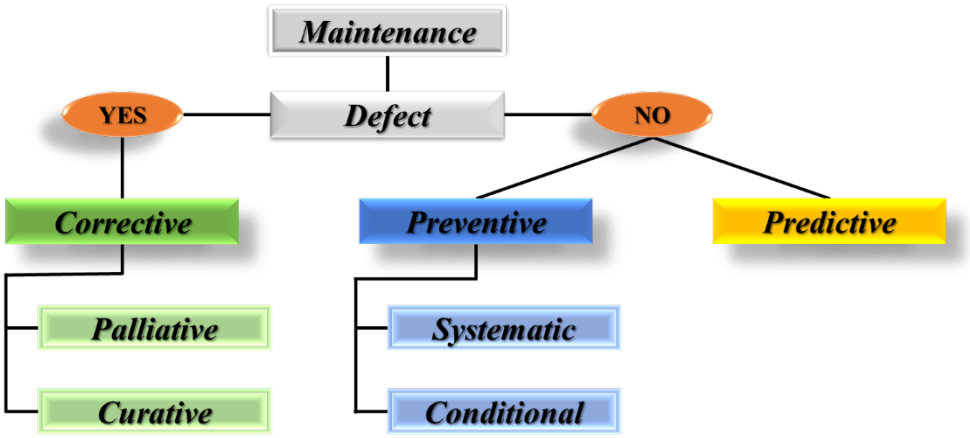

Figure 1.1. Different types of maintenance.

Corrective maintenance takes place after a failure to restore the functionality of machines, either in a palliative manner (temporary restoration to an acceptable performance level) or a curative manner (restoration to optimal performance levels).

Preventive maintenance, on the other hand, acts proactively to prevent failures and follows two approaches: systematic maintenance, which involves planned interventions based on fixed schedules, and condition-based maintenance, which relies on real-time performance monitoring to trigger actions when anomalies are detected.

Finally, predictive maintenance leverages advanced data analysis, including artificial intelligence and machine learning, to anticipate failures by identifying early warning signs.

3. Conditional preventive maintenance techniques

Condition-based preventive maintenance is the most widely used maintenance method globally. It relies on various techniques that utilize the measurement of physical parameters such as vibration analysis, oil analysis, and others (Figure 1.2) to continuously monitor the condition and performance of operating equipment in real time.

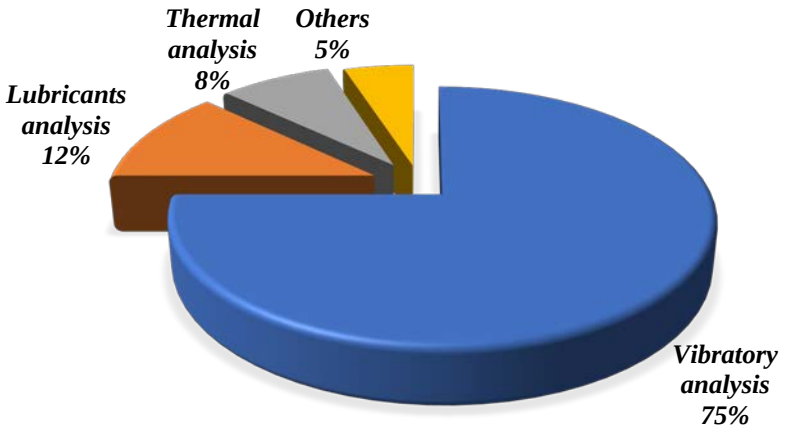

Figure 1.2. Different analysis methods used in conditional preventive maintenance [7].

Its objective is to diagnose anomalies and plan maintenance interventions in advance based on collected data, allowing for proactive maintenance planning.

Vibration analysis is a fundamental diagnostic method in industrial maintenance, focusing on the study of vibrations generated by operating machines. This technique enables the detection of anomalies such as turbulence, shocks, and instability, providing real-time monitoring and precise diagnostics to identify the root causes of faults. Additionally, other diagnostic techniques are sometimes used as complementary tools:

- Lubricant analysis: Evaluates fluid quality to detect signs of component wear.
- Acoustic analysis: Detects anomalies based on the sounds emitted by machines.
- Ultrasonic analysis: Identifies internal defects and leaks using ultrasonic waves.
- Thermography: Visualizes temperature variations to detect friction points or mechanical defects.

Among the various condition-based preventive maintenance methods, vibration analysis stands out as a key tool due to its sensitivity and versatility. It enables the detection of early signs of machine degradation, providing accurate fault diagnostics before failures occur.

While other methods remain valuable, vibration signals often provide the most revealing indicators of impending issues. The following discussion delves deeper into the principles, methodologies, and applications of vibration analysis.

4. Vibration analysis practices

Fault diagnosis in the industrial sector is crucial for productivity gains and competitiveness, as it depends on the essential control of equipment availability and the quality of manufactured goods or services. Vibration analysis (Figure 1.3) plays a key role in achieving this objective by ensuring efficient fault detection and predictive maintenance.

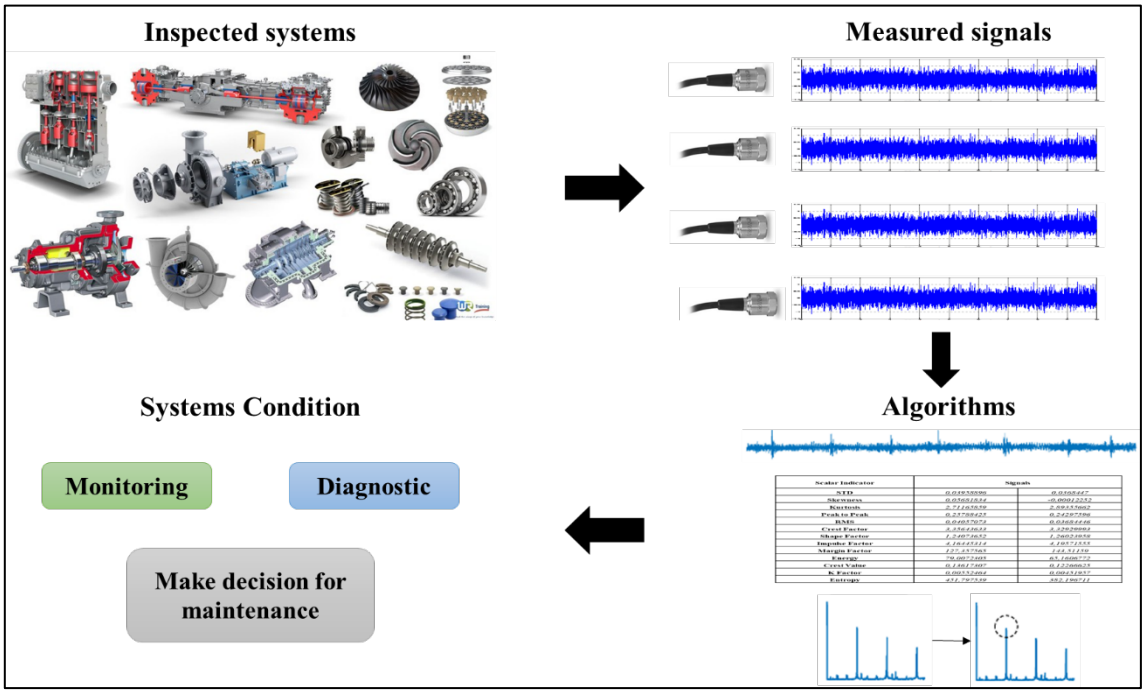

Figure 1.3. Practice of vibration analysis for monitoring rotating machines.

There are two essential tasks in vibration analysis practice [4]: observing failure symptoms, known as "monitoring," and identifying the root cause of the failure using logical reasoning based on observations, referred to as "diagnosis." These two tasks are explained in detail in the following sections.

4.1. Monitoring by vibration analysis

Vibration-based monitoring is a key approach in industrial machine maintenance. This technique involves the collection and analysis of vibration signals emitted by operating equipment. Its primary objective is to detect anomalies, imbalances, or potential mechanical faults in machinery. Monitoring relies on scalar indicators to track changes in a derived quantity related to the power or maximum amplitude of the signal (Figure 1.4).

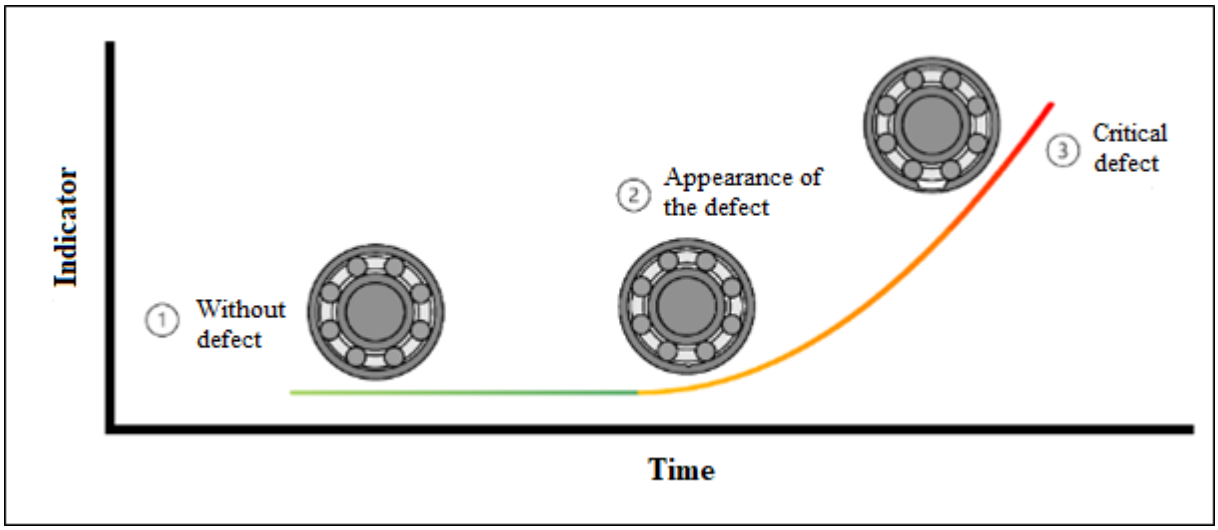

Figure 1.4. The evolution of monitoring indicators over time [8].

Although their absolute values may lack intrinsic significance, the temporal evolution of these quantities is crucial for fault detection. Table 1.1 presents the most commonly used scalar indicators in vibration-based monitoring [9].

Table 1.1. Main scalar indicators.

Indicator	Mathematical expression	Advantages	Disadvantages
Kurtosis (K): indicates whether the data distribution is more or less peaked than a normal distribution.	$K = \frac{\frac{1}{N_e}\sum_{n-1}^{N_e}\left(S(t)-\tilde{S}\right)^4}{\left(\frac{1}{N_e}\sum_{n-1}^{N_e}\left(S(t)-\tilde{S}\right)^2\right)^2}$	Useful for detecting non-Gaussian signals and defects such as bearing faults	Sensitive to non-stationary signals
Crest Factor (CF): The ratio of a signal's peak value to its RMS value, indicating the peak or spikes of the signal.	$FC = \frac{Sup\lvert S_K\rvert}{\sqrt{\frac{1}{N_e}\sum_{k=1}^{N_e}(S_K)^2}}$	Indicates vibration peaks relative to RMS value, useful for detecting high amplitude peaks.	Does not provide a complete indication of overall vibration behavior, sensitive to background noise.

Spectral Center of Gravity (CGS): The weighted average of the frequency spectrum; represents the "center" or predominant frequency components of the signal.	$CGS = \frac{\int f \times L(f)\,df}{L(f)\,df}$	Provides a measure of frequency distribution, useful for identifying changes in the frequency signature.	Require expertise to correctly interpret spectral variations.
Root Mean Square (RMS): The square root of the mean of the squares of a set of values; represents the effective or average amplitude of the signal.	$RMS = \sqrt{\frac{1}{N_e}\sum_{k=1}^{N_e}(S_K)^2}$	Provides an overall measure of vibrational energy, commonly used as a general indicator of vibration.	Not effectively detecting sudden vibration spikes or abrupt changes.
Peak-to-Peak (P2P): The difference between the maximum positive and maximum negative amplitudes of a signal; shows the total variation of the signal.	$C\grave{a}C = \max\left(S(t)\right) - \min\left(S(t)\right)$	Indicates the total amplitude of the signal, useful for assessing extreme variations.	Does not provide details on frequency distribution.
Peak Value (PV): The maximum amplitude of the signal.	$VC = Sup\left\|S_K\right\|$	Gives the maximum value of the vibration amplitude.	Does not take into account the average of vibrations, does not provide an overview of vibrational energy.

K-factor (KF): A parameter used to assess the deviation of actual vibration from a normal distribution; particularly relevant for detecting defects in rolling element bearings.	$FK = Sup\|S_K\| * \sqrt{\frac{1}{N_e}\sum_{k=1}^{N_e}(S_K)^2}$	Used to assess bearing faults and frequency anomalies.	May require calibration and adjustments for specific applications, does not always provide complete information on overall machine condition.

4.2. Diagnosis by vibration analysis

In the field of vibration-based diagnostics, several well-established classical methods continue to play a central role due to their proven effectiveness. These techniques enable the analysis of vibration signals to detect faults and anomalies, including but not limited to:

- Spectral Analysis: This method relies on the Fourier Transform, which represents a time-domain signal x(t) in the frequency domain X(f). It is particularly useful for identifying dominant frequencies and harmonics in vibrations, although it is limited by its time resolution [10]:

$$X(f) = \int_{-\infty}^{+\infty} x(t).e^{-i2\pi ft}dt \tag{1.1}$$

- Cepstral Analysis: This technique applies a double Fourier Transform to the logarithm of the Fourier Transform of a signal x(t) to obtain the cepstral representation C(τ). It is highly effective in identifying periodicities in frequency spectra, enabling the detection of intermittent or hidden faults [11]:

$$C(\tau) = F^{-1}\left\{\log\left(\left|F\left\{x(t)\right\}\right|\right)\right\} \tag{1.2}$$

- High-Frequency Resonance Technique (HFRT) Envelope Analysis: This method focuses on extracting the envelope of a signal, often using the Hilbert Transform. It is particularly suitable for detecting subtle defects, such as those related to bearings or lubrication issues [12]:

$$H\left[x(t)\right] = \frac{1}{\pi}\int_{-\infty}^{+\infty}\frac{x(t)}{t-\tau}d\tau \tag{1.3}$$

- Short-Time Fourier Transform (STFT): This technique enables localized time-frequency analysis by applying a windowing function w(t). It is effective for studying non-stationary signals, although the window size affects both time and frequency resolution [13]:

$$X(\tau, f) = \int_{-\infty}^{\infty} x(t) w(t-\tau) e^{-j2\pi ft} dt \tag{1.4}$$

These traditional methods form a solid foundation for vibration analysis and are still widely used in various industrial applications. However, the increasing demands for predictive maintenance and high-precision diagnostics have led to the development of more advanced techniques.

4.2.1. Wavelet Multi-Resolution Analysis

Wavelet Multi-Resolution Analysis (WMRA) involves decomposing a signal into multiple components at different spatial and frequency resolutions using wavelet filters (Figure 1.5). This decomposition allows the analysis of a signal at different scales of resolution. WMRA decomposes a signal into a series of details $D_i(t)$ and an approximation $A_j(t)$ at different scales *(j)* and resolution levels *(i)* [5].

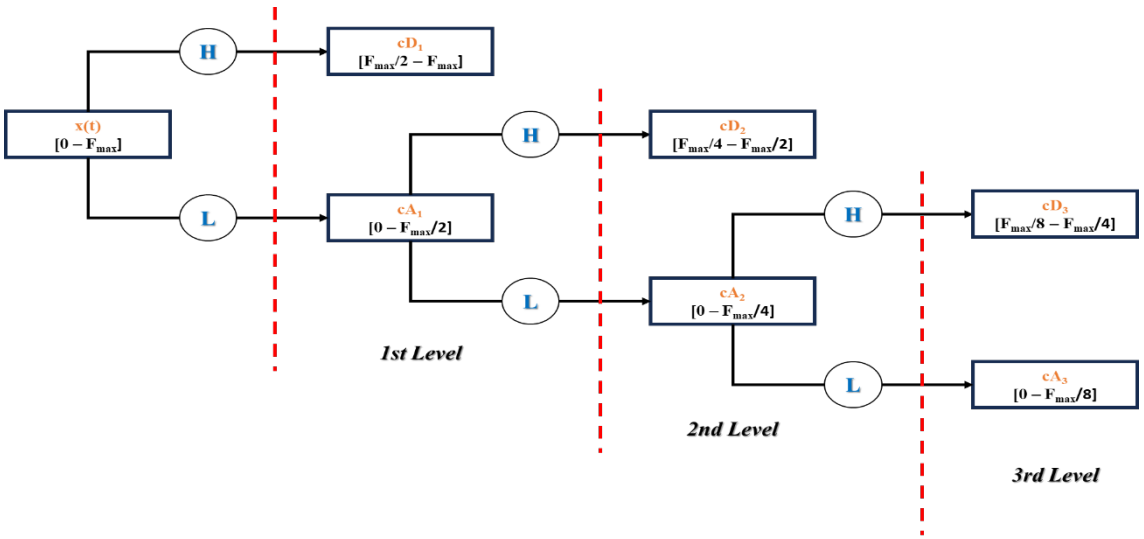

Figure 1.5. WMRA decomposition scheme [14].

WMRA is widely used in various fields, including signal processing and vibration analysis in machinery. It enables the identification of important signal features at different scales, making it particularly useful for detecting faults in machines.

This method offers better temporal localization of transient events and higher frequency resolution than traditional techniques such as the Fourier Transform. However, WMRA requires an appropriate selection of wavelet functions and decomposition parameters, which can be a complex process.

4.2.2. Cyclostationary Analysis

Cyclostationary analysis is a signal processing method used to study signals whose statistical characteristics vary periodically over time, a property known as cyclostationarity [15]. Unlike stationary signals, which have constant statistical properties, cyclostationary signals exhibit periodic variations in their spectral structure.

This technique is particularly useful for detecting intermittent or periodic faults in machine vibration signals. It helps identify cyclic variations in vibrations caused by bearing defects, faulty gear teeth, or other periodic anomalies. Cyclostationary analysis is highly effective in detecting periodic faults in vibration signals, making it easier to identify specific mechanical issues. However, it can be sensitive to variations in cyclostationarity and requires precisely tuned parameters for an accurate analysis.

The mathematical foundations of cyclostationarity are characterized by its power spectral density (PSD) or second-order statistics, such as autocorrelation or dual-lag autocorrelation. A cyclostationary signal presents peaks at specific cyclic frequencies, indicating periodic variations and the presence of faults.

4.2.3. EMD analysis

EMD is a technique for decomposing nonlinear and non-stationary signals into components known as Intrinsic Mode Functions (IMFs). EMD is adaptive and data-driven, enabling the processing of complex and time-varying signals without requiring prior assumptions about their structure [7]. It facilitates the decomposition of complex signals into different characteristic frequency components, thereby enhancing the detection of mechanical faults.

Mathematically, EMD follows an iterative decomposition process. At each step, IMFs are extracted by identifying the oscillatory components present in the original signal. This is achieved by subtracting the mean of the upper and lower envelopes of the signal until reaching a non-decomposable residue. The sum of the IMFs and the residue reconstructs the original signal.

The main advantage of EMD is its ability to handle nonlinear and non-stationary signals. It is adaptive and can be applied in scenarios where traditional methods may fail. However, EMD is known to be sensitive to noise.

The EMD approach has evolved into a broad family of techniques [9], including: Ensemble Empirical Mode Decomposition (EEMD), Complete Ensemble Empirical Mode Decomposition with Adaptive Noise (CEEMDAN), Improved Complete Ensemble Empirical Mode Decomposition with Adaptive Noise (ICEEMDAN). These advanced EMD-based techniques are designed to handle noisy data and trends in vibration signals, improving the accuracy of fault diagnosis.

4.2.4. VMD analysis

To overcome the mode-mixing issues in EMD, Variational Mode Decomposition (VMD) [3] was introduced. VMD is an advanced signal processing technique designed to extract intrinsic modal components from a signal by decomposing it into a sum of modes. This method provides a precise separation of different frequency components within a signal, facilitating the identification of vibration phenomena and fault sources in rotating machinery.

Initially, the decomposition modes are initialized and then iteratively adjusted to minimize their correlation while preserving the total signal energy. At each iteration, the modes undergo spectral filtering to eliminate unwanted components. This process repeats until convergence is achieved, producing the intrinsic modal components of the signal. By combining weighted modes, the modal components of the signal are obtained, allowing for a precise separation of different frequency components.

VMD offers several significant advantages including accurate separation of frequency components, making it easier to identify vibration sources in rotating machinery, adaptability to non-stationary signals, making it a versatile tool for condition monitoring of mechanical systems and higher robustness than traditional techniques, as VMD is less sensitive to distortions and noise, making it suitable for complex industrial environments. By providing greater precision in modal decomposition, VMD enhances fault detection in rotating machines, enabling preventive and proactive maintenance strategies.

It is important to emphasize that all these different techniques converge toward the spectral or envelope spectrum analysis to extract specific frequency characteristics. These approaches aim to analyze the vibrational characteristics of machines, with vibration and envelope spectra being essential tools for identifying fault-related frequencies.

5. Major faults in rotating machines

Rotating machinery is susceptible to various types of faults that can compromise its proper functioning and longevity. The main categories of faults encountered include shaft-related faults, bearing faults, gear faults, and belt faults.

The detection and monitoring of these faults are crucial in the field of preventive maintenance for rotating machinery to prevent costly failures and ensure operational efficiency. Each type of fault has a distinct vibration signature, which allows for detection by analyzing the frequency spectrum of the measured signal.

Figure 1.6 illustrates a typical signal from a healthy machine. The time-domain signal (Figure 1.6.a) exhibits no noticeable periodicities, and its corresponding frequency spectrum (Figure 1.6.b) displays only a peak at the system's rotational frequency, indicating a normal operating condition.

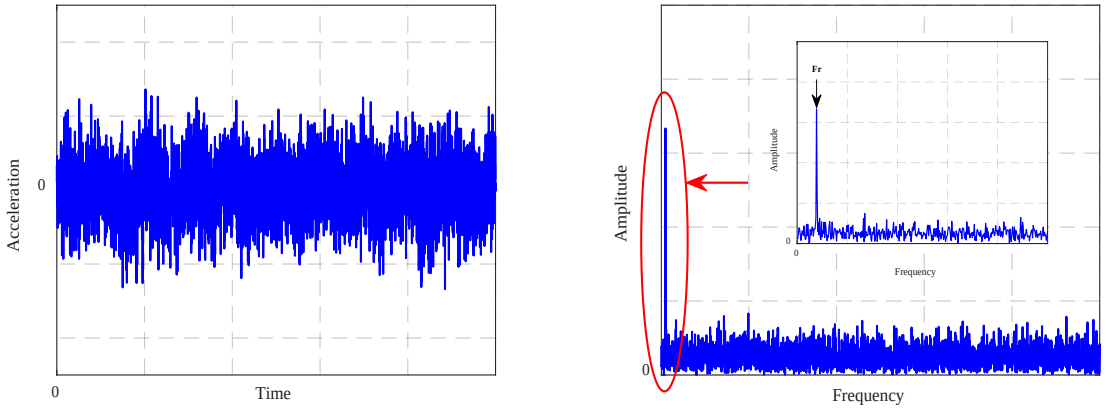

a. b.

Figure 1.6. Vibrational signature of the simulated system:
a. acceleration signal, b. corresponding spectrum.

5.1. Shaft defects

Shaft faults can result from structural issues or excessive stresses, leading to abnormal vibrations and shaft deformation. Here, we explore some of the main faults that can occur in shafts.

5.1.1. Unbalance

Unbalance refers to an uneven distribution of mass around the axis of rotation, which induces non-zero centrifugal forces during rotation. This can lead to undesirable vibrations and premature wear of components.

We can distinguish two types of unbalances: static and dynamic, as shown in Figure 1.7. Static unbalance (Figure 1.7.a) results from an uneven mass distribution relative to the axis of rotation, even when the machine is at rest. On the other hand, dynamic unbalance (Figure 1.7.b) occurs when the mass distribution varies during machine operation, generating variable centrifugal forces.

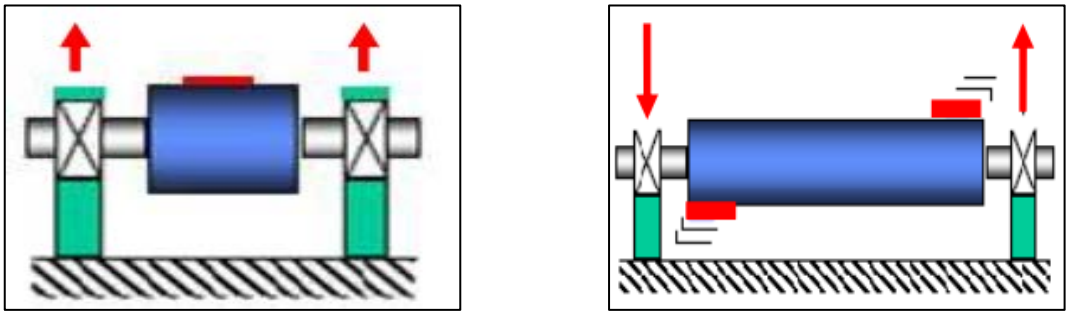

a. b.

Figure 1.7. Unbalance defects: a. static unbalance, b. dynamic unbalance.

To illustrate the vibration signature of an unbalance fault, we examine the spectrum in Figure 1.8. The spectrum exhibits a dominant peak at the rotational frequency of the shaft carrying the unbalance, denoted as *Fr*, along with its harmonics (*×2, ×3*) of lower amplitude.

Unbalance thus induces a vibration whose spectrum features a component with a base frequency corresponding to the rotational frequency *Fr*. This frequency represents the highest peak, accompanied by smaller amplitude peaks at the harmonics of *Fr*.

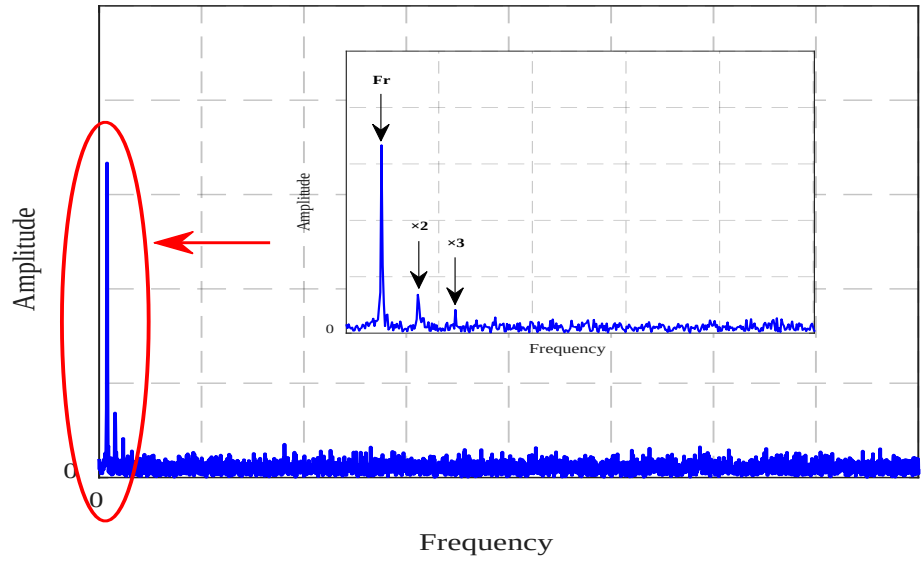

Figure 1.8. Typological spectrum of an unbalance defect.

5.1.2. Misalignment

Misalignment is a condition where the rotational axes of two components are not perfectly aligned. This can occur between two shafts or between a shaft and a coupling. Misalignment can lead to excessive lateral forces, premature wear, and reduced system efficiency. There are two main types of misalignments: radial misalignment, where the rotational axes are not perfectly parallel (Figure 1.9.a), and angular misalignment, where the axes form an angle other than 180° (Figure 1.9.b).

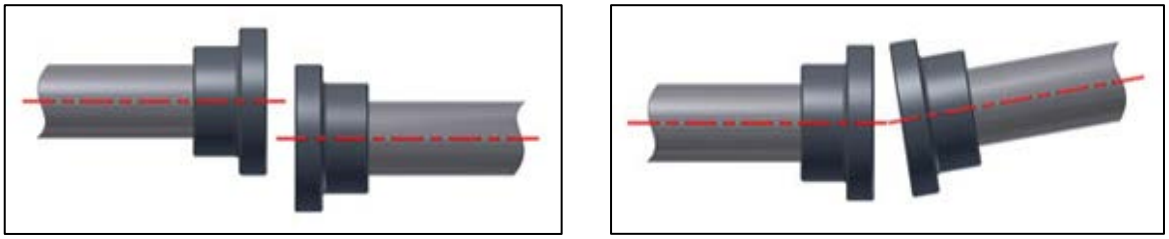

a. b.

Figure 1.9. Misalignment defects: a. radial misalignment, b. angular misalignment.

Let's consider the vibration spectrum of a radial misalignment in a coupling, as illustrated in Figure 1.10. The presence of a misalignment fault is characterized by the emergence of a significant amplitude peak, typically at a frequency equivalent to twice the rotational frequency, $2\times Fr$ (sometimes at three or four times this frequency).

This anomaly generates a characteristic vibration in the radial direction, primarily consisting of a second-order component relative to the rotational frequency (sometimes third-order, or exceptionally fourth-order), with amplitudes exceeding those of the first-order components.

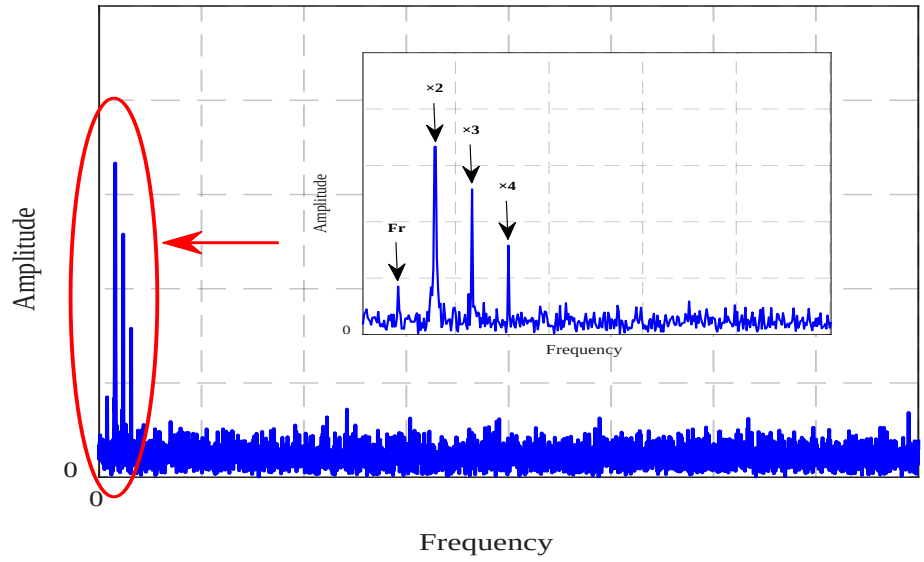

Figure 1.10. Typological spectrum of a misalignment defect.

The diagnosis of an angular misalignment fault requires measurements in two axes (radial and axial). It is characterized by axial vibration with second-, third-, or fourth-order components of the rotational frequency, exhibiting amplitudes higher than those of the corresponding radial components.

5.1.3. Clearance and wear

Clearance and wear represent a common fault in rotating machinery, resulting from the constant interaction of mechanical components over time. This fault can manifest as increased gaps between moving parts, leading to undesirable vibrations and reduced system efficiency. The primary causes of clearance and wear include harsh operating conditions, inadequate maintenance, or the use of low-quality materials.

Mechanical clearance/wear typically manifests in mounts or bearing caps and often produces a large number of harmonics in the vibration spectrum. The spectrum of a clearance/wear fault, as shown in Figure 1.11, reveals the presence of a series of harmonics of the rotational frequency (*Fr, ×2, ×3*) along with sub- and inter-harmonics (with intervals equal to *0.5*×Fr).

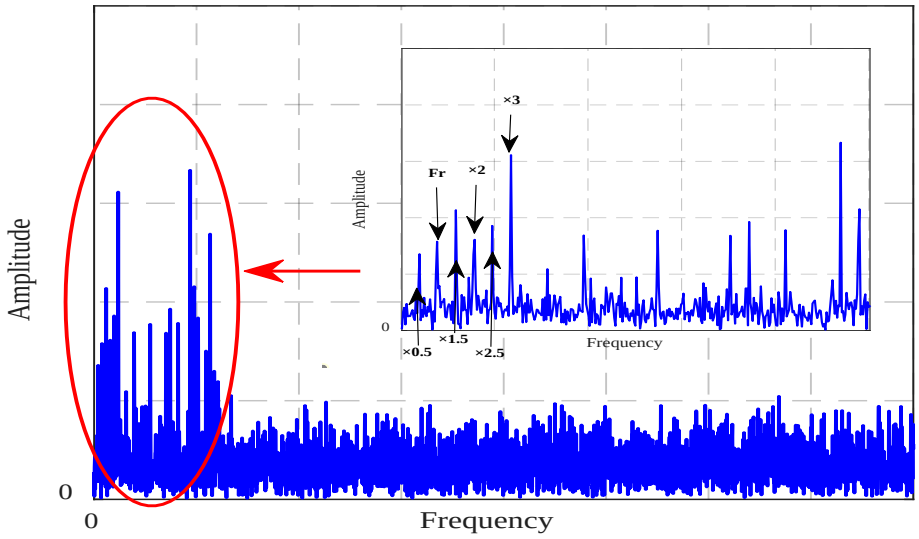

Figure 1.11. Typological spectrum of a shaft clearance/wear defect.

5.2. Bearing defects

Bearing faults are a major concern in the field of rotating machinery, causing significant disruptions. The primary cause of these faults often lies in harsh operating conditions, such as excessive loads, high speeds, or unfavorable operating environments. These faults generally manifest in four main categories [9]: the inner ring, the outer ring, the rolling element, and the cage, as illustrated in Figure 1.12.

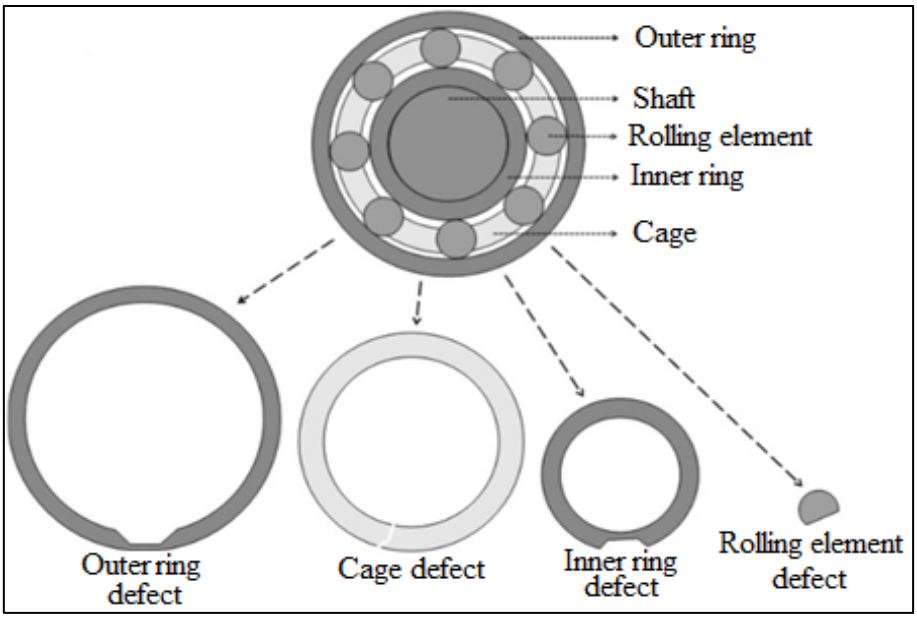

Figure 1.12. Defects present in bearings [9].

Each category of fault exhibits a characteristic natural frequency, which can be identified and analyzed to diagnose the nature and severity of the malfunction. Table 1.2 summarizes these natural frequencies associated with each type of fault.

Table 1.2. Characteristic frequencies of bearing defects.

Frequency of the defect	**Mathematical expression**
Inner Ring Fault Frequency *(BPFI)*	$F_{bi} = \frac{nN}{2}\left(1+\frac{d}{D}\cos\alpha\right)$
Outer Ring Fault Frequency *(BPFO)*	$F_{be} = \frac{nN}{2}\left(1-\frac{d}{D}\cos\alpha\right)$
Rolling Element Fault Frequency *(BPF)*	$F_{er} = \frac{DN}{d}\left(1-\frac{d^2}{D^2}\cos^2\alpha\right)$
Frequency of Cage Defect *(CF)*	$F_c = \frac{N}{2}\left(1-\frac{d}{D}\cos\alpha\right)$

While: N is the rotation frequency in *Hz*

D is the average diameter of the bearing in *mm*

n is the number of rolling elements

d is the diameter of the rolling elements

α is the contact angle in degrees.

5.2.1. Inner ring

The inner race fault in bearings is associated with specific anomalies on the inner raceway of the bearing. This can result from mechanical stresses, excessive loads, or inappropriate operating conditions. This type of fault evolves rapidly and can compromise the stability of the bearing, leading to undesirable vibrations and a decline in the overall performance of the machine.

The characteristic frequency BPFI occurs when a rolling element passes over a defect on the inner raceway. This fault is subject to modulations due to the shaft speed, resulting in a large number of sidebands [16]. Figure 1.13 shows the typical vibration response of an inner race fault in the frequency domain. We can observe the BPFI and its second harmonic (×*2*), as well as sidebands of the rotational frequency *Fr* around the BPFI and its harmonics.

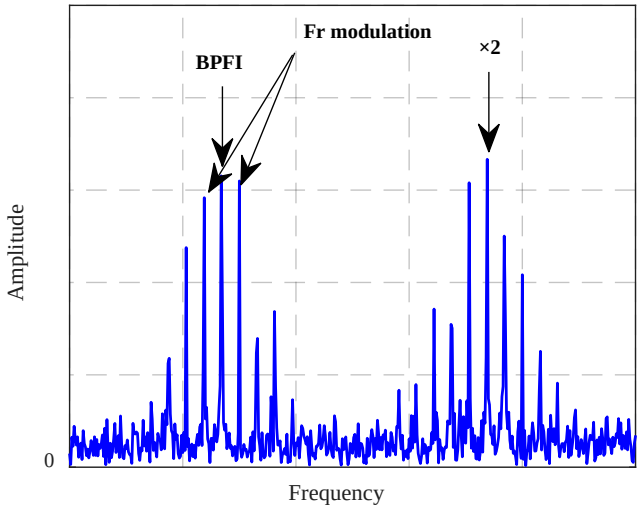

Figure 1.13. Typological spectrum of an inner ring defect.

5.2.2. Outer ring

The outer race is one of the main components of a ball or roller bearing, providing external support for the rolling elements and enabling the rotation of the assembly. Outer race faults evolve over months and manifest as anomalies on its outer surface, typically caused by wear, fatigue, cracks, spalling, pitting, or manufacturing defects.

The typological spectrum of an outer race fault, shown in Figure 1.14, highlights the characteristic frequency peak BPFO and its second harmonic (×*2*), which are indicative of the presence and severity of outer race faults. Sometimes, there may be multiple harmonics of the BPFO, even exceeding it.

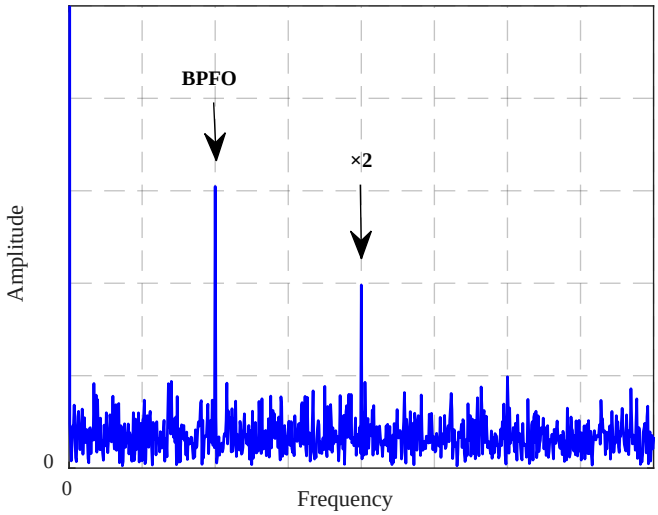

Figure 1.14. Typological spectrum of an outer ring defect.

5.2.3. Rolling element

In the context of bearings, the rolling element refers to the moving part of the bearing that rolls between the inner and outer races. This element can take the form of balls, cylindrical rollers, or tapered cones, depending on the type of bearing. Its primary role is to reduce friction between moving surfaces and facilitate the rotation of the entire mechanism. Faults affecting rolling elements can include shape defects, surface defects, or material defects.

These faults result in distinct characteristics in the typological vibration spectrum, as shown in Figure 1.15. The frequency peaks associated with rolling element faults, BPF and its second harmonic (×*2*), dominate the spectrum and provide valuable insights for diagnosing bearing problems, thereby contributing to improved predictive maintenance of rotating machinery.

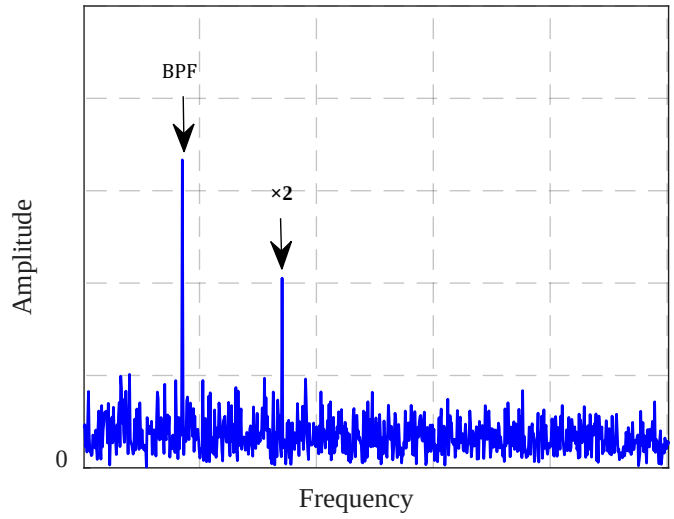

Figure 1.15. Typological spectrum of a rolling element defect.

5.2.4. Cage

The cage fault in bearings refers to a failure or deterioration of the cage structure, the component that maintains the rolling elements (balls or rollers) at regular intervals and prevents them from touching each other. Cage faults are rapidly destructive and are often detected too late. They are rarely energetic, hence the need for high resolution.

The vibrations from a cage fault generate distinct characteristics. In the typological spectrum shown in Figure 1.16, we observe the manifestation of the characteristic frequency CF and its harmonics (×2, ×3). The CF appears between 35% and 46% of the rotational frequency *Fr*, and the cage fault is sometimes accompanied by another fault, such as a ball fault, appearing as sidebands.

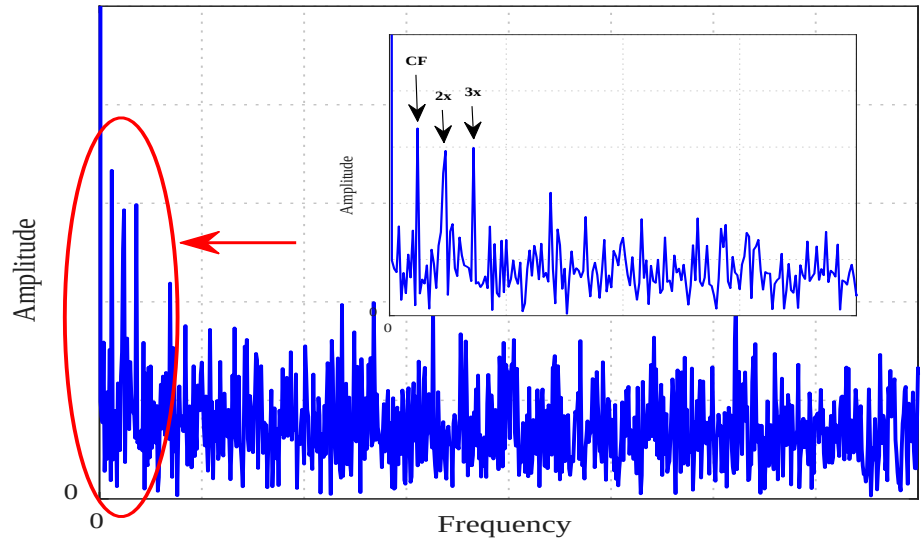

Figure 1.16. Typological spectrum of a cage defect.

5.3. Gear defects

Gear Faults refer to any anomaly or deterioration that affects the proper functioning of gears. These faults can be caused by various factors such as wear, corrosion, fatigue, poor assembly, overload, and manufacturing defects.

Among the major gear faults, as shown in Figure 1.17, are tooth breakage, pitting, complete tooth removal, root cracking, and wear: Tooth Breakage occurs when one of the gear teeth breaks or detaches, while pitting is characterized by the formation of small depressions on the tooth surface, generally caused by high contact stresses. Missing Tooth refers to the complete absence of a gear tooth, which disrupts the gear's motion and root crack refers to a crack or fracture developing from the base of a gear tooth. Finally, wear occurs when the contact surfaces of the teeth gradually deteriorate over time due to continuous use.

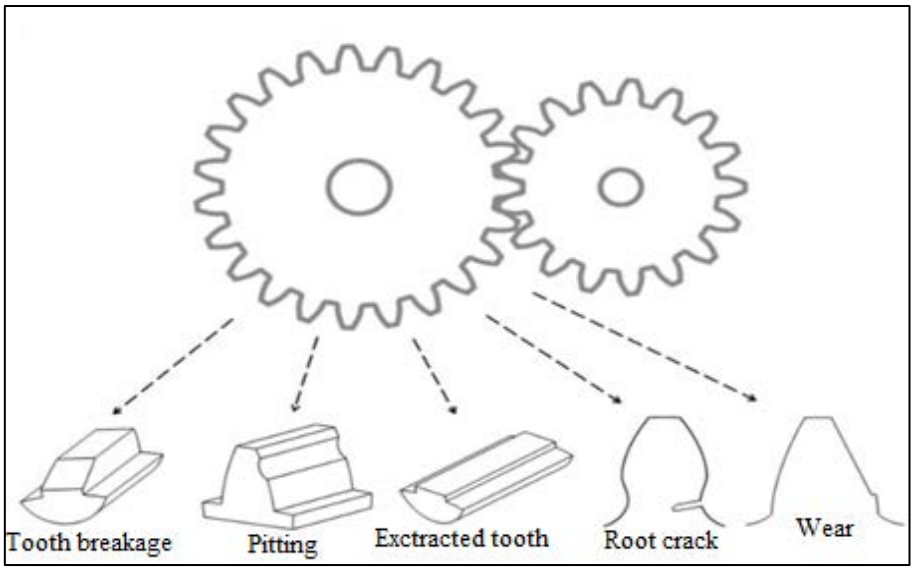

Figure 1.17. Major defects present in gears [8].

Each gear pair has a characteristic frequency, known as the meshing frequency *Fm*, which can be calculated using the following equation:

$$Fm = Z_1 \times Fr_1 = Z_2 \times Fr_2 \tag{1.7}$$

Where: Z_1 and Z_2 are the number of teeth on the two gears.

Fr_1 and Fr_2 are the rotational frequencies of the two gears.

In a measured signal from a gearbox, the presence of the meshing frequency is normal and results from the natural meshing of the gears. Low-amplitude sidebands around *Fm* are also common, reflecting slight differences between the teeth. However, gear faults amplify this modulation, resulting in symmetrical sidebands (with equal spacing) on either side of *Fm* and its harmonics.

As shown in Figure 1.18, the vibration signature characteristic of a gear fault consists of a comb-like pattern of lines at *Fm* and its harmonics (×*2*, ×*3*), modulated by *Fr* of the shaft connected to the defective gear. To observe these families of spectral lines, it is necessary to analyze a frequency range covering multiple times *Fm*.

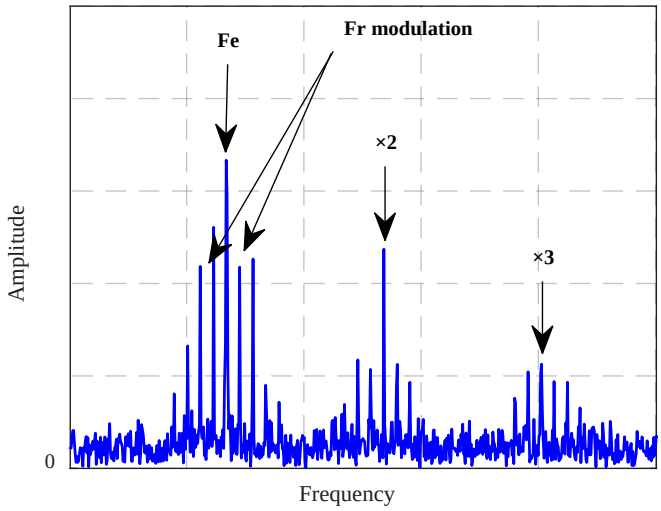

Figure 1.18. Typological spectrum of a gear defect.

In some cases, the spectral pattern may exhibit changes in its shape, such as:

- Wear: Diagnosed by an increase in the 2nd and 3rd harmonics of *Fm*. A significantly higher amplitude of these harmonics compared to *Fm* indicates the severity of the damage.
- Insufficient Center Distance: Between the two gears, this manifests as the appearance of a dominant spectral line at $2\times Fm$ and a partial or complete disappearance of *Fm*'s amplitude.
- Deterioration of Both Gears: Can cause strong impacts when both defects align, a phenomenon known as "coincidence." This alignment generates a coincidence frequency F_{co}: $F_{co} = Fm / PPCM\left(Z_1, Z_2\right)$. The spectrum not only displays the two comb-like patterns corresponding to the rotational frequencies of each gear but also an additional comb of spectral lines corresponding to F_{co}.

5.4. Belt defect

Belt faults typically manifest as signs of slipping, cracking, or breaking, leading to a disruption in the transmission of motion between components. The predominant fault observed in this type of transmission results from localized deterioration of the belt (Figure 1.19.a), causing a specific force or impact at the belt defect frequency *Fc*, which can be calculated using Equation 1.8.

$$F_c = \frac{\pi D_1}{L} F_1 = \frac{\pi D_2}{L} F_2 \tag{1.8}$$

Vibration analysis of this fault reveals significant amplitudes at the belt pass frequency and its harmonics (Figure 1.19.b).

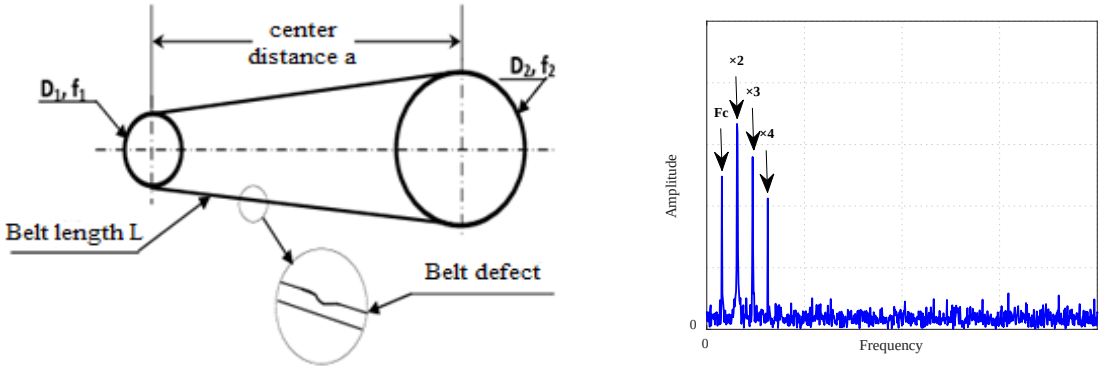

a. b.

Figure 1.19. Belt defect: a. Defect image, b. Typological vibration signature of the defect.

Despite the faults already mentioned, it is important to recognize the existence of other potential anomalies in the mechanical components of rotating machinery, such as turbines, fans, cavitation faults, and faults due to lubrication issues, among others. Vibration analysis, by monitoring the vibrations emitted by these machines, remains a valuable tool for detecting the characteristic signatures of a multitude of faults, thereby enabling effective predictive maintenance and proactive management of industrial equipment.

6. Bibliography

Numerous investigations have been conducted in the field of condition-based maintenance through vibration analysis, aiming to identify characteristic vibration signatures of specific faults in rotating machinery based on acceleration signals. These studies have played a crucial role in the development and determination of suitable diagnostic tools, thereby facilitating the monitoring of rotating machinery behavior.

This section provides a synthesis of various research efforts, highlighting the methods employed and the results obtained in the vibration-based diagnosis of faults. These methods can be grouped into four major categories: time-domain methods, frequency-domain methods, time-frequency methods, and advanced diagnostic methods [17].

In the field of machinery diagnostics through vibration analysis, early work focused on the time-domain analysis of raw vibration signals [18, 19]. This direct approach generates a wealth of information, revealing aspects such as amplitude modulation, transitions, and higher-frequency components [20]. However, the simplicity of evaluating these vibration signals is offset by the inherent noise in the data. To address this challenge, signal processing methods become imperative to extract essential information from time-domain signals. This involves transforming raw signals into relevant statistical parameters [17]. The calculation of scalar

indicators sensitive to the signal's shape provides an indication of the presence of a fault [21–24]. Several statistical parameters are typically extracted from the time-domain signal, such as RMS, crest factor, kurtosis, energy, and others [25]. These parameters enable the differentiated characterization of healthy and faulty machine vibration signals [26].

To diagnose bearing faults, Shrivastava and Wadhwani [27] acquired vibration signals from both healthy and artificially damaged motor bearings, followed by feature extraction and analysis. The main findings indicate that features such as RMS, skewness, and crest factor clearly distinguish healthy conditions from faulty ones. The sensitivity of different features to various types of faults highlights the need to combine these features for robust diagnostics. The study concludes that time-domain features derived from vibration signals can effectively detect faults in rotating electrical machines but cannot determine the type of fault.

Benchaabane et al. [28] present an in-depth study on the detection and monitoring of gear tooth pitting faults through vibration analysis. Their methodology combines numerical simulation of gear faults with experimental testing on a gear test bench, using scalar indicators such as kurtosis, crest factor, and RMS. Key results indicate that while kurtosis is highly effective for detecting impact-type faults, its sensitivity decreases as the number of faults increases. The crest factor shows lower sensitivity, and RMS and energy indicators are more responsive to amplitude variations. Additionally, the study highlights the significant impact of lubrication and applied torque on vibration levels, with non-lubricated gears exhibiting higher vibrations.

Subsequently, frequency-domain vibration analysis emerges as a fundamental tool for uncovering crucial information from machine signals. The Fast Fourier Transform (FFT) is widely used [29, 30] and yields good results. Other studies have introduced FFT-based algorithms such as power spectra [31] and bicoherence [32]. Cepstral analysis has also been introduced and has proven advantageous for rapid fault detection [33, 34].

Ameid et al. [35] used FFT analysis to diagnose broken rotor bar faults in induction motors. By applying FFT to the stator current, the authors were able to identify faulty components, confirming the effectiveness of this method through simulations and experimental tests, particularly with Field-Oriented Control (FOC).

Complementarily, Vernekar et al. [36] explored fault detection in internal combustion engine gearboxes. Their approach, based on vibration and cepstral analysis, demonstrated the effectiveness of these methods for predicting faults, primarily influenced by the Gear Mesh Frequency (GMF) and its harmonics.

El Morsy and Achtenová [37] also emphasized cepstral analysis for diagnosing vehicle gearbox faults. By introducing an artificial pitting fault on a gear tooth, they showed that this method clearly identifies anomalies even under high-load conditions, confirming its utility.

Furthermore, Randall [33] proposed an empirical approach for diagnosing gearbox faults by analyzing vibration signals without resorting to complex dynamic models. By combining spectral and cepstral analysis, the study demonstrated that specific changes in the vibration spectrum can be correlated with gear faults, offering a practical method for condition monitoring.

Nacib et al. [34] used vibration and cepstral analysis to detect gear faults in helicopter gearboxes. Based on in-flight vibration data, they proved that cepstral analysis effectively identifies gear tooth cracks from sidebands, demonstrating its early detection capability.

Time-frequency analysis represents an advanced approach in the evaluation of rotating machinery vibration signals. Unlike classical frequency analysis, this method tracks the evolution of a signal's vibration characteristics over time. It provides a dynamic perspective, particularly relevant for detecting transient variations, intermittent anomalies, or progressive behavioral changes. Several methods have been developed in this domain, including the Short-Time Fourier Transform (STFT) [38], Power Spectral Density (PSD) [39], Cyclostationarity [40], Wavelet Transform (WT) [41], Empirical Mode Decomposition (EMD) [2], and more recently, Variational Mode Decomposition (VMD) [3], which was proposed to overcome the limitations of EMD.

Xuan and Ge [42] investigated the Hilbert-Huang Transform (HHT) for diagnosing faults in rotating machinery from vibration signals, showing that HHT detects rotor eccentricity fault frequencies better than the Fourier Transform.

Cusidó et al. [43] developed an improved method using wavelet analysis and Power Spectral Density (PSD) to detect faults in induction motors under variable load conditions, outperforming traditional Motor Current Signature Analysis (MCSA) techniques.

To demonstrate the superiority of time-frequency methods, Bendjama et al. [44] explored various vibration signal processing techniques for the monitoring and diagnosis of faults in rotating machinery. Their study demonstrates that time-frequency analysis methods outperform traditional methods in terms of effectiveness for detecting faults, particularly gear and unbalance faults, from vibration signals collected on experimental systems.

Wavelet analysis, widely addressed in recent works in both its continuous [45, 46] and discrete [47] forms, has yielded promising results. Early work using wavelets was initiated by Wang and McFadden [48], who processed vibration signals from a helicopter gearbox, enabling

the localization of gear faults. Nikolaou and Antoniadis [49] proposed the use of the wavelet transform as an alternative to traditional time-frequency analysis methods for detecting bearing faults using data collected from a test platform, with results showing promise for monitoring the condition of rotating machinery. Other studies have used continuous wavelets as diagnostic tools for detecting gear faults, such as those by Sung et al. [50], Yoshida et al. [51], and Meltzer and Dien [52]. In the article by Djebala et al. [53], the authors optimized the Wavelet Multi-Resolution Analysis (WMRA) using kurtosis as an optimization criterion to determine the number of decomposition levels, the relevant detail, and other parameters. This technique was used in [54] to detect bearing faults, where optimization yielded excellent results in fault detection. Other works have combined wavelet analysis with other analysis methods, achieving good results in the field [55–58].

Furthermore, Huang et al. [2] proposed a new method called Empirical Mode Decomposition (EMD), where the signal is decomposed adaptively. EMD has been widely used for detecting bearing and gear faults [59–61]. Despite its reliability in fault detection, this method encountered the problem of mode mixing, where different scales can be contained in a single Intrinsic Mode Function (IMF), potentially leading to erroneous diagnostics. To address this issue, a new version of EMD, called Ensemble EMD (EEMD), was proposed [62]. EEMD is a noise-assisted data analysis method, involving the addition of white noise to the signal and computing an ensemble of trials using the original EMD. The average of the results from each trial represents the true IMF. Unfortunately, this solution requires more computational time. Despite this, EEMD has been used for detecting bearing [63, 64] and gear faults [65, 66]. EEMD also has another limitation related to the residual white noise that remains in the reconstructed components from the IMFs, even after the averaging process. To overcome this limitation, a new algorithm called Complete EEMD with Adaptive Noise (CEEMDAN) was introduced by Torres et al. [67]. It offers a complete decomposition with numerically negligible error. Many authors have found that CEEMDAN can be successfully implemented in the monitoring and diagnosis of machine faults [68–70]. To improve CEEMDAN and address its shortcomings, Colominas et al. [71] proposed an improved version called Improved CEEMDAN (ICEEMDAN). Several real biomedical signals were processed, and the results show that the obtained components have less noise and more physical significance. However, ICEEMDAN is still in its early stages of application in the field of fault detection in rotating machinery [72].

However, cyclostationary analysis has proven to be a highly effective method for diagnosing faults in rotating machinery, often surpassing traditional techniques in terms of accuracy and reliability [73]. Urbanek et al. [74, 75] demonstrated that the Modulation Intensity Distribution

(MID) provides information similar to the Spectral Correlation Density. They established that the Integrated MID (IMID) is optimal for detecting secondary cyclostationary components in vibration signals. Kebabsa et al. [76, 77] applied cyclostationarity to diagnose faults in turboalternators and turbofans in industrial settings, effectively identifying issues such as rubbing, oil whirl, blade faults, and gear wear. Their work highlighted the utility of MID and IMID for detecting modulations at different frequencies. Babouri et al. [78] compared cyclostationarity to other signal processing methods, such as FFT, envelope analysis, and Wavelet Multi-Resolution Analysis (WMRA). The study confirmed the superiority of cyclostationarity for diagnosing real mechanical faults, particularly in non-stationary and non-linear signals. Assad et al. [79] processed cyclostationary signals from a multi-stage planetary gearbox, using first-order cyclostationarity to synchronize and average vibration signals, thereby improving fault localization. The combination of cyclostationarity with autoregressive modeling further enhanced detection and diagnostic capabilities.

In the literature, there are two research directions on VMD: the use of the method for fault diagnosis and the optimization of its parameters [80]. In the first direction, the work of Mohanty et al. [81] used VMD to decompose measured signals from a ball bearing. The FFT analysis of the resulting Intrinsic Mode Functions (IMFs) proved the superiority of VMD in analyzing bearing health conditions compared to EMD, even in the presence of noise. An et al. [82] performed envelope demodulation on the IMFs obtained from the VMD of a gear fault signal, where the results from processing simulated and real signals demonstrated the method's effectiveness in detecting gear faults. Mahgoun et al. [83] studied the effectiveness of VMD for diagnosing gear faults under variable speed conditions. Wang et al. [84] applied VMD combined with envelope spectrum analysis for gear fault detection. Chen et al. [85] proposed a scheme for gearbox fault detection using VMD for feature extraction from acoustic emissions, successfully diagnosing a failure. Lin et al. [86] took a further step by combining VMD with a probabilistic neural network for gear fault detection, achieving excellent results that confirmed the advantages of VMD.

In the second direction, focusing on VMD optimization, the work of Li et al. [87] proposed an independent-oriented VMD using the Locally Weighted Scatterplot Smoothing (LOWESS) method, providing a more reliable and stable strategy for selecting the number of intrinsic modes. Additionally, Feng et al. [88] suggested choosing an appropriate value for the number of IMFs (K) based on spectral characteristics. Zhang et al. [89] used correlation and energy ratio in an iterative process to select the value of K. Jiang et al. [90] published a paper in which they used initial center frequencies as an optimization strategy to obtain effective intrinsic

modes. Jiang et al. [91] proposed a coarse-to-fine decomposition technique where VMD is used to evaluate different types of signals for detecting incipient faults in rotating machinery. Many other studies have been conducted on this topic using various techniques [92–96], opening new avenues in the field of vibration analysis.

Recent advances in fault detection have seen the integration of artificial intelligence (AI) techniques to enhance signal analysis, feature extraction, and fault classification. Unsupervised techniques [97] include Principal Component Analysis (PCA) [98], Competitive Learning [99], and Self-Organizing Maps (SOM) [100].

For supervised approaches [101], the literature reports studies on methods such as Support Vector Machines (SVM) [102], Convolutional Neural Networks (CNN) [103], and k-Nearest Neighbors (k-NN) algorithms [104]. One of the most effective AI techniques is Long Short-Term Memory (LSTM) [105], a type of Recurrent Neural Network (RNN) architecture. LSTM was specifically designed to address the limitations of traditional RNNs in capturing and retaining long-term dependencies in sequential data.

Xie and Zhang [106] demonstrated the superiority of the LSTM approach over other methods for the prognosis of complex bearing systems. Anwarsha and Narendiranath [107] found that LSTM networks are capable of detecting faults in various components of rotating machinery. To evaluate the performance of LSTM in real-world scenarios, Cao et al. [108] used LSTM networks to diagnose wind turbine gearbox faults, with results confirming the effectiveness of this technique. Masri and Al-Jabi [109] applied LSTM neural networks to develop predictive models for wind speed, direction, and mechanical power, achieving an average error of less than 3% and an R^2 value of 0.95.

In recent years, the combination of advanced signal processing techniques with AI has emerged as a promising pathway to enhance fault detection capabilities. Damou et al. [110] proposed a new hybrid method for the automatic classification and identification of defective bearings in gearbox systems with identical rotational frequencies. This approach combines signal processing techniques like Ensemble Empirical Mode Decomposition (EEMD), Wavelet Packet Transform (WPT), and Empirical Wavelet Transform (EWT) with machine learning algorithms such as Random Forests for effective fault diagnosis. Moumene and Ouelaa [111] combined Wavelet Transform and Pattern Recognition to detect faults in gears and bearings, achieving perfect results for detecting combined fault types. Gu et al. [112] integrated Variational Mode Decomposition (VMD) and Continuous Wavelet Transform (CWT) to enhance CNN performance in fault diagnosis of rotating machinery. Almutairi and Sinha [113] conducted an experimental study on Vibration-based Machine Learning (VML) for fault

diagnosis in rotating machinery, focusing on the classification of rotor and bearing faults. Their VML approach was tested at two different rotational speeds. Tong et al. [114] proposed a novel fault diagnosis approach for rolling element bearings by combining Dual-Tree Complex Wavelet Packet Transform, Improved Intrinsic Time-Scale Decomposition, Singular Value Decomposition, and Online Sequential Extreme Learning Machine. This method extracts meaningful fault features and accurately identifies fault patterns from vibration signals.

7. Conclusions

This introductory chapter addressed the fundamental concepts, common methodologies, and research advances in the field of vibration analysis for machine condition monitoring. The use of predictive maintenance techniques to maximize equipment reliability and uptime has established the critical role of maintenance in modern industry.

An overview of the fundamental vibration analysis techniques demonstrated their capability to extract sensitive information about machine health from vibration data. By revealing characteristic vibration patterns, time-domain, frequency-domain, and time-frequency analysis methods have been shown to facilitate the detection of common faults in rotating machinery.

The chapter also discussed recent advancements in fault diagnosis through the integration of machine learning and artificial intelligence, which have significantly improved the accuracy of fault detection. Key research contributions applying various vibration analysis methodologies for diagnosing faults were summarized.

A literature review highlighted the crucial importance of vibration monitoring for effective condition-based maintenance. The collective studies emphasize the efficacy of vibration analysis for preventive maintenance and early fault detection, making it an indispensable tool for improving the reliability and operational efficiency of industrial equipment.

Chapter 02

Comparative study between VMD and EMD for the diagnosis of rotating machine faults

In this chapter, we compare EMD and VMD in the context of gear fault diagnosis. After presenting the theoretical principles of each method, we apply these techniques to real vibrational signals obtained from a test bench simulating various fault conditions. Our study shows that VMD achieves better isolation of significant signal components with fewer modes, whereas EMD generates a larger number of Intrinsic Mode Functions (IMFs) with less effective separation. VMD demonstrates superior accuracy, particularly for detecting subtle faults. However, determining the optimal number of modes for VMD remains a major challenge. This comparison highlights the importance of selecting the most appropriate decomposition method based on the specific characteristics of the signal and the type of fault being analyzed.

1. Introduction

In the field of industrial maintenance, vibration signal analysis has established itself as a particularly relevant diagnostic approach. This non-invasive technique allows for the anticipation of mechanical failures by detecting anomalies as soon as they appear, thereby promoting a predictive rather than reactive approach. However, the complexity of modern machinery generates non-linear and non-stationary signals that require sophisticated analysis tools. In response to these challenges, the scientific community has developed various signal processing methods, each with distinct characteristics.

Among these methods, the EMD and VMD have emerged as promising techniques for the diagnosis of rotating machinery. This chapter provides an in-depth comparative analysis of these two approaches, evaluating their relevance and effectiveness in the specific context of gear faults. Our study is based on experimental data from a test bench replicating different fault conditions, enabling a pragmatic assessment of the performance of each method.

This investigation aims to provide practitioners and researchers with insights into the choice of the most suitable method for their specific needs, while opening new perspectives for improving rotating machinery diagnostic techniques. The results of this analysis will contribute to optimizing predictive maintenance strategies in the modern industrial context.

2. Principle of the EMD method

EMD is an adaptive signal processing method that decomposes a signal into a series of basic functions called Intrinsic Mode Functions (IMFs) [2]. Each IMF represents an oscillatory component of the original signal [60]. The decomposition process relies on an algorithm known as the sifting process [115], which iteratively extracts the IMFs.

The EMD decomposition process, as illustrated in Figure 2.1, can be described by the following steps [116]:

- Introduce the original signal.
- Identify all local maxima and minima of the signal.
- Construct the upper envelope $e_{upper}(t)$ by interpolating the local maxima, and the lower envelope $e_{lower}(t)$ by interpolating the local minima.
- Compute the mean of the two envelopes $m(t)$ using the relation:

$$m(t) = \frac{e_{upper}(t) + e_{lower}(t)}{2} \tag{2.1}$$

- Extract the candidate IMF h(t) by subtracting the mean envelope from the original signal:

$$h(t) = x(t) - m(t) \tag{2.2}$$

- Validation of the IMF, verify if *h(t)* satisfies the conditions to be considered an IMF:
  - The number of zero crossings and local extrema must be equal or differ by at most one.
  - The mean of the upper and lower envelopes should be zero at every point.

If these conditions are not met, repeat steps 1 to 4 using *h(t)* as the new signal.

- Extraction of IMFs: once an IMF $c_i(t)$ is obtained, subtract $c_i(t)$ from the original signal to obtain the residue *r(t)*:

$$r(t) = x(t) - c_i(t) \tag{2.3}$$

- Repeat the same process to the residue *r(t)* to extract subsequent IMFs.

The original signal can be reconstructed as the sum of all IMFs and the final residue $r_n(t)$:

$$x(t) = \sum_{i=1}^{n} c_i(t) + r_n(t) \tag{2.4}$$

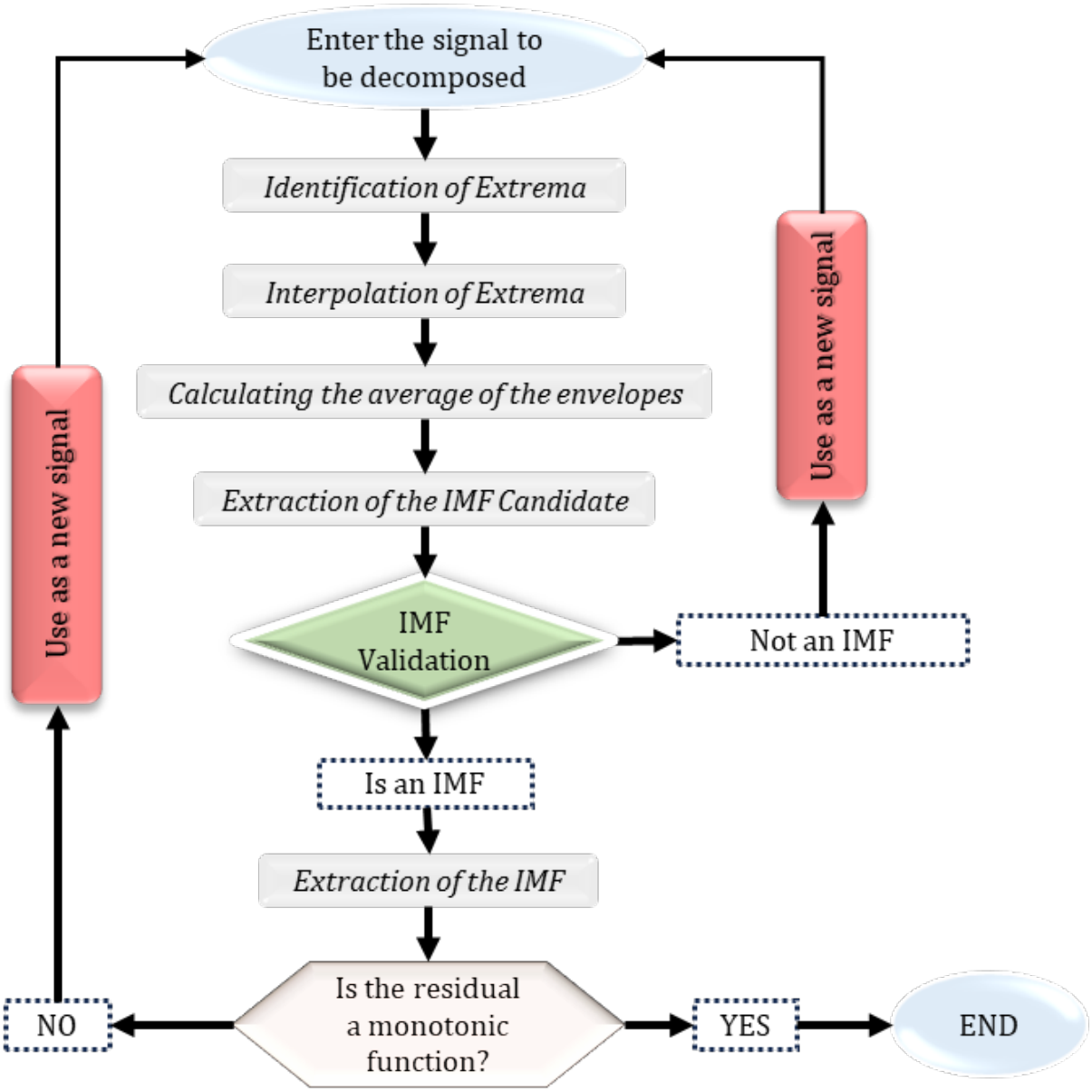

Figure 2.1. Organizational chart for the EMD.

3. Principle of the VMD method

VMD is an innovative and adaptive signal processing method, proposed in [3], which decomposes a signal *S(t)* into its band-limited intrinsic mode functions (IMFs) $u_k(t)$ [84], each characterized by a specific center frequency ω_k and bandwidth [117]. This method aims to minimize a cost function defined in terms of the mode spectra [89]:

$$\min_{\{u_k\},\{\omega_k\}} \left\{ \sum_k \left\| \partial_t \left[\left(\delta(t) + \frac{j}{\pi t} \right) * u_k(t) \right] e^{-j\omega_k t} \right\|_2^2 \right\} \tag{2.5}$$

Where: $*$ denotes convolution, $\|\cdot\|_2^2$ is the squared $L^2 - norm$, and δ is the Dirac function.

To overcome the minimization problem proposed in Equation (2.5), the augmented Lagrangian *L* was introduced [3]:

$$\boldsymbol{L}\left(\{u_k\},\{\omega_k\},\lambda\right) := \alpha\sum_k \left\| \partial_t \left[\left(\delta(t) + \frac{j}{\pi t} \right) * u_k(t) \right] e^{-j\omega_k t} \right\|_2^2 + \left\| S(t) - \sum_k u_k(t) \right\|_2^2 + \left\langle \lambda(t), S(t) - \sum_k u_k(t) \right\rangle \quad (2.6)$$

Here, α is the bandwidth constraint.

The steps of the VMD method, as shown in Figure 2.2, are as follows:

- Introduce the signal for decomposition.
- Initialize Parameters: **s**et the decomposition parameters for VMD, including the number of IMFs *K* and the bandwidth constraint α.
- Update the Modes $u_k(t)$, using gradient descent to minimize the cost function:

$$u_k(t) = \arg\min_{u_k} \left\{ \sum_{k=1}^{K} \left\| \partial_t \left[\left(\delta(t) + \frac{j}{\pi t} \right) * u_k(t) \right] e^{-j\omega_k t} \right\|_2^2 \right\} \quad (2.7)$$

- Update the Center Frequencies ω_k, using gradient descent to minimize the cost function:

$$\omega_k = \arg\min_{\omega_k} \left\{ \sum_{k=1}^{K} \left\| \partial_t \left[\left(\delta(t) + \frac{j}{\pi t} \right) * u_k(t) \right] e^{-j\omega_k t} \right\|_2^2 \right\} \quad (2.8)$$

- Calculate the Residual $r(t)$, by subtracting the sum of the obtained modes from the original signal:

$$r(t) = s(t) - \sum u_k(t) \quad (2.9)$$

- Check for Convergence: verify whether the updates to the modes and frequencies have stabilized (i.e., no significant changes).
  - If the algorithm has converged, save the modes $u_k(t)$ and their center frequencies ω_k.
  - If the algorithm has not converged, use $r(t)$ as the new signal and repeat the update steps.

The original signal can be reconstructed as the sum of the IMFs and the final residual $r(t)$:

$$s(t) = \sum_{i=1}^{K} u_k(t) + r(t) \quad (2.10)$$

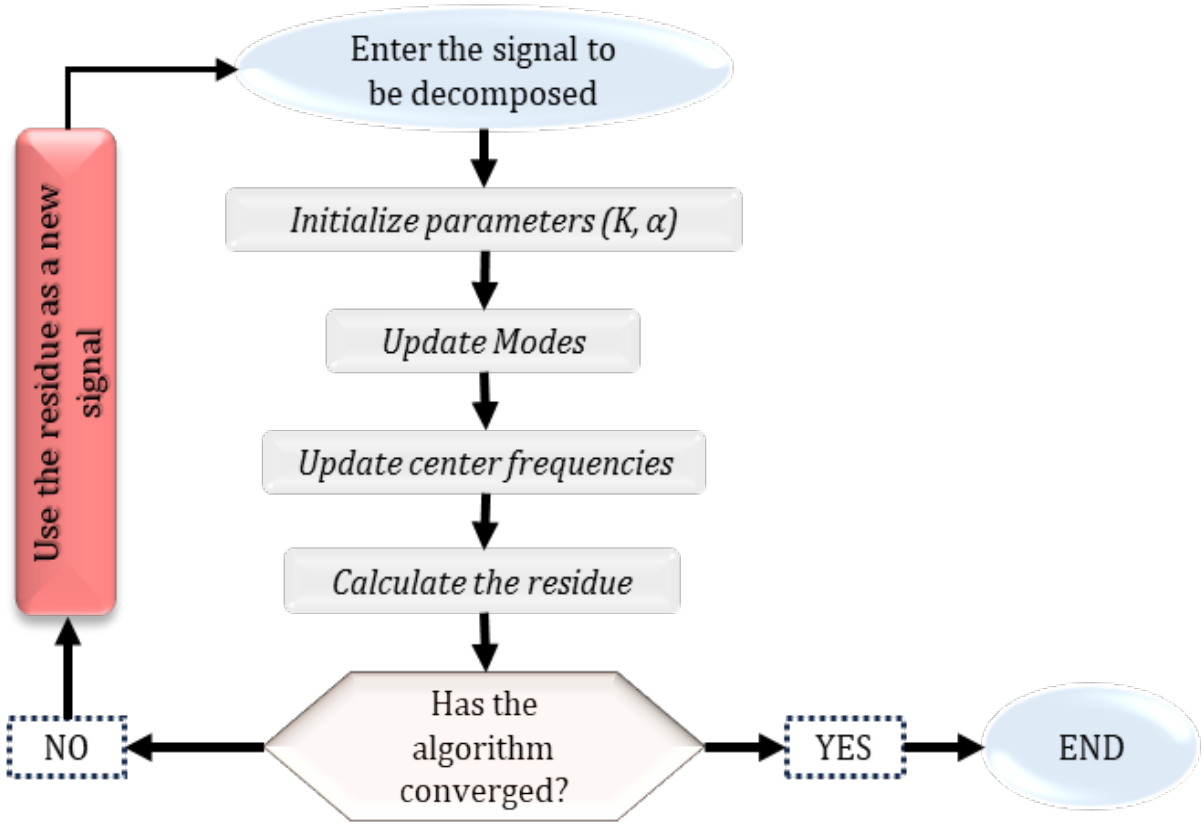

Figure 2.2. Organization chart for the VMD.

4. Comparison between EMD and VMD

Table 2.1 presents a comparison of the main differences between EMD and VMD. EMD is highly adaptive and performs well without requiring prior parameters, offering excellent local resolution. However, it is sensitive to noise and may suffer from mode mixing.

In contrast, VMD, although requiring initial parameters such as the number of modes and center frequencies, provides greater robustness against noise and reduces the phenomenon of mode mixing through its optimization of bandwidths. VMD, while more computationally complex, often converges more quickly and efficiently.

Table 2.1. Comparison between EMD and VMD.

Criteria	***EMD***	***VMD***
Adaptivity [118]	Highly adaptive, without a priori parameters.	Partial adaptivity, requires number of modes.
Locality [119]	Very local, excellent temporal resolution.	Less local, less fine temporal resolution but more stable.
Stopping criterion [120, 121]	Based on local criteria (crossed zeros, envelopes).	Based on the convergence of the global cost function.
Noise robustness [122]	Sensitive to noise and extreme local variations, risk of mode-mixing.	Less sensitive to noise, better separation of components.
Mode-mixing [96]	Susceptible to the mode-mixing phenomenon.	Reduces mode-mixing phenomenon by optimizing bandwidths.
Computational Complexity [2, 3]	Less complex, but may require many sifting iterations.	More complex due to Variational optimization, but often converges faster.
Parameter Specification [64, 90]	No parameters required a priori.	Requires specification of number of modes
Processing of Nonlinear and Nonstationary Signals [83]	Efficient, naturally adapts to signal dynamics.	Very efficient, but requires a good estimation of the initial parameters.
Applications [59, 84, 88, 123]	Used in various applications due to its simplicity and adaptability.	Increasingly used thanks to its robustness and its bandwidth separation capacity.
Bibliographic References [80, 124]	Older, widely studied and documented.	More recent method, but growing rapidly in the literature.

Theoretically, VMD is more effective than EMD for applications requiring precise separation of signal components and increased robustness against perturbations. Its ability to provide more stable modes and better noise management makes it a more advanced method for fault diagnosis in rotating machinery.

5. Application to gear defects

To better understand the difference between the two methods and to observe their real implications as well as the diagnostic results, we propose in the following section an application of both methods for diagnosing gear faults using signals measured from a test bench.

5.1. Description of the test bench

The data used in this study were measured on the Machine Fault Simulator (MFS) test bench using the SpectraQuest processing software. The MFS test bench primarily consists of a *0.75 kW* electric motor with a maximum rotational speed of *6000 rpm*, a coupling, and a belt transmission system (with pulleys *d1=51 mm, d2=126 mm*, and belt length *L=965 mm*), offering a transmission ratio of *0.4*. Finally, a gearbox is included, as illustrated in Figure 2.3.

The single-stage gearbox contains two straight bevel gears with a ratio of *1.5:1*. A magnetic brake is used to simulate the load. The input and output gears have *18* and *27* teeth, respectively, resulting in a transmission ratio of *0.67*. Two accelerometers were used to measure the vibration signals: the first accelerometer is a bi-directional sensor placed on top of the gearbox reducer, capturing both axial and radial vibrations, while the second accelerometer is mounted horizontally to capture additional vibration data.

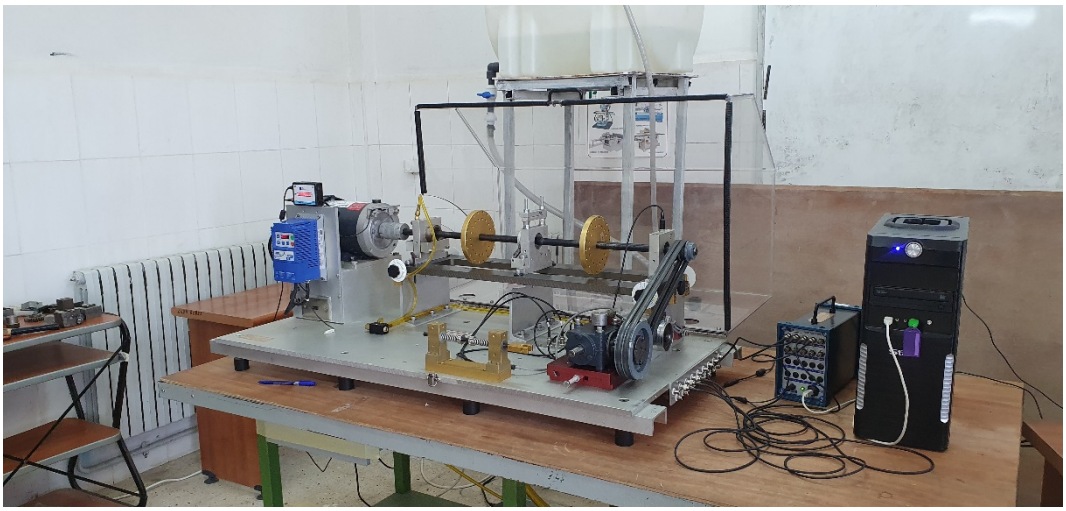

Figure 2.3. MFS test bench.

Based on the selected dataset from the MFS, two signals are chosen for this study, each representing a state of the machine. The first signal corresponds to the case of a half-extracted tooth (Figure 2.4 (a)), and the second corresponds to the case of a fully extracted tooth (Figure 2.4 (b)).

a. b.

Figure 2.4. Defective gear: a. half tooth extracted, b. tooth extracted completely.

The chosen signals (Figure 2.5) are measured for a motor shaft rotational frequency of $F = 36\ Hz$, resulting in an input frequency to the gearbox corresponding to the faulty gear of $F_{r1} = 14.54\ Hz$, an output frequency of $F_{r2} = 9.69\ Hz$, and a meshing frequency of $Fm = 261.87\ Hz$. These signals are subsequently processed using EMD and VMD to highlight the differences in the results. Figure 2.5 (a) presents the case with a half-extracted tooth, while Figure 2.5 (b) presents the case of a fully extracted tooth.

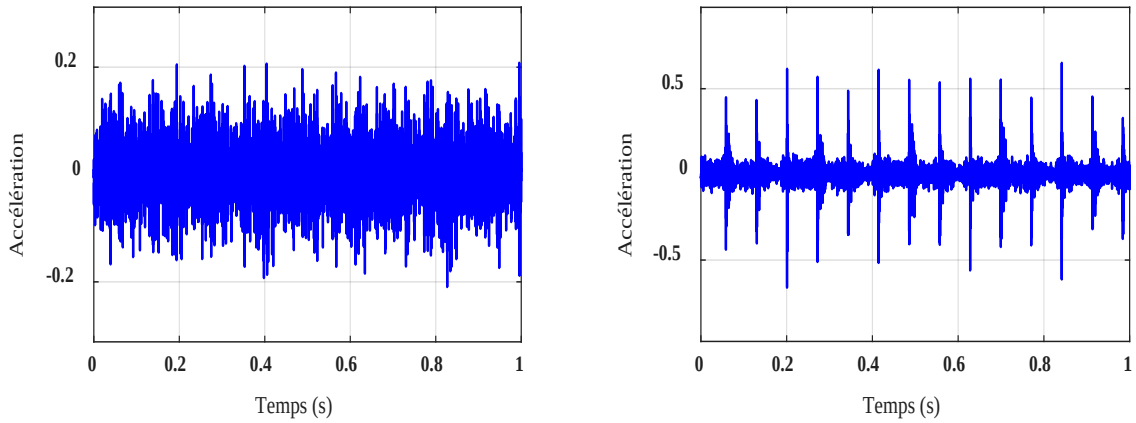

a. b.

Figure 2.5. The signals chosen for the study:
a. Case of a half tooth extracted, b. Case of a tooth extracted.

5.2. EMD analysis

The EMD was first applied to the signal of a gear with a half-tooth extracted. This decomposition resulted in 14 IMFs, as illustrated in Figure 2.6(a). Each IMF represents a distinct oscillatory component extracted from the original signal, as shown in Figure 2.6(b).

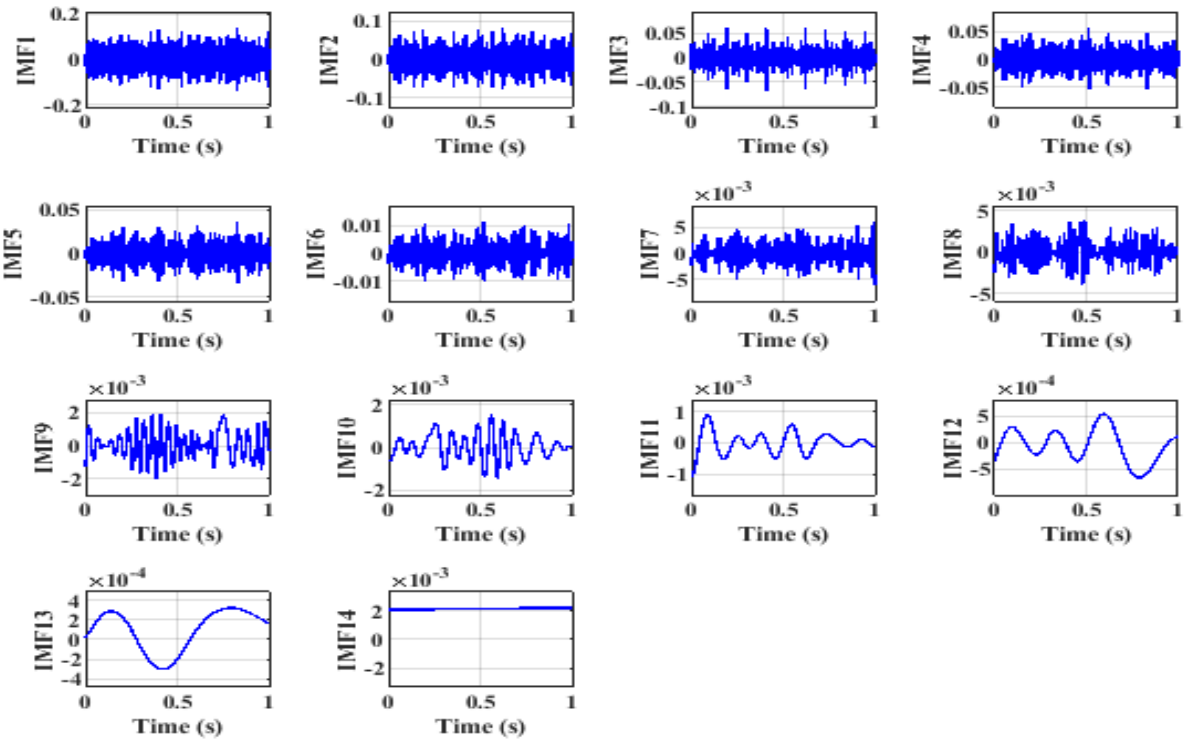

a.

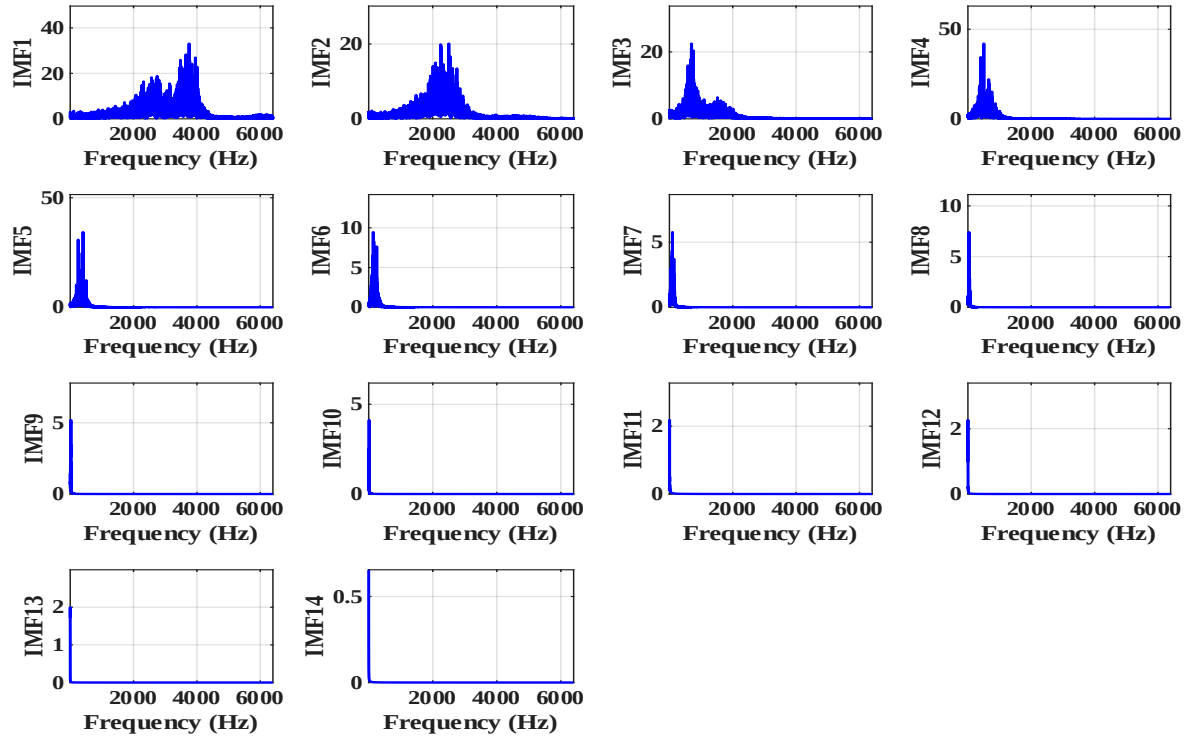

b.

Figure 2.6. The resulting IMFs by EMD for a defect of a half-extracted tooth: a. time representation, b. frequency representation.

The analysis of these 14 IMFs reveals how each component can be associated with specific characteristics of the signal: high-frequency oscillations (IMF1 to IMF4) are influenced by

noise, while low-frequency trends (IMF9 to IMF14) represent the overall behavior of the system. However, only the first four IMFs are relevant for diagnostics, as they may contain information about the machine's condition. Therefore, these are the IMFs to be further investigated.

Table 2.2 presents various scalar indicators calculated for each IMF obtained through EMD. These indicators include: Kurtosis, Peak-to-Peak Value, Root Mean Square (RMS), Crest Factor, Energy, Peak Value, and *K*-Factor. It is evident that the first four IMFs are the most relevant for fault diagnosis. They exhibit high values of kurtosis, peak-to-peak, RMS, and energy, indicating that they capture the frequency components associated with faults. In contrast, the higher-order IMFs capture lower-frequency components and more uniform variations, contributing less to the direct identification of faults. The analysis of this table confirms the observations made in Figure 2.6.

Table 2.2. Scalar indicators of IMFs obtained by EMD: case of a half-extracted tooth.

IMFs	**Indicators**						
	Kurtosis	Peak to Peak	RMS	Crest Factor	Energie	Peak Value	K-Factor
IMF1	3,96	0,27	0,032	4,34	16,88	0,13	0,004
IMF2	4,17	0,16	0,018	4,61	5,32	0,08	0,001
IMF3	5,61	0,13	0,012	5,03	2,59	0,06	0,0008
IMF4	3,13	0,11	0,014	4,01	3,37	0,05	0,0008
IMF5	3,04	0,07	0,009	3,65	1,60	0,03	0,0003
IMF6	2,83	0,02	0,003	3,13	0,22	0,01	4,27E-05
IMF7	2,84	0,01	0,001	3,18	0,06	0,006	1,19E-05
IMF8	2,37	0,007	0,001	2,42	0,03	0,003	6,06E-06
IMF9	2,28	0,003	0,0008	2,14	0,01	0,002	1,71E-06
IMF10	2,61	0,002	0,0005	2,50	0,005	0,001	8,93E-07
IMF11	3,67	0,002	0,0003	2,62	0,002	0,001	3,96E-07
IMF12	2,31	0,001	0,0003	1,70	0,001	0,0006	2,09E-07
IMF13	2,09	0,0006	0,0002	1,40	0,0008	0,0003	7,41E-08
IMF14	1,53	0,0001	0,002	1,02	0,07	0,002	4,82E-06

To diagnose the fault, the first 4 IMFs are subsequently processed using envelope analysis to obtain the envelope spectra shown in Figure 2.7. The envelope spectra of the IMFs clearly show the presence of the rotational frequencies F_{r1}, F_{r2} and some of their harmonics $(2\times F_{r1}, 2\times F_{r2}, 3\times F_{r2}, ...)$, but we are not able to achieve a clear fault detection (based on the typological spectrum). The presence of F_{r1} and its harmonics is explained by the intentionally simulated fault on the input shaft gear. However, the extraction of half a tooth from a spur gear does not produce enough impact, and the contact between the teeth was not significantly affected, which requires more advanced analysis methods. On the other hand, the presence of F_{r2} and its harmonics may indicate the emergence of a second fault on the output shaft gear. It should be noted that this latter fault could arise due to the manipulation of the test bench (assembly and disassembly of the gears).

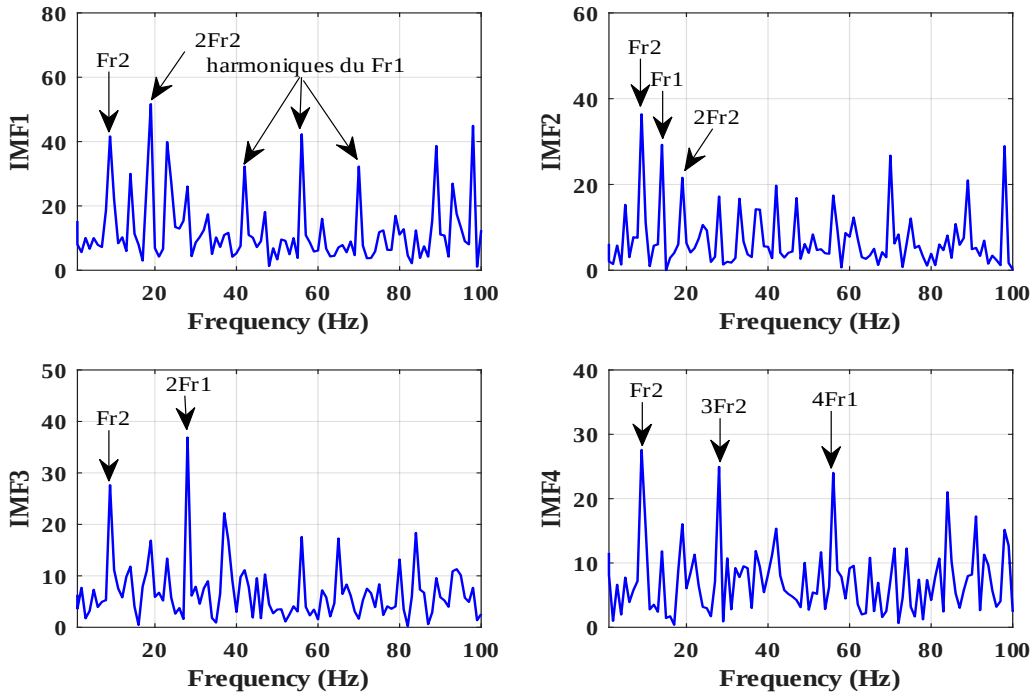

Figure 2.7. Envelope spectra of the first 4 IMFs obtained by EMD for the case of a half-extracted tooth.

In contrast, for the second case, where the EMD was applied to the signal from a gear with a completely extracted tooth, the decomposition resulted in 16 IMFs. After observing these IMFs and analyzing their corresponding scalar indicators, we again selected the first four IMFs for fault diagnosis. The selected IMFs are presented in Figure 2.8. In this case, the fault detection is much clearer: we observe very high kurtosis values for the selected IMFs (see figure 2.8 (b)).

The envelope spectra in Figure 2.8(c) show a dominance of the rotational frequency of the defective gear F_{r1}, along with a rich presence of harmonics (2×, 3×, 4×, ...) forming pattern consistent with a gear fault. We observe that for the complete removal of a tooth, the defect masks all other frequency components.

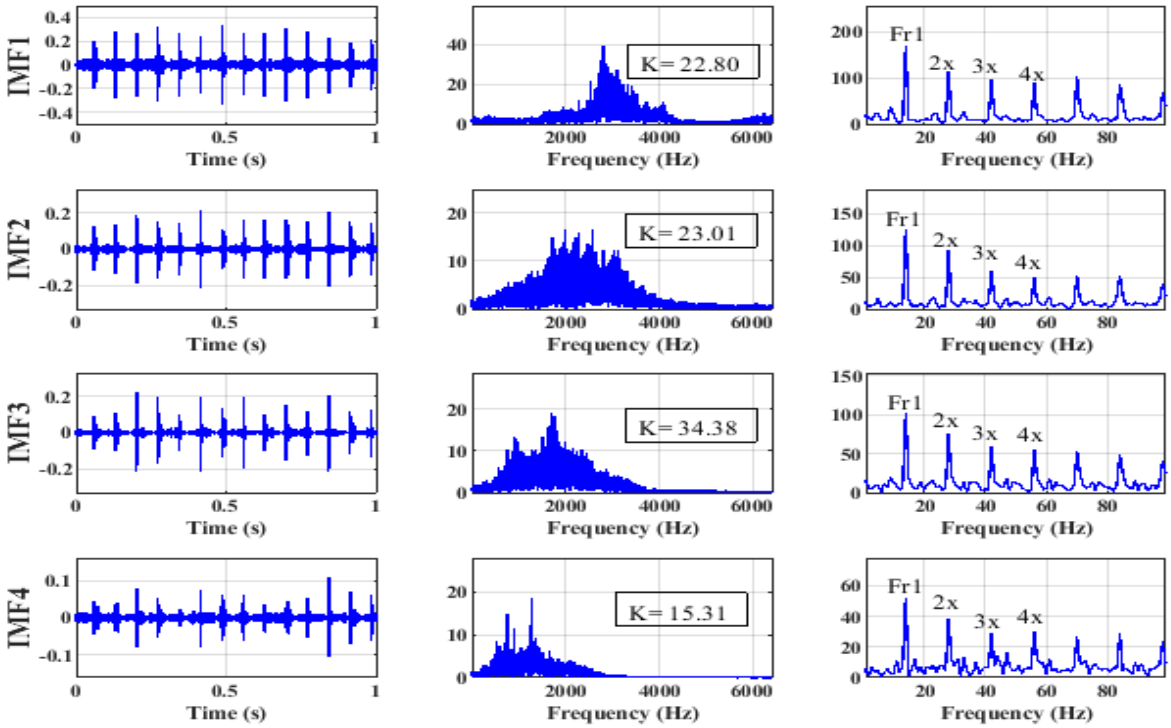

a. b. c.

Figure 2.8. The IMFs chosen for the case of an extracted tooth obtained by EMD: a. time representation, b. frequency representation, c. envelope spectra.

5.3. VMD analysis

Unlike EMD, VMD requires the prior selection of the number of IMFs. To allow for a direct comparison between the two methods, we selected 14 IMFs for VMD. The results of this decomposition are presented in Figure 2.9.

We observe that the IMFs obtained by VMD differ significantly from those produced by EMD. First, each IMF covers a narrow frequency band around a central frequency, which aligns with the principle of VMD. Second, the resulting IMFs are organized from low to high frequencies, reflecting a better separation of the frequency components of the original signal.

However, we also note the existence of some IMFs that do not contain relevant information for diagnosis, as well as redundant IMFs containing the same information. This observation underscores the critical importance of selecting the appropriate number of modes for the effective application of VMD. A judicious choice of K allows for the capture of essential information while minimizing redundancy and non-informative components.

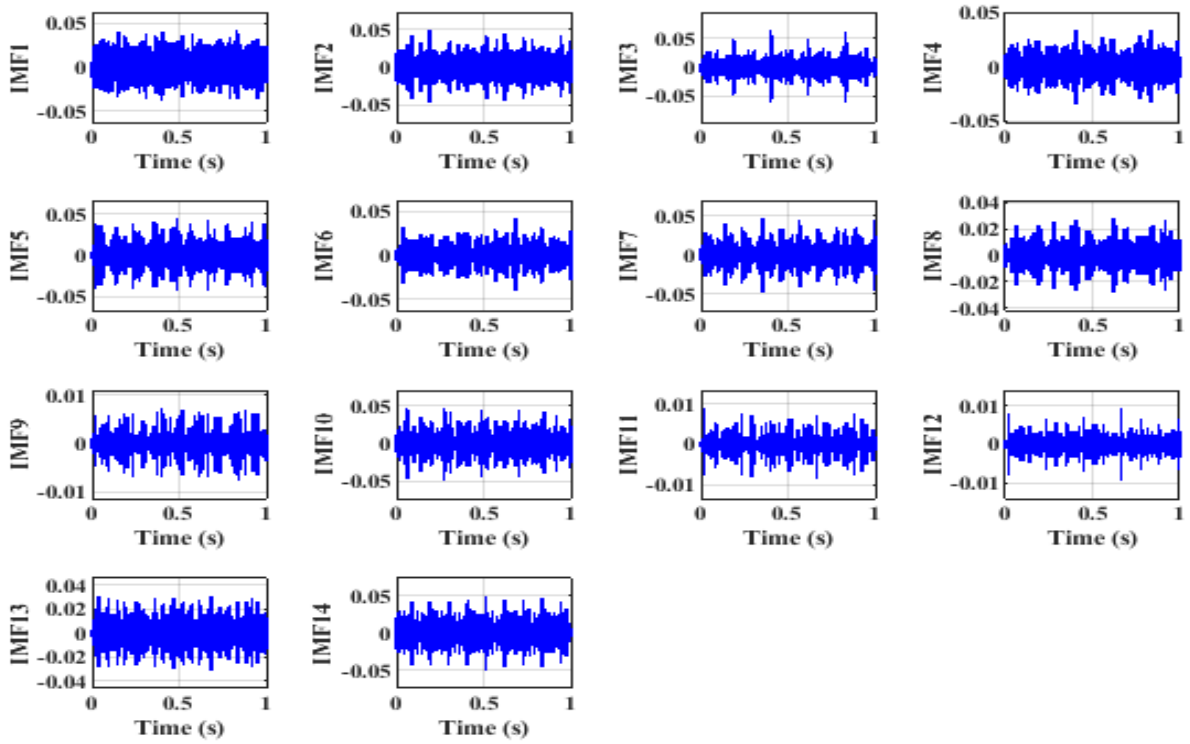

a.

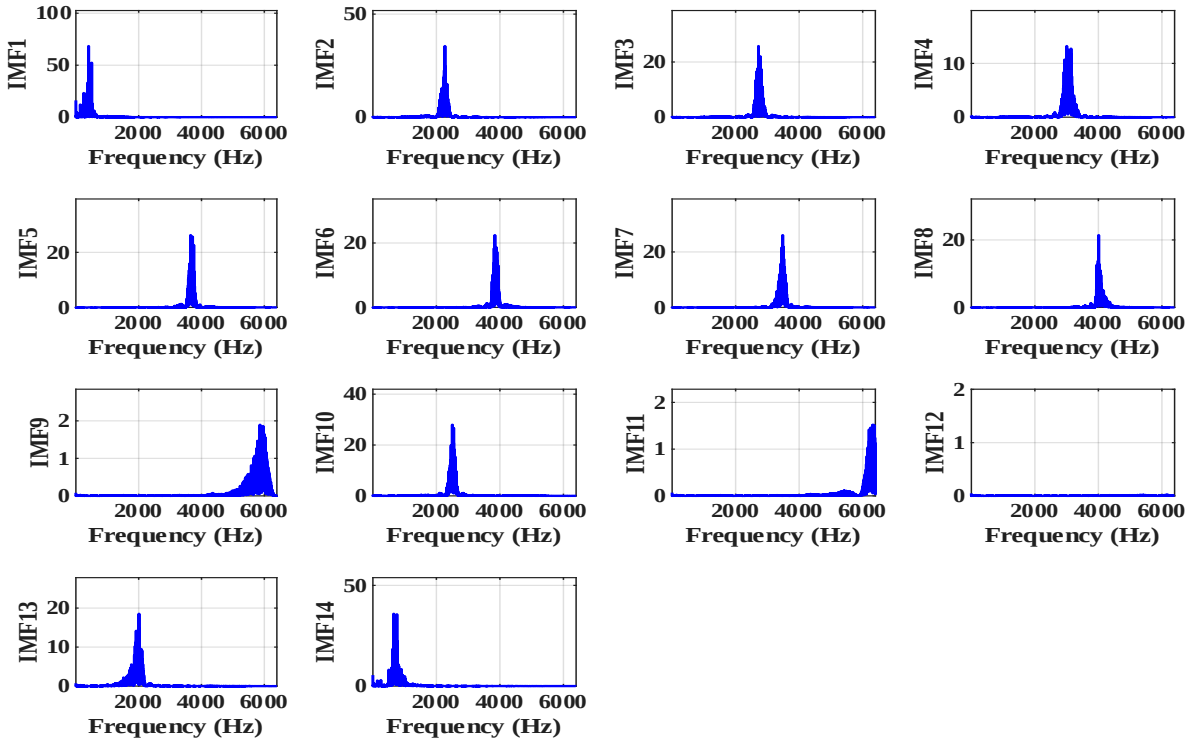

b.

Figure 2.9. The resulting IMFs by VMD for a defect of a half-extracted tooth: a. temporal representation, b. frequency representation.

Table 2.3, which presents scalar indicators for the 14 IMFs obtained by VMD, shows a non-uniform distribution of values. This variability in indicators does not provide clear distinctions regarding the relevance of the IMFs for fault diagnosis. Unlike EMD, where scalar indicators can help identify relevant IMFs for diagnosis, VMD produces indicator values that do not effectively differentiate informative IMFs from non-informative ones. Consequently, the scalar indicators from VMD do not provide sufficiently discriminative information to assess the relevance of the IMFs in the context of fault diagnosis. This observation highlights the need for additional approaches or alternative criteria to select the most relevant IMFs when using VMD.

Table 2.3. Scalar indicators of IMFs obtained by VMD: case of a half-extracted tooth.

IMFs	**Indicators**						
	Kurtosis	Peak to Peak	RMS	Crest Factor	Energie	Peak Value	K-Factor
IMF1	2,37	0,08	0,014	2,98	3,19	0,04	5,80E-04
IMF2	3,24	0,10	0,012	3,99	2,43	0,05	5,92E-04
IMF3	5,81	0,13	0,011	5,62	2,09	0,06	7,17E-04
IMF4	3,33	0,07	0,008	4,03	1,13	0,03	2,84E-04
IMF5	3,16	0,09	0,013	3,44	2,78	0,04	5,85E-04
IMF6	3,38	0,08	0,009	4,45	1,46	0,04	3,96E-04
IMF7	3,50	0,09	0,011	4,19	2,06	0,05	5,31E-04
IMF8	3,56	0,06	0,007	3,84	0,84	0,03	1,98E-04
IMF9	6,65	0,01	0,001	5,41	0,03	0,01	1,03E-05
IMF10	3,32	0,10	0,013	3,77	2,58	0,05	6,09E-04
IMF11	7,19	0,02	0,001	6,95	0,03	0,01	1,16E-05
IMF12	9,89	0,02	0,001	8,48	0,02	0,01	1,05E-05
IMF13	3,48	0,06	0,008	3,58	1,17	0,03	2,60E-04
IMF14	3,15	0,10	0,013	3,77	2,75	0,05	6,44E-04

The initial choice of 14 IMFs for VMD, although intended to provide a comprehensive comparison with EMD, revealed limitations in terms of the relevance of scalar indicators for diagnosis. Moreover, the 14 IMFs obtained by VMD included many redundant and non-informative components, complicating the analysis.

To optimize the efficiency of VMD, we propose reducing the number of IMFs to 3. This choice is based on the characteristics of VMD, which extracts IMFs within a band around a central frequency [88]. After a spectral investigation of the signal to be decomposed, as shown in Figure 2.10, we observe the presence of 3 relevant frequency zones.

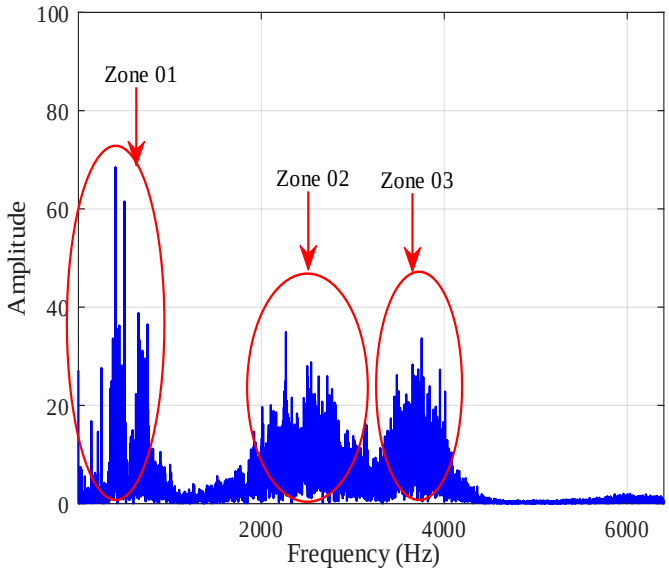

Figure 2.10. Signal spectrum with half a tooth extracted.

The 3 resulting IMFs from VMD for these 3 zones are presented in Figure 2.11. We can observe the effectiveness of VMD in isolating significant parts of the signal with an appropriate choice of the number of modes (highlighting zones with high energy levels). The inspection of the envelope spectra of the three IMFs revealed the presence of the rotational frequency F_{r1} and its harmonics $(2\times, 3\times, 4\times, ...)$, notably in IMF2, confirming the gear defect induced in the system. The presence of F_{r2} and its harmonics in IMFs 1 and 3 further indicates the existence of another defect within the system. This defect may have been introduced due to handling of the test bench during the assembly and disassembly of the faulty teeth.

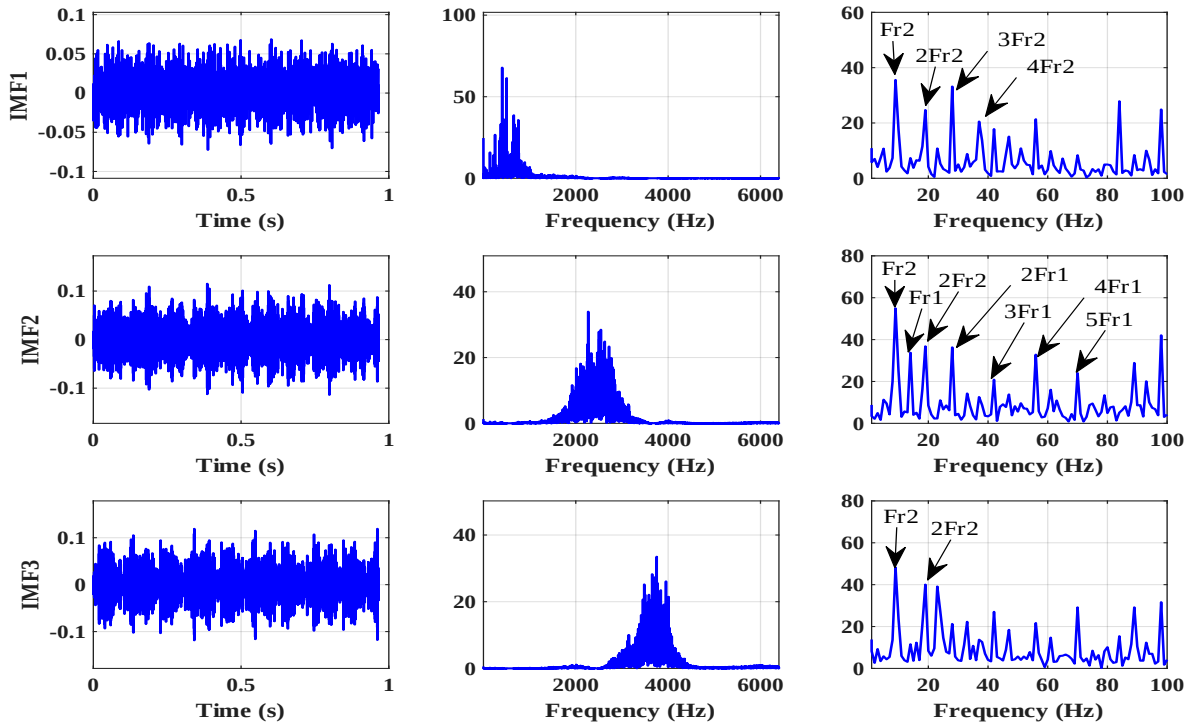

a. b. c.

Figure 2.11. The 3 IMFs chosen for the case of an extracted half tooth obtained by VMD: a. time representation, b. frequency representation, c. envelope spectra.

For the second case, where a tooth was fully extracted, we applied VMD by choosing to decompose the signal into 2 IMFs. This choice is motivated by the need to simplify the analysis while capturing the most relevant information for diagnosis. The results of this decomposition are presented in Figure 2.12. Inspection of the envelope spectra of the 2 IMFs obtained revealed the presence of the rotational frequency F_{r1} and its harmonics in the envelope spectra, clearly indicating the manifestation of the fault caused by the tooth extraction. This precise detection demonstrates the effectiveness of VMD in isolating and identifying significant signal components related to specific mechanical faults.

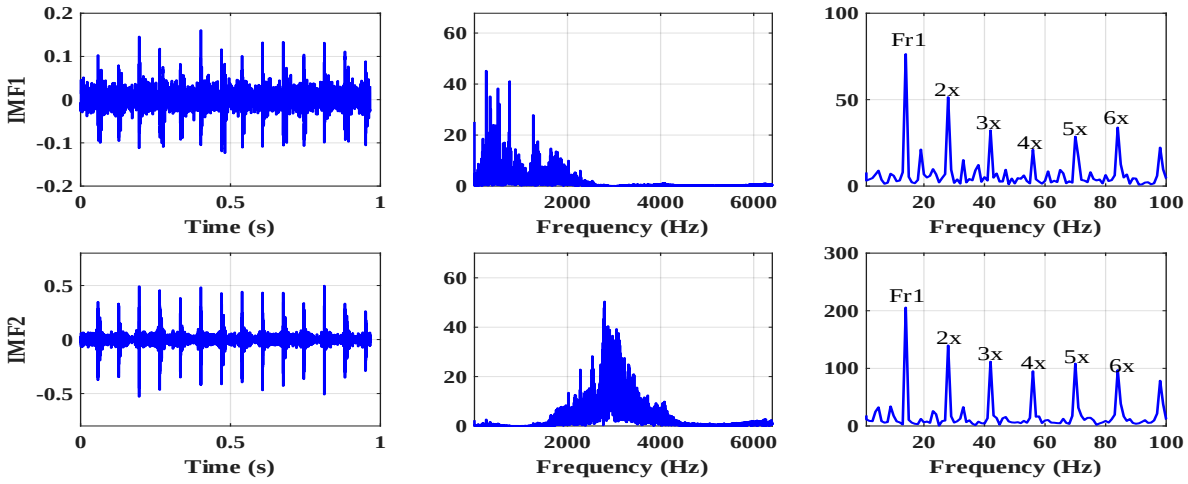

a. b. c.

Figure 2.12. The 2 IMFs chosen for the case of an extracted tooth obtained by VMD: a. temporal representation, b. frequency representation, c. envelope spectra.

The comparative analysis of the two cases demonstrates the superiority of VMD over EMD. For the first case, EMD produced 14 IMFs, of which only the first 4 were relevant for diagnosis. In contrast, VMD effectively identified faults with only 3 IMFs, showing a better ability to isolate significant signal components. For the second case, VMD, by decomposing the signal into only 2 IMFs, also successfully detected the fault, illustrating its efficiency and precision in fault identification. This comparison highlights that VMD offers better adaptability and superior diagnostic capability with a reduced number of modes, simplifying the analysis and making diagnosis more efficient.

The importance of selecting the number of IMFs in VMD is crucial for achieving an optimal and precise decomposition. A reliable criterion for determining this number is necessary to maximize the method's efficiency. This issue will be addressed in detail in the next chapter, where we will propose a criterion for optimal decomposition using VMD.

6. Conclusions

In conclusion, the comparative analysis between EMD and VMD in the context of gear fault diagnosis has revealed several key findings:

- VMD has proven to be more effective in isolating significant signal components with a reduced number of modes, offering better adaptability and precision in fault detection.
- However, the optimal selection of the number of modes for VMD remains a crucial challenge that requires careful consideration.
- While EMD generates a larger number of Intrinsic Mode Functions (IMFs), it has shown limitations in effectively separating signal components, especially when dealing with subtle faults.

This study highlights the importance of a judicious selection of the decomposition method based on the nature of the fault and the characteristics of the analyzed signal. It also paves the way for future research focused on optimizing VMD parameters to further enhance its effectiveness in the diagnosis of rotating machinery.

Chapter 03

Fault diagnosis by a new VMD-WMRA approach, optimized by a new criterion

In this chapter, we develop an innovative method for diagnosing mechanical faults in gearboxes by combining VMD with WMRA. We introduce an optimization criterion based on Shannon entropy to determine the optimal number of IMFs in the VMD, significantly improving analytical accuracy, even in the presence of noisy vibrational signals. This method is validated through numerical simulations and experimental tests, demonstrating its robustness and effectiveness in detecting and localizing gear faults in complex environments. The results show that our approach outperforms traditional techniques by providing a reliable and high-performing solution tailored to the industrial needs of vibrational diagnostics.

1. Introduction

Vibratory analysis plays a crucial role in preventing catastrophic machine failures, which can lead to unexpected downtime, production losses, and safety hazards. It also helps identify the root causes of defects, facilitating maintenance operations such as adjustments, troubleshooting, and repairs. Consequently, vibration monitoring has consistently attracted the interest of researchers due to its effectiveness in detecting anomalies.

However, despite significant advancements, determining the optimal number of modes in VMD remains a major challenge due to the complexity of existing methods. Moreover, analyzing the obtained IMFs is often complicated by noise or disturbances in the measured signals, particularly in the context of gearbox fault diagnosis.

In this chapter, we propose a novel approach that combines VMD with WMRA for diagnosing gearbox faults under noisy conditions. This method includes an innovative optimization criterion to effectively determine the number of modes in VMD, providing a robust solution suited to complex industrial environments.

2. Mathematical formulation

The purpose of this section is to provide an overview of the Shannon Entropy (SE) theory and the fundamentals of WMRA to help readers better understand the background and functioning of these techniques. It is important to note that the fundamentals of VMD were already discussed in the previous chapter.

2.1 Wavelet multi-resolution analysis WMRA

WMRA is a highly effective signal processing method that has gained popularity in recent years. It involves the use of the Wavelet Transform, a mathematical technique for representing a signal *S(t)* using functions derived from scaling and translating a basic function known as the mother wavelet $\psi(t)$ [14]. The wavelet family is characterized as follows [125]:

$$\psi_{a,b}(t) = \frac{1}{\sqrt{a}}\psi\left(\frac{t-b}{a}\right) \tag{3.1}$$

where a and b are the scaling and translation parameters, respectively.

Since ψ^* is the conjugate of ψ, the Continuous Wavelet Transform (CWT) of the function *S(t)* is defined as [125]:

$$CWT(a,b) = \frac{1}{\sqrt{a}}\int_{-\infty}^{+\infty} S(t) * \psi^*\left(\frac{t-b}{a}\right)dt \tag{3.2}$$

Replacing *a* with 2^m and *b* with $n2^m$, where *n* and *m* are integers, we obtain the Discrete Wavelet Transform (DWT) [125]:

$$DWT(m,n) = 2^{-\frac{m}{n}} \int_{-\infty}^{+\infty} S(t) * \psi^* \left(2^{-m} t - n\right) dt \tag{3.3}$$

The DWT involves a cascade decomposition as proposed by [126], using low-pass and high-pass filters to separate the signal, yielding two sets of coefficients:

- Approximation coefficients cA_j for low-frequency components.

These vectors undergo down-sampling during the decomposition process and are subsequently reconstructed through additional filters to obtain the approximations A_j and details D_j. The sub-signals can be reconstructed using the following model [126]:

$$\begin{aligned} A_{j-1} &= A_j + D_j \\ S &= A_j + \sum_{i \le j}^{n} D_j \end{aligned} \tag{3.4}$$

An Optimized WMRA (OWMRA) was proposed by [55] specifically designed for shock signal analysis. This optimized version involves selecting different parameters to determine the appropriate number of levels for gear fault analysis, using kurtosis as the optimization criterion. The number of levels is expressed as [55]:

$$n \le 1.44 \log\left(\frac{F_{\max}(S)}{F_c}\right) \tag{3.5}$$

where F_{max} is the maximum frequency of the signal *S(t)* and F_c is the shock frequency.

In this study, the WMRA was performed using the Daubechies 5 (db5) wavelet. This choice was motivated by the db5 wavelet's proven effectiveness in vibration signal analysis, particularly for fault detection in rotating machinery [5].

2.2 Shannon entropy

Shannon Entropy (SE) measures the uncertainty or randomness of a probability distribution. It is calculated as follows [127]:

$$SE(n) = -\sum_{i=1}^{N} p(n_i) \log_2 \left(p(n_i)\right) \tag{3.6}$$

where $p(n_i)$ represents the probability of obtaining the value n_i.

In fault detection of transmission systems, SE quantifies the uncertainty and information content of the vibration signal produced by a gearbox. It helps identify gearbox failures by evaluating the degree of randomness in the gear signals [111].

Consequently, SE serves as a practical criterion for analyzing and measuring the similarity between vibration signals [128]. In our case, the similarity between IMFs of a signal is based on changes in the frequency spectrum of the vibration signal.

3. Proposed approach

As previously mentioned, our approach aims to detect gear faults from highly noisy signals. To improve diagnostic results, we propose a new criterion based on the normalized variation of SE between two successive IMFs to determine the optimal number of IMFs required for VMD-based signal decomposition. Subsequently, WMRA is used to demodulate the obtained IMFs, enhancing fault detection.

The detailed methodology of the proposed procedure, illustrated in the flowchart of Figure 3.1, is as follows:

- Measure the vibration signals and calculate their SE.
- Initialize VMD decomposition parameters, such as the initial number of IMFs *k0*, which should be high for gear fault detection (typically between 20 and 30). Other parameters, such as the bandwidth constraint α and tolerance, are selected based on studies from [3] and [89].
- Iterate the VMD process, where *j* ranges from *2* to k_0, incrementing by *1*. For each iteration, calculate SE for each IMF, denoted as SE_{IMF}. This indicator is then normalized relative to the overall SE to obtain NSE_{IMF} using the following formula:

$$NSE_{IMF} = \frac{SE_{IMF}}{SE} \tag{3.7}$$

- Check the stopping criterion after each iteration by calculating the difference between two consecutive NSE_{IMF} values: $\Delta_{NSE} = NSE_{IMF_{(j)}} - NSE_{IMF_{(j-1)}}$. If Δ_{NSE} is less than 1%, it indicates that the similarity between the two IMFs exceeds 99%, and the iteration stops.
- Determine the optimal number of IMFs by selecting the last iteration before reaching the similarity threshold. This avoids the over-segmentation phenomenon, where two IMFs carry redundant information [3]. The signals are then decomposed again using this new *k* value to obtain optimal IMFs suitable for fault detection.
- Finally, the selected IMFs are processed through WMRA to identify demodulation frequencies (bearing resonance frequencies, gear meshing frequencies, belt resonance frequencies, etc.) that help explain the nature of the fault.

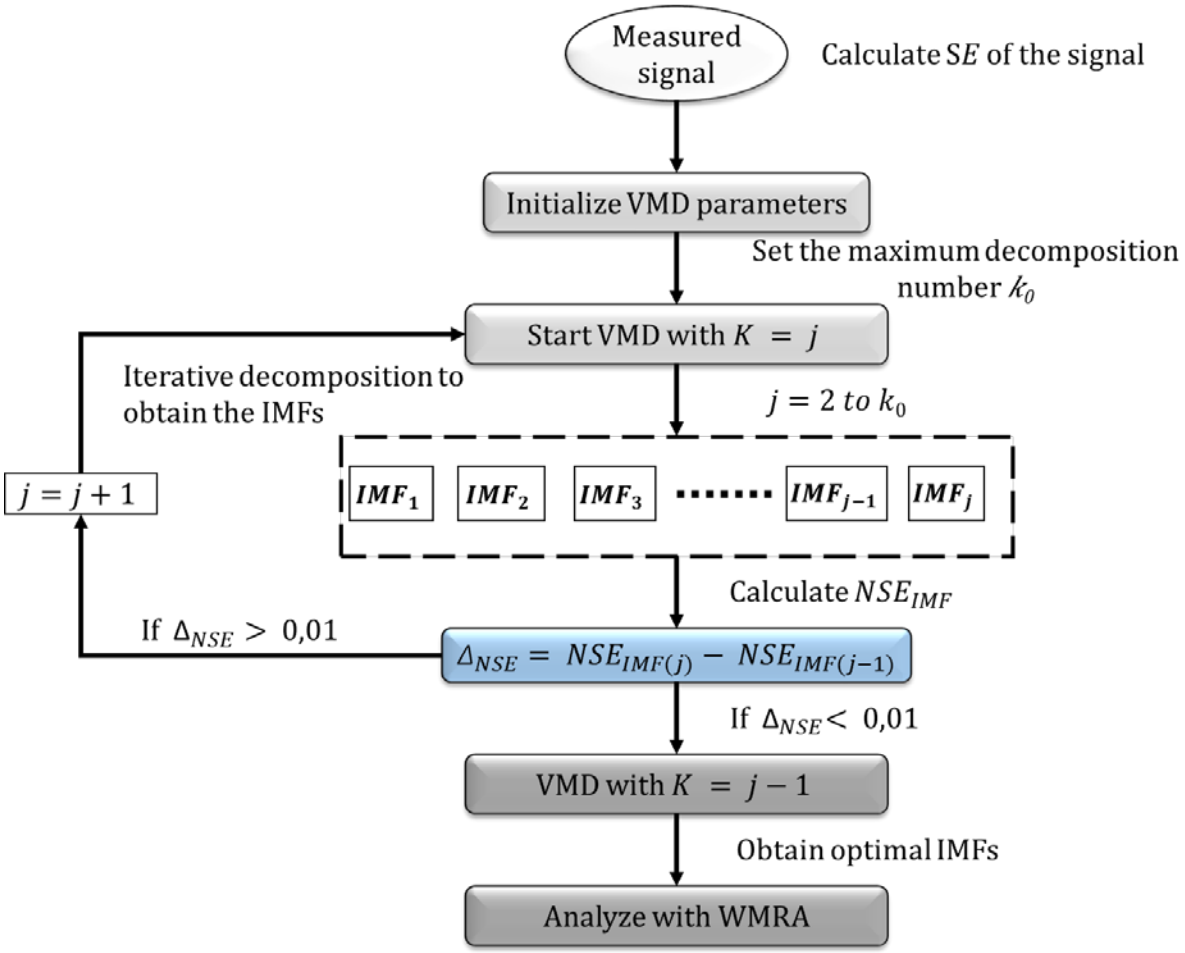

Figure 3.1. The flowchart of the proposed approach for fault detection.

4. Numerical simulation

4.1 Determining the number of IMFs in a sinusoidal signal

To verify the effectiveness of the proposed criterion for determining the number of IMFs in the decomposition using the VMD method, we conducted tests on a simulated signal $X(t)$, composed of the sum of three distinct sinusoidal signals $X1(t), X2(t)$ and $X3(t)$, given by the expressions (3.8) [129]:

$$\begin{aligned} X(t) &= X1(t) + X2(t) + X3(t) \\ X1(t) &= 3\sin(2\pi 5t) \\ X2(t) &= 0.4\sin(2\pi 200t) \\ X3(t) &= 1.2\sin(2\pi 50t) \end{aligned} \tag{3.8}$$

Figures 3.2 and 3.3 illustrate these three signals and the overall signal, respectively. In this application example, we have prior knowledge of the exact number of IMFs contained in the signal $X(t)$, which is three.

The objective is to confirm the effectiveness of the proposed criterion for selecting the optimal number of IMFs during decomposition. Each of the obtained IMFs should represent a distinct component of the signal we constructed. By validating the effectiveness of this criterion in accurately extracting the different components of the original signal, we can subsequently use it for the decomposition of simulated and measured gear signals.

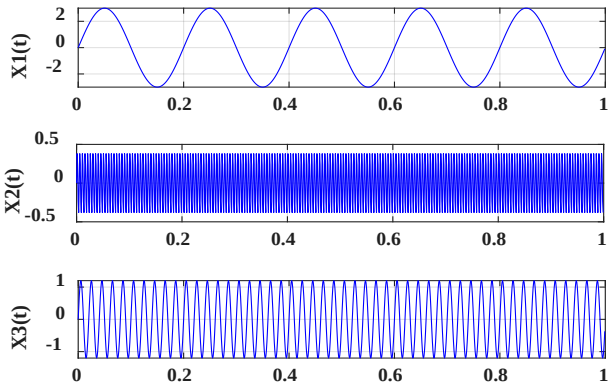

Figure 3.2. Three simulated sinusoidal signals.

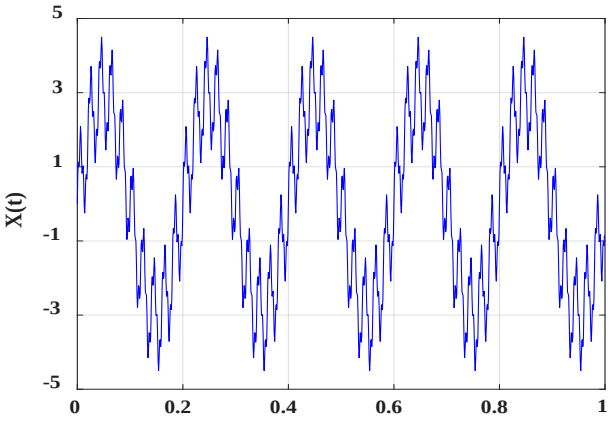

Figure 3.3. The signal obtained from the sum of the three simulated signals.

The decomposition of the signal $X(t)$ using the proposed approach, following the flowchart in Figure 3.1, yields the value of the proposed criterion Δ_{NSE} after each iteration. These values are presented in Table 3.1 and Figure 3.4. We observe that for Δ_{NSE} less than 0.01, the selected number of IMFs is *K=3*.

Table 3.1. Value of the criterion Δ_{NSE} and the number of corresponding IMFs.

Δ_{NSE}	*0,7159*	*0,0136*	*0,0099*	*0,0043*	*0,0056*	*0*	*0,0025*	*0.0051*	*0.003*
Number of IMFs *K*	*2*	*3*	*4*	*5*	*6*	*7*	*8*	*9*	*10*

The decomposition of the signal X(t) using VMD with the optimal number of IMFs, determined by the proposed criterion, is illustrated in Figure 3.5. We observe that the IMFs obtained from this decomposition highlight the three components of the original signal, confirming the effectiveness of the proposed criterion in determining the optimal number of IMFs.

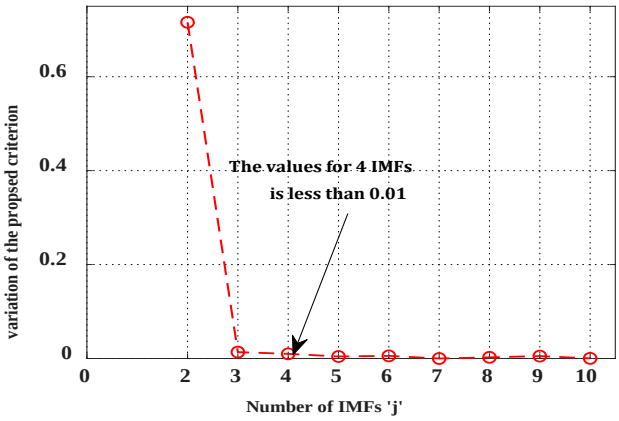

Figure 3.4. Variation of the proposed criterion Δ_{NSE} for the signal $X(t)$.

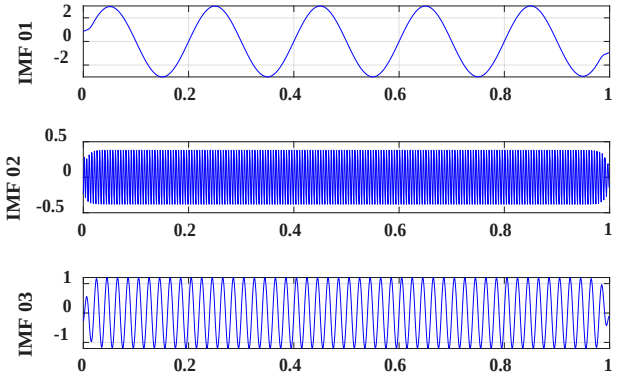

Figure 3.5. The resulting IMFs from VMD for *K = 3*.

To further strengthen the validation of our criterion, we present the IMFs obtained from the VMD decomposition for *K=2* and *K=4* in Figures 3.6(a) and 3.6(b), respectively. In Figure 3.6(a), we can clearly observe mode mixing and its influence on IMF1. This indicates a case of under-segmentation, where two combined IMFs are insufficient to capture all the characteristics of the original signal. In Figure 3.6(b), we notice shared information between IMF2 and IMF4. This represents a case of over-segmentation, where an excessive number of IMFs are generated, and some of them may contain redundant or similar information. These observations are mentioned in reference [3]. By examining the results of these two cases, we can confirm the performance of our criterion for achieving a precise and complete signal decomposition.

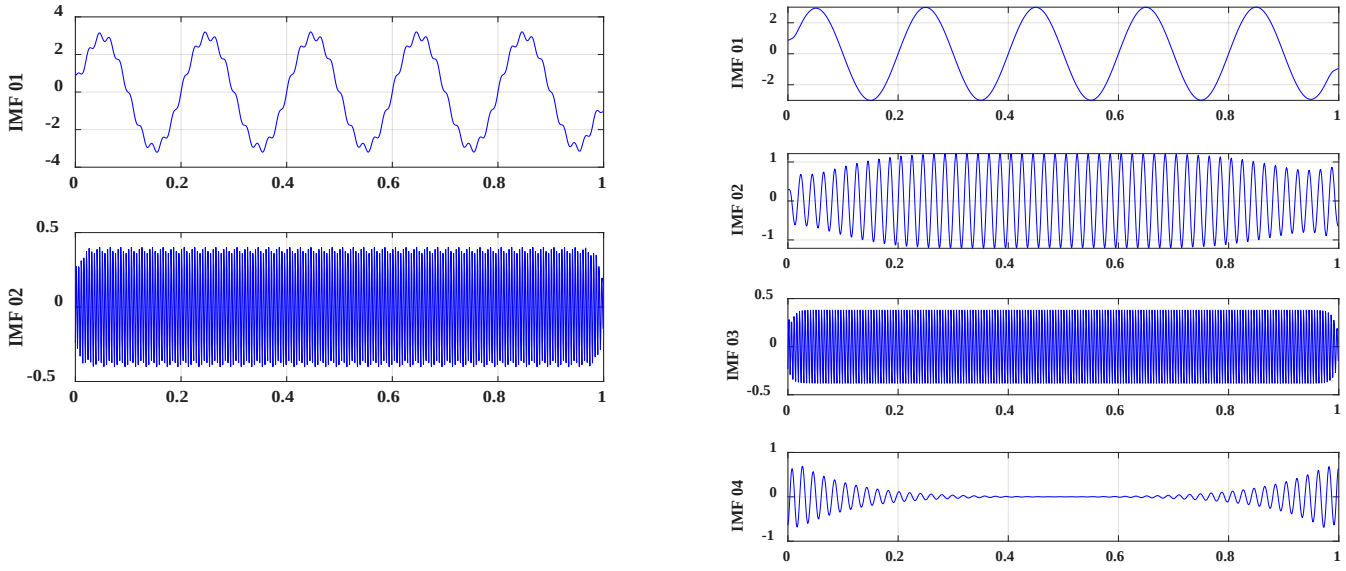

a. b.

Figure 3.6. Resulted IMFs from VMD: a. for *K = 2*, b. for *K = 4*.

4.2 Numerical simulation of gear faults

Gear faults manifest in both vibration spectra and envelope spectra at the rotational frequencies of the shafts on which the gears are mounted. The amplitudes of these rotational frequencies are amplified at the gear meshing frequencies and their harmonics for each gear pair. For this reason, it is advisable to select these resonance frequencies and conduct detailed analyses around them. The combined VMD-WMRA approach, based on the proposed criterion, can be used with high efficiency for diagnosing this type of fault.

In this section, we simulate a gear fault signal $S_{en}(t)$, based on the mathematical model provided by [130]. The gearbox shown in Figure 3.7 consists of three shafts rotating at frequencies of *15 Hz, 12 Hz,* and *17 Hz*, respectively. The gear mounted on the first shaft has $Z_1 = 42$ teeth, while the gears mounted on the second shaft have $Z_2 = 50$ and $Z_3 = 65$ teeth, and the gear on the third shaft has $Z_4 = 45$ teeth. The following expression (3.9) is used to generate the signal $S_{en}(t)$ for studying gear faults. Processing this signal with the proposed approach allows us to identify gear faults in this gearbox.

$$S_{en}(t) = \left(\sum_{n=-\infty}^{+\infty} S_e(t - n \times \tau_e)\right) * \begin{pmatrix} 1 + \sum_{m=-\infty}^{+\infty} S_{r1}(t - m \times \tau_{r1}) + \\ \sum_{p=-\infty}^{+\infty} S_{r2}(t - p \times \tau_{r2}) \end{pmatrix} + n(t) \qquad (3.9)$$

Where: $S_e(t)$ is the response signal of gear meshing.

τ_e is the meshing period, calculated as: $\tau_e = 1/F_m$.

τ_{r1} , τ_{r2} are the rotation periods of the defective gears, defined as:

$\tau_{r1} = 1/F_{r1}$, $\tau_{r2} = 1/F_{r2}$.

n(t) is a white Gaussian noise added to simulate real-world conditions.

$F_{m1} = F_{r1} \times Z_1 = F_{r2} \times Z_2 = 588Hz$ and $F_{m2} = F_{r2} \times Z_3 = F_{r3} \times Z_4 = 760Hz$ are the first and second meshing frequencies.

Gear defects were simulated on Gear Z_2 of the intermediate shaft and Gear Z_4 of the output shaft of the gearbox.

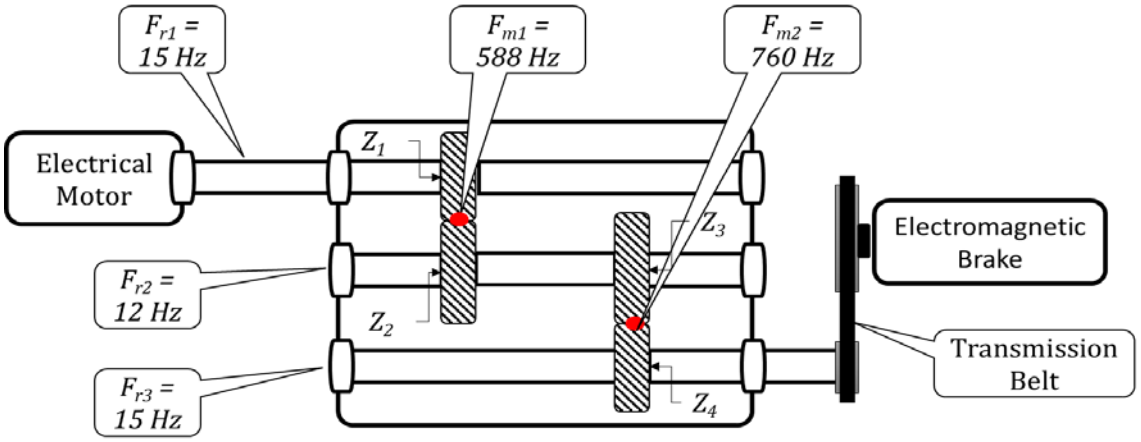

Figure 3.7. Gearbox configuration: schematic representation.

In Figures 3.8, we present the simulated signal of the two gear faults and its spectrum, respectively. The spectrum clearly shows the appearance of the two meshing frequencies (F_{m1} and F_{m2}) and their harmonics. A simple zoom around the meshing frequencies reveals that they are modulated by the rotational frequencies F_{r2} and F_{r3}, corresponding to the faults on gears Z_2 and Z_4, respectively. Thus, the simulated signal accurately reflects the different frequency characteristics of the gearbox with good precision.

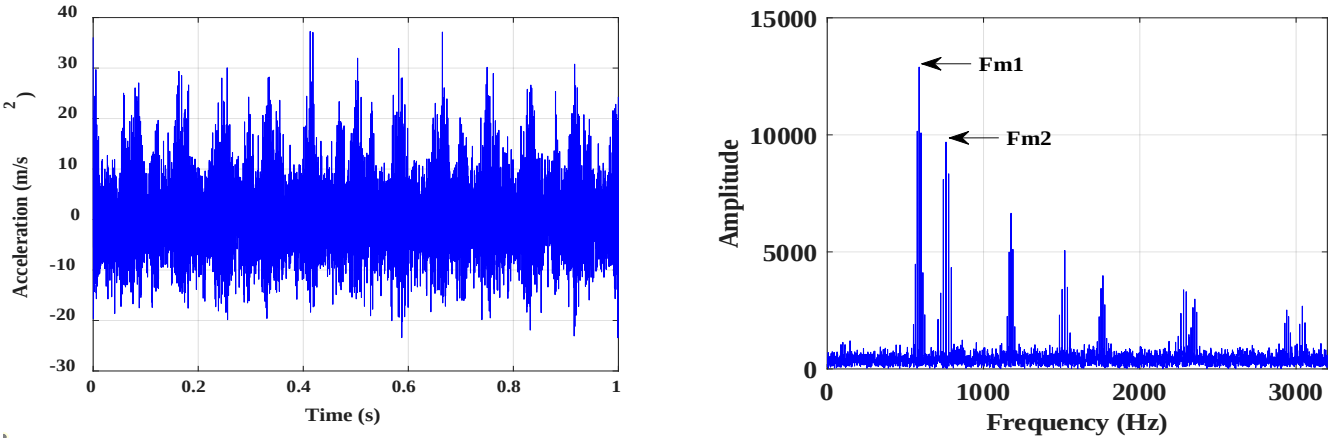

Figure 3.8. Simulated signal $S_{en}(t)$ of the combined gear fault in the time and frequency domains.

The decomposition of the signal simulating the gear faults using the VMD method, based on the proposed criterion, yields 4 IMFs, as shown in Figure 3.9. In Figure 3.10, we present the signals and spectra of the four IMFs. We observe a highly effective isolation of the meshing frequencies and some of their harmonics, enabling a more precise diagnosis of potential failures in the gearbox.

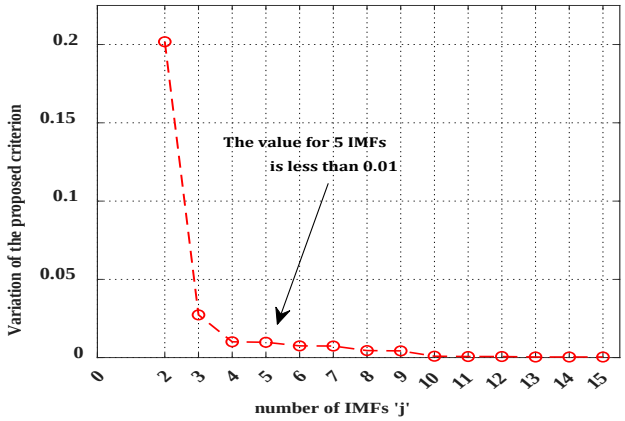

Figure 3.9. Variation of the Δ_{NSE} for $S_{en}(t)$.

The main advantage of the proposed criterion is to minimize the number of IMFs likely to contain information about potential faults. As a result, the combination of the two signal processing methods, VMD and WMRA, becomes simpler and more effective.

In the case of simulated signals or measured signals with minimal noise, VMD alone can provide a correct diagnosis. However, for highly noisy signals, VMD must be combined with WMRA for superior diagnostic efficiency

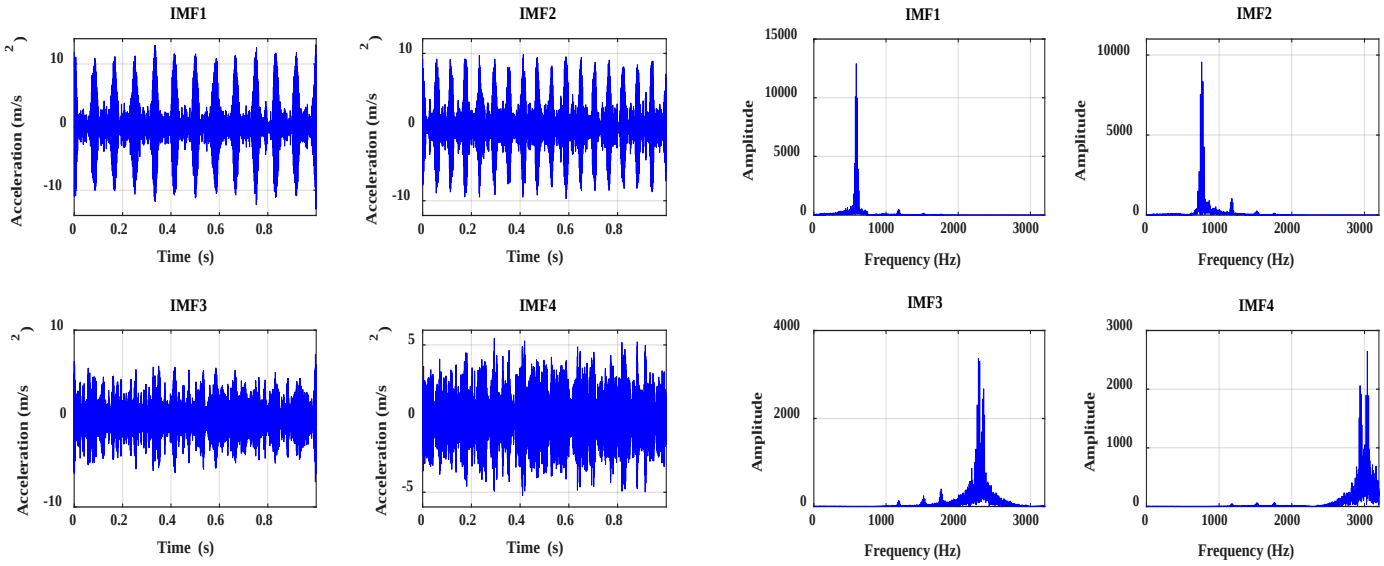

Figure 3.10. IMFs obtained from VMD of simulated signal $S_{en}(t)$ in the time (left) and frequency (right) domains.

Applying WMRA to each of the four IMFs in Figure 3.10 allows us to obtain the envelope spectra of each, as shown in Figure 3.11. It is clear that IMF1, which covers the first meshing frequency $F_{m1} = 588Hz$, has an envelope spectrum showing the modulation of F_{m1} by the

rotational frequency of the intermediate shaft $F_{r2} = 12Hz$, on which we simulated the fault (Figure 3.11(a)).

Meanwhile, IMF2, which covers the second meshing frequency $F_{m2} = 760Hz$, has an envelope spectrum showing the modulation of F_{m2} by the rotational frequency of the output shaft $F_{r3} = 17Hz$ (Figure 3.11(b)). IMFs 3 and 4, which cover the combinations of $3F_{m2}$ plus $4F_{m1}$ and $4F_{m2}$ plus $5F_{m1}$, respectively, have envelope spectra that reveal the combination of the two fault frequencies F_{r2} and F_{r3}.

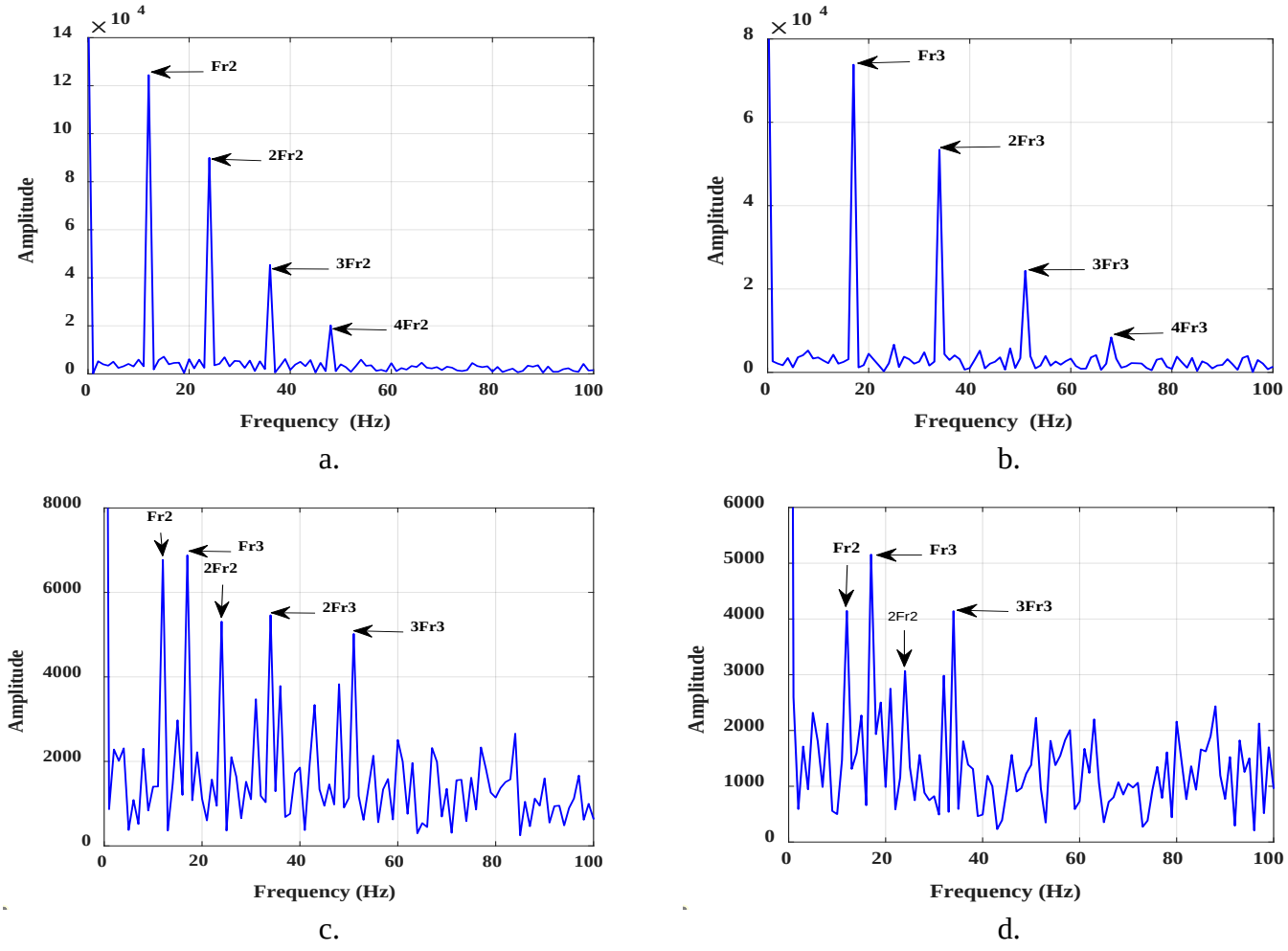

Figure 3.11. Envelope spectra obtained from WMRA for each IMF: a. IMF 01, b. IMF 02, c. IMF 03 and d. IMF 04

5. Experimental Study

The vibration signals analyzed in this section were measured on a test bench designed and built at the Laboratory of Mechanics and Structures of the University of Guelma, Algeria, as shown in Figure 3.12(a). The experimental setup consists of the following components:

- Electric motor with a power of 2.2 kW and a rotational speed of 1500 rpm.

- Elastic coupling to transmit motion between the motor and the gearbox.
- Gearbox, with its mechanical characteristics detailed in Table 3.2.
- Electromagnetic brake used to apply varying loads on the gearbox.
- V-ribbed belt for power transmission between the output shaft and the electromagnetic brake.

Vibration signals were experimentally measured at two rotational frequencies: *14 Hz* and *23 Hz*, under both healthy and faulty gear conditions. Data acquisition was performed using the Bruel & Kjær PULSE 16.1 analyzer and the Pulse LabShop software, as shown in Figure 3.12(a).

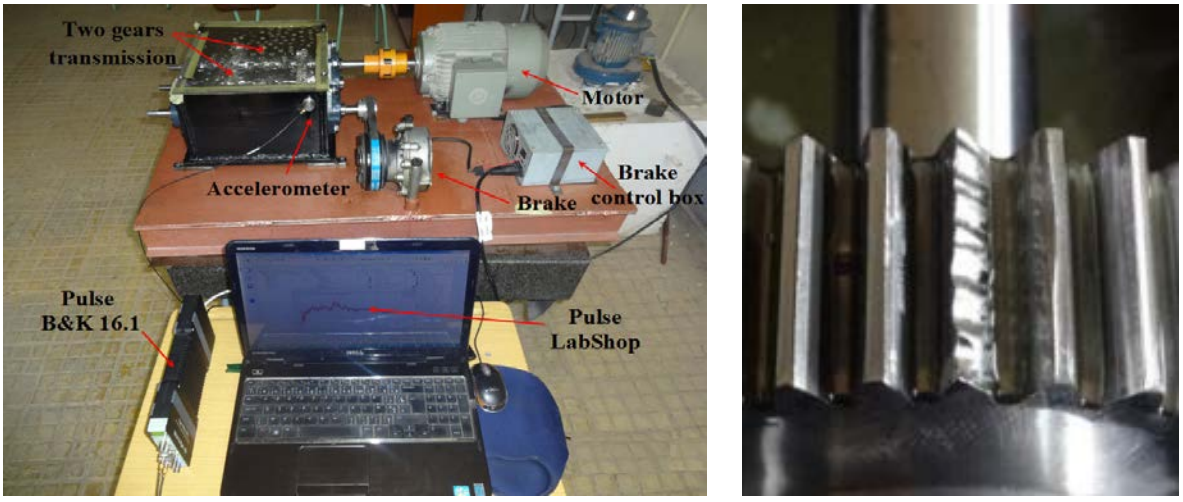

a. b.

Figure 3.12. The experimental setup: a. test rig and b. defected gear.

To validate the results from the numerical simulations presented in Section 4, the experimental setup was designed to replicate the same mechanical components of the previously simulated gearbox. Table 3.2 provides the mechanical characteristics of the gears, including: transmission ratios for each gear stage (U_1 and U_2), rotational frequencies of the three shafts (F_{r1}, F_{r2} and F_{r3}), and gear meshing frequencies (F_{m1} and F_{m2}) for two motor speeds.

Table 3.2. Used gears and characteristic frequencies.

<table>
<tr><td>Gear type</td><td colspan="3">Straight teeth</td></tr>
<tr><td rowspan="3">Gear characteristics</td><td>Transmission ratios</td><td colspan="2">$U1 = 42/50 = 0.84$
$U2 = 65/45 = 1.444$</td></tr>
<tr><td rowspan="2">Rotation Frequencies</td><td>First case:</td><td>$F_{r1} = 14$ Hz
$F_{r2} = 12$ Hz
$F_{r3} = 17$ Hz</td></tr>
<tr><td>Second case:</td><td>$F_{r1} = 23$ Hz
$F_{r2} = 20$ Hz
$F_{r3} = 28$ Hz</td></tr>
<tr><td rowspan="2">Meshing frequency</td><td>First case:</td><td colspan="2">$F_{m1} = 588\ Hz$
$F_{m2} = 761\ Hz$</td></tr>
<tr><td>Second case:</td><td colspan="2">$F_{m1} = 966\ Hz$
$F_{m2} = 1300\ Hz$</td></tr>
</table>

Three Bruel & Kjær Type 4533-B accelerometers were mounted horizontally on the gearbox casing, positioned near each gear stage. A total of four vibration signals were recorded within a frequency bandwidth of 6400 Hz: *S1* and *S2*: signals without gear faults, and *S3* and *S4*: signals with gear faults. These signals illustrated in Figure 3.13, will be processed using the proposed diagnostic method.

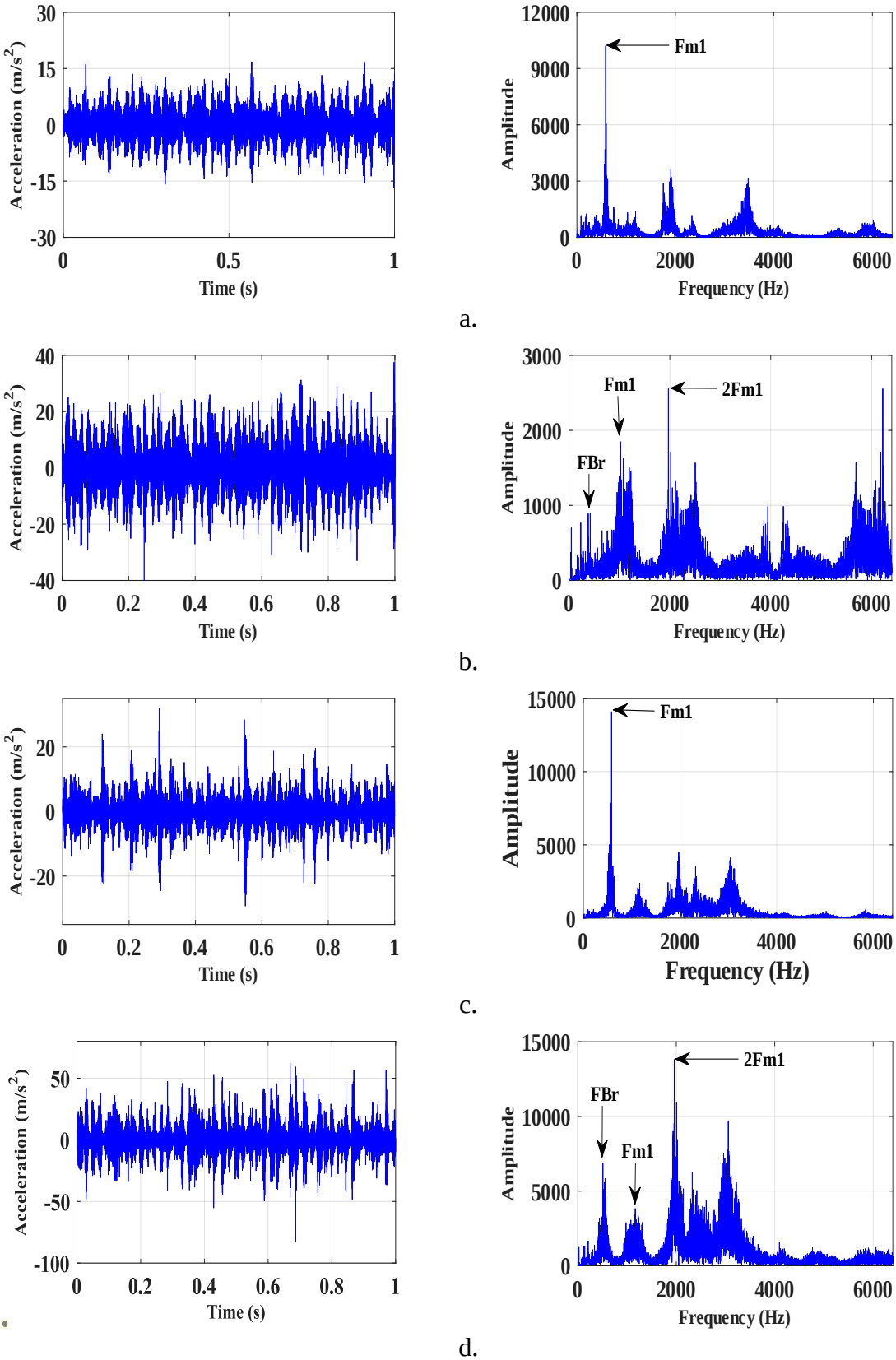

Figure 3.13. Vibratory signals measured for different cases and their spectra:
a. *S1* without gear defect and $F_{r1} = 14Hz$, b. *S2* without gear defect and $F_{r1} = 23Hz$,
c. *S3* with gear defect and $F_{r1} = 14Hz$, d. *S4* with gear defect and $F_{r1} = 23Hz$.

To achieve precise fault diagnosis, an analysis of scalar indicators was performed. In this study, six scalar indicators were calculated and are presented in Table 3.3, some of which are energy-sensitive indicators: Peak Value (PV), Root Mean Square (RMS), Energy (E), Power (P), while others are shape-sensitive indicators: Kurtosis (K), Crest Factor (CF).

Upon examining these indicators, it is evident that the signals exhibit not only the experimentally simulated gear faults but also additional anomalies. Moreover, the signals are heavily contaminated with noise, complicating fault detection. For example, in signal *S1*, the kurtosis value reaches 5.08, while under normal conditions without impulsive defects, this value should not exceed 3. The high noise levels present in the signals pose significant challenges for fault detection, highlighting the need for an effective diagnostic method. These observations underscore the importance of implementing a robust diagnostic approach capable of identifying faults despite substantial signal noise. An in-depth analysis based on the proposed VMD-WMRA approach will be essential for accurate fault detection in the studied gearbox.

Table 3.3. Scalar indicators' value.

		RMS	**CF**	**PV**	**E*10^3**	**K**	**P**
Without gear defect	***S1***	5.56	5.96	33.10	506.22	5.08	30.90
	S2	3.77	4.38	16.90	116.29	3.76	14.19
With gear defect	***S3***	4.80	6.55	33.60	378.84	6.12	23.12
	S4	10.04	6.20	82.10	165.07	6.05	100.75

6. Results and discussions

This section is dedicated to the experimental validation of the proposed approach for detecting faults in gearboxes. As previously mentioned, the vibration signals (*S1, S2, S3,* and *S4*) were measured under two operational conditions: without gear faults (*S1* and *S2*) and with gear faults (*S3* and *S4*). These measurements were conducted at two different rotational speeds, $F_{r1}=14\ Hz$ and $F_{r1}=23\ Hz$.

The work involves first processing the four signals using WMRA. The results obtained will be compared with those from the proposed approach applied in numerical simulations, i.e., determining the optimal number of IMFs based on the proposed criterion, followed by decomposing the same signals using VMD and finally processing each IMF using WMRA.

6.1. Signal processing without gear fault

The signals *S1* and *S2*, along with their corresponding spectra, are presented in Figure 3.14. These signals, which correspond to the gearbox without gear faults, exhibit abnormal values of scalar indicators, suggesting the presence of another type of fault.

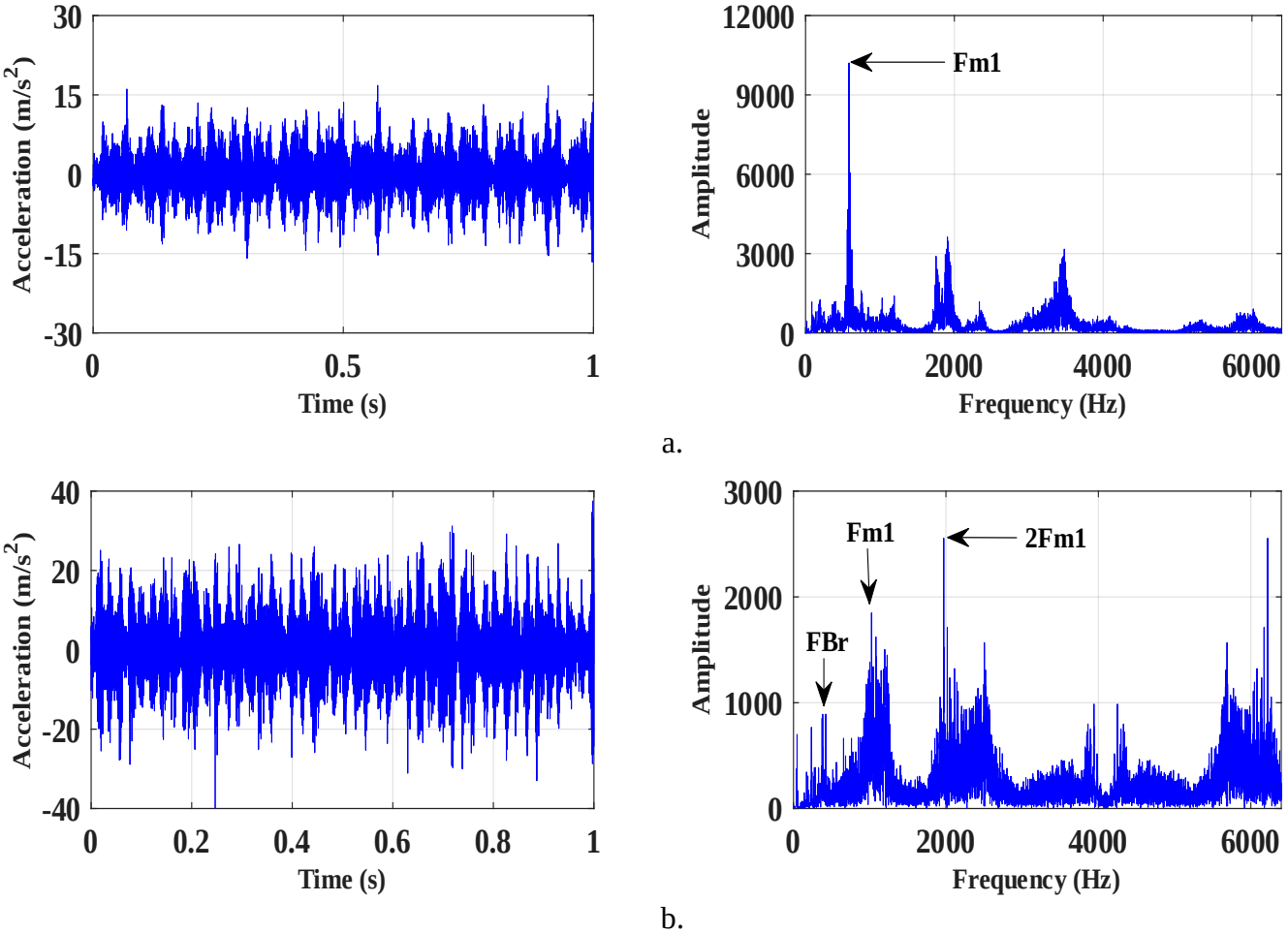

Figure 3.14. Signals without gear defects and their corresponding spectra:
a. *S1* with $F_{r1} = 14$ *Hz*, b. *S2* with $F_{r1} = 23$ *Hz*.

For *S1*, shown in Figure 3.14(a), the spectral analysis reveals a dominance of the meshing frequency F_{m1}, which overshadows the other frequencies, making diagnosis difficult and necessitating the use of more advanced signal processing methods. On the other hand, for *S2*, shown in Figure 3.14(b), we can clearly observe noise in the signal. The corresponding spectrum shows the appearance of F_{m1} and its harmonic $2F_{m1}$, where the amplitude of $2F_{m1}$ is approximately 1.5 times greater than that of F_{m1}, indicating insufficient backlash (insufficient tooth root clearance).

6.1.1. Results obtained by WMRA.

Processing the two signals *S1* and *S2* using WMRA for both rotational speeds yield the envelope spectra shown in Figure 3.15. We observe that the amplitudes of the harmonics of the input shaft rotational frequency $2F_{r1}$, $3F_{r1}$ and $4F_{r4}$ are higher than that of the fundamental frequency F_{r1}, indicating misalignment of the input shaft. The misalignment is more pronounced, especially at the rotational frequency of *14 Hz*, as shown in Figure 3.15(a). The vibration amplitude at this frequency is twice that observed at *23 Hz*, as shown in Figure 3.15(b). This result is confirmed by the doctoral work of J. Bouyer [131], which shows that the amplitude of misalignment increases with the intensity of the misalignment torque, particularly when the load or rotational speed is low.

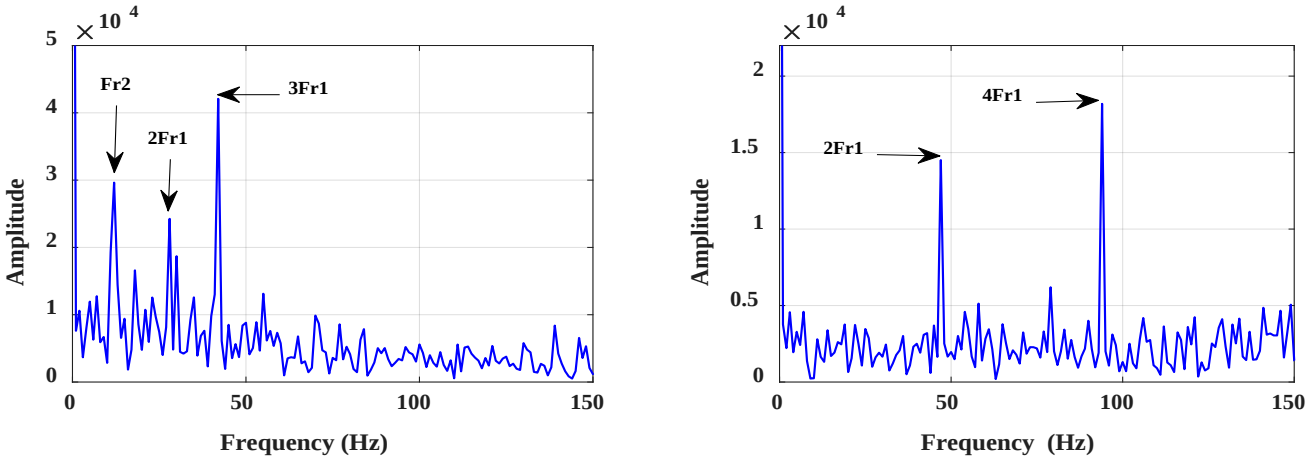

a. b.

Figure 3.15. Envelope spectra obtained from WMRA:
a. *S1* with F_{r1} = *14 Hz*, b. *S2* with F_{r1} = *23 Hz*.

6.1.2. Results obtained by VMD-WMRA combination

Decomposing the same signals using VMD, based on the proposed criterion, yields the signals and spectra of the different IMFs, as shown in Figure 3.16. For *S1* (Figure 3.16(a)), we observe that the spectra of the obtained IMFs perfectly isolate the meshing frequency F_{m1} (IMF1) and some of its harmonics (IMFs 2, 3, and 4). Similarly, for *S2* (Figure 3.16(b)), we observe the isolation of the meshing frequency F_{m1} (IMF2) and its fifth harmonic (IMF3). Additionally, IMF1 isolates a resonance at *422 Hz*, with an amplitude lower than that of F_{m1}.

After investigating this resonance and based on the calculations below, we conclude that this resonance represents the natural frequency of the belt F_{Br} . The values of F_{Br} for the two rotational speeds are presented in Table 3.4. The absence of F_{Br} in *S1* is due to its proximity in value to Fm1Fm1, which has a high amplitude, causing F_{m1} to overshadow F_{Br} , unlike in *S2*.

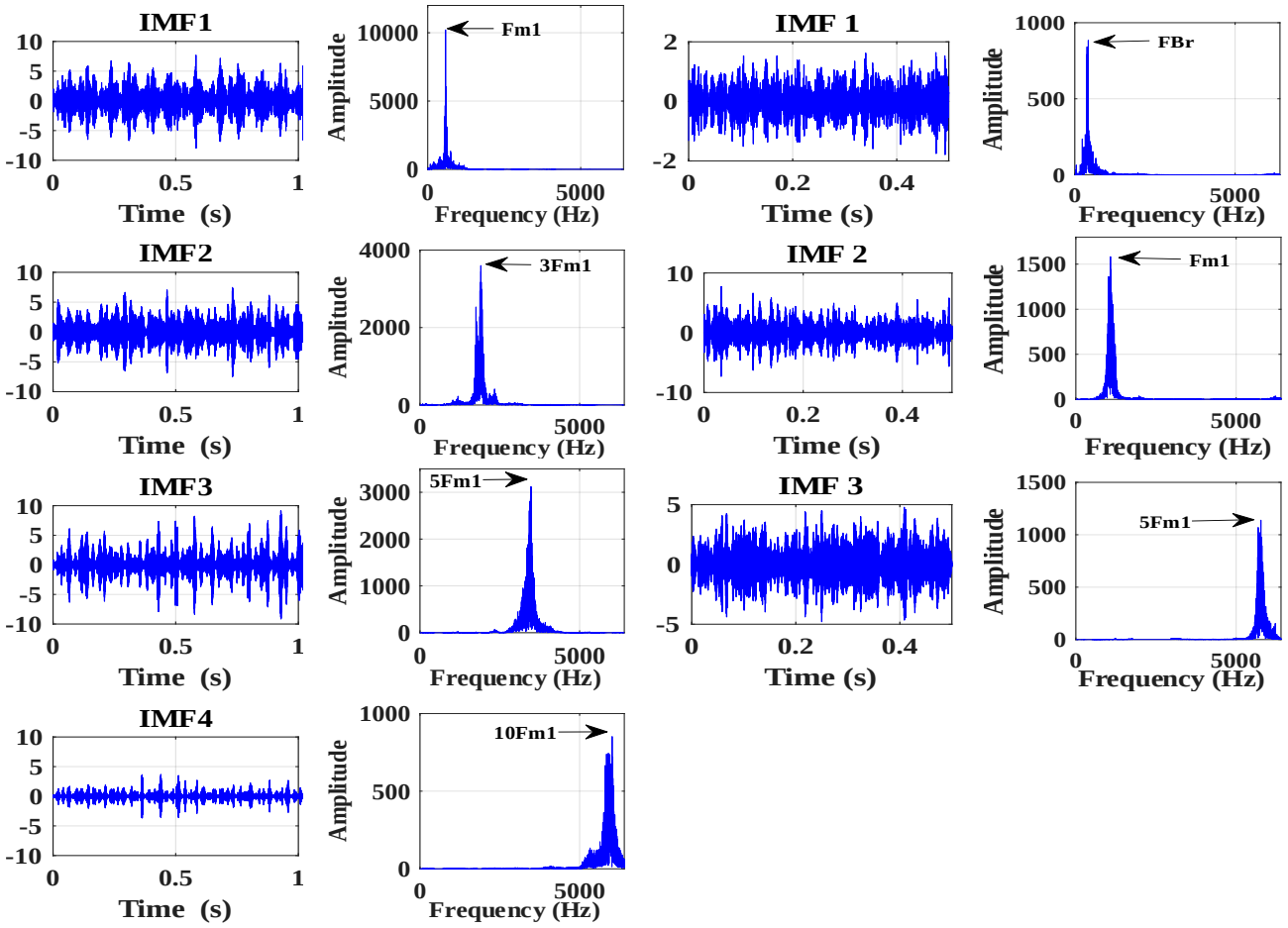

a. b.

Figure 3.16. Resulting IMFs and the corresponding spectrum obtained from VMD:

a. *S1* with $F_{r1} = 14\ Hz$, b. *S2* with $F_{r1} = 23\ Hz$.

The values of the belt resonance frequency can be obtained using the following expressions:

$C_e = 9.555 \times \frac{P}{N_e}$, where C_e is the input torque, P_e is the input power, and N_e is the input rotational speed.

$C_s = \frac{C_e}{u}$, where C_s is the output torque and u is the total transmission ratio.

$T = \frac{P}{V_s}$, where T is the belt tension and V_s is the linear speed of the belt.

$F_{Br} = \frac{1}{2L_b}\sqrt{\frac{T}{\mu}}$, where L_b is the free length of the belt and μ is the linear mass of the belt.

Table 3.4. Calculation results for the two rotation frequencies.

Rotation frequency F_{r1}	**Input torque C_e**	**Output torque C_s**	**Belt tension T**	**The resonant frequency F_{Br}**
14 Hz	*25.01 N.m*	*20.68 N.m*	*827 N*	*535 Hz*
23 Hz	*15.22 N.m*	*12.55 N.m*	*502 N*	*417 Hz*

To diagnose the faults, WMRA is applied to each IMF for both rotational speeds, as shown in Figures 3.17 and 3.18. For *S1*, the presence of input shaft misalignment is confirmed by the modulation of the rotational frequency harmonics ($2Fr_1$, $3Fr_1$), which exceed the amplitude of the rotational frequency itself, as shown in IMFs 1, 2, and 4.

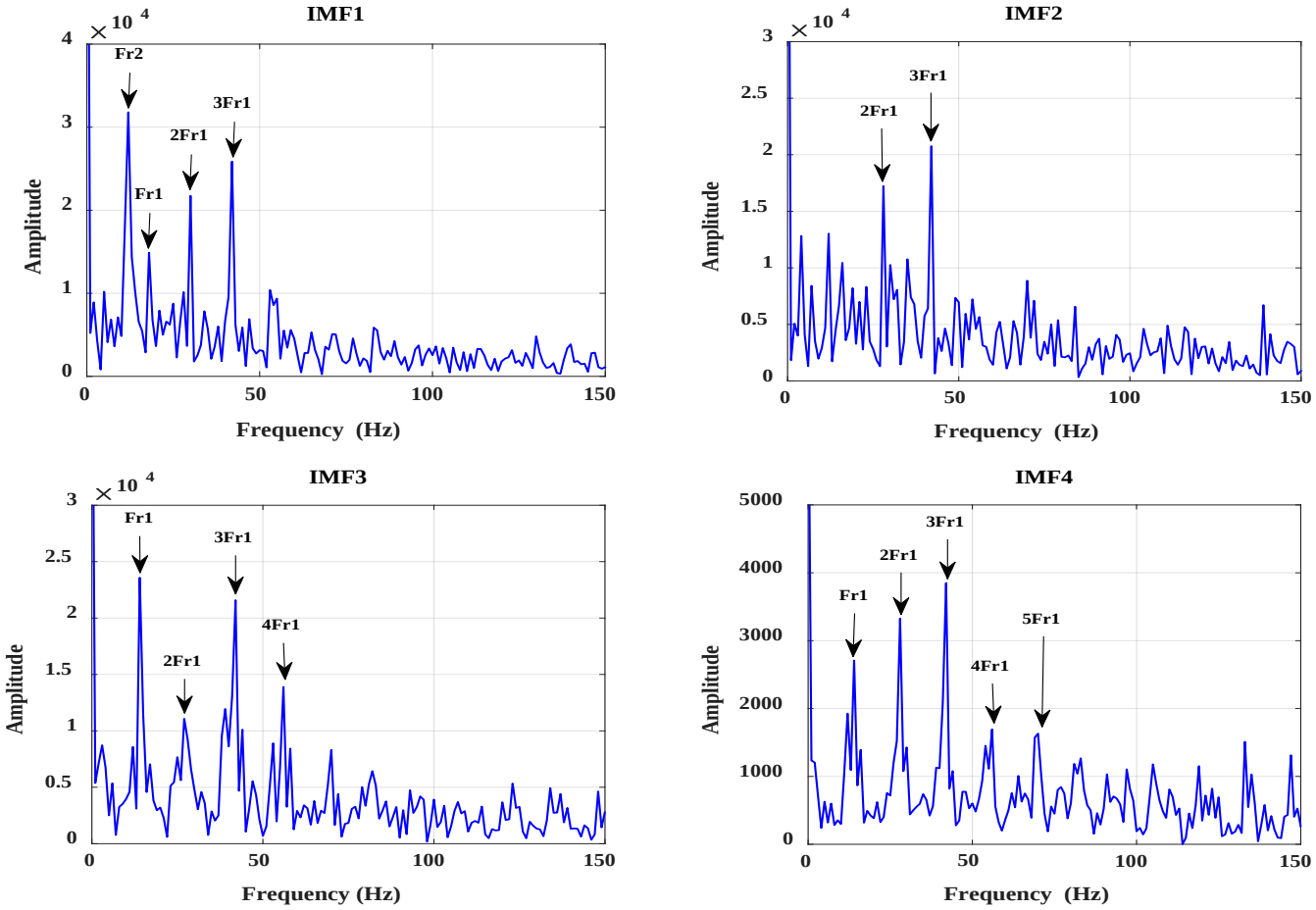

Figure 3.17. Envelope spectra obtained by the WMRA for each IMF of *S1*.

For *S2*, shown in Figure 3.18, the input shaft misalignment is confirmed by the presence of the $2F_{r1}$ peak, which exceeds the rotational frequency F_{r1} , as shown in IMFs 2 and 3. The presence of input shaft misalignment, combined with insufficient backlash between the two gears (identified in the spectrum of Figure 3.14(b)), caused misalignment in the second shaft, detected in IMFs 1 and 2 by the presence of a peak at $2F_{r2}$ in the absence of the rotational frequency F_{r2}. Additionally, in IMF3, we observe a peak at *4 Hz*.

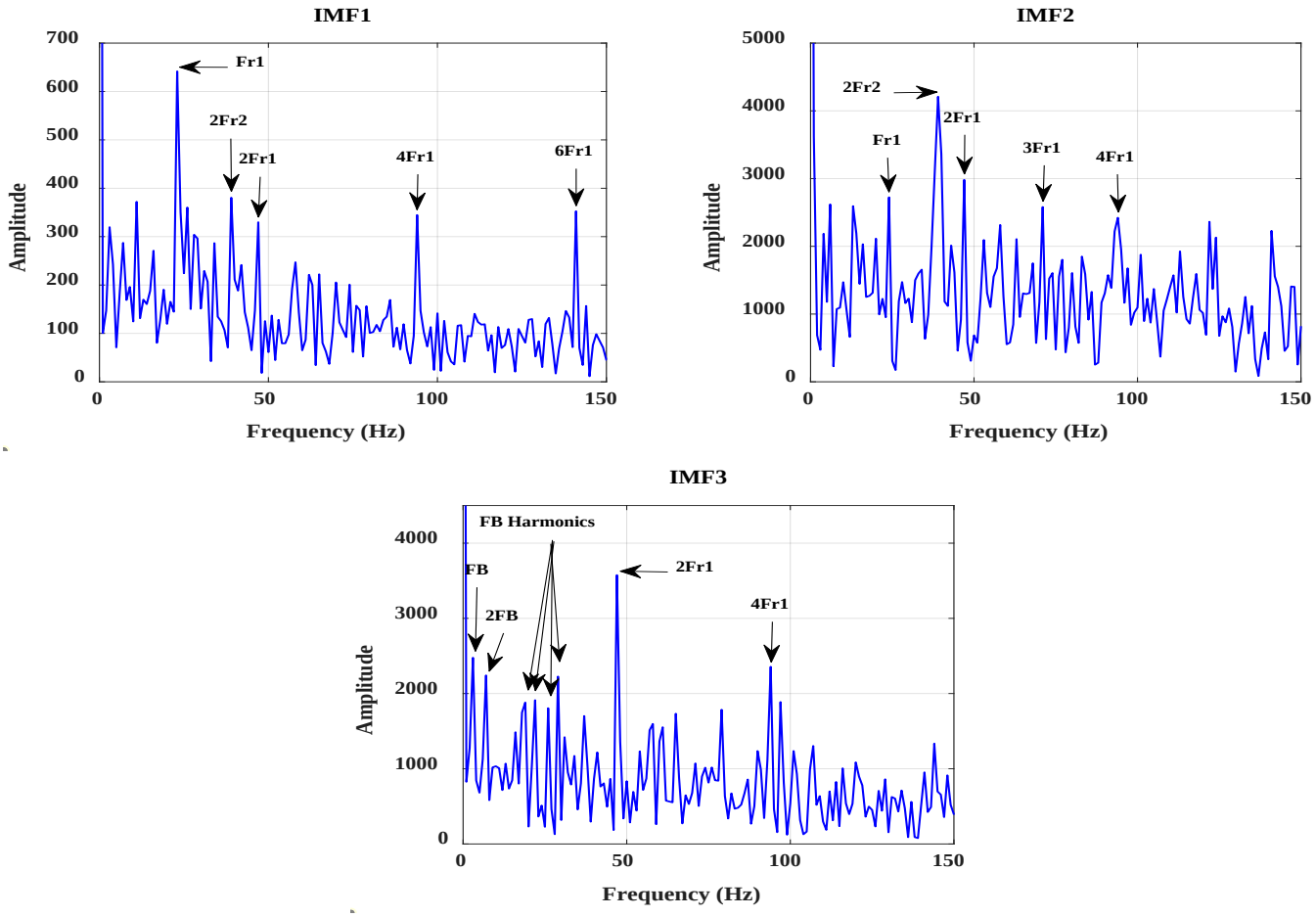

Figure 3.18. Envelope spectra obtained by the WMRA for each IMF of *S2*.

After inspecting the belt condition, we found two defects in the grooves of the poly-V belt, as shown in Figure 3.19. These defects justify the presence of the peak at *4 Hz*, corresponding to the belt passage frequency F_B and a large number of its harmonics.

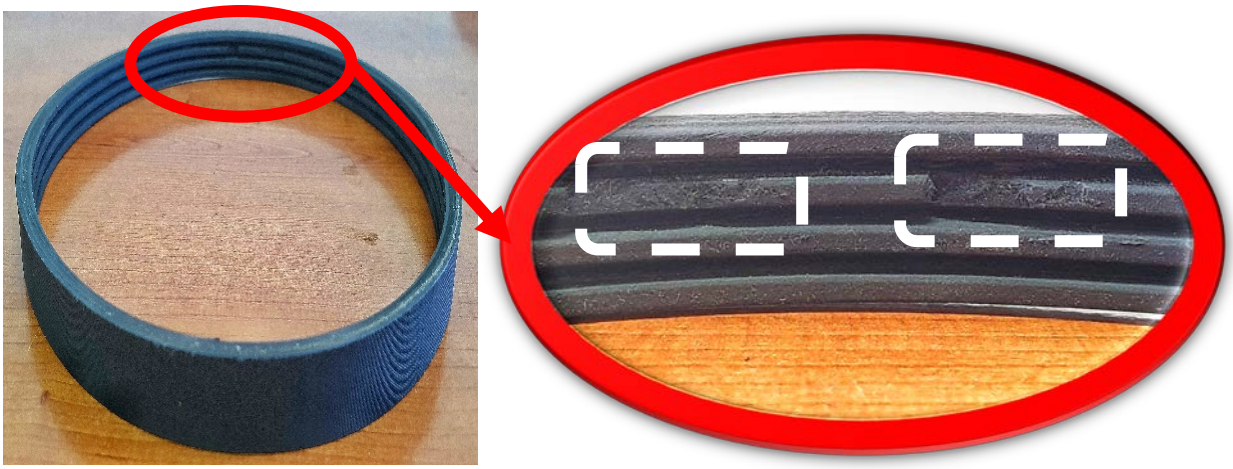

Figure 3.19. Defects identified on the V-ribbed belt.

6.2. Signal processing with gear fault

The signals exhibiting gear faults, *S3* and *S4*, shown in Figure 3.20, were also studied in this section. Following the presence of a fault on a tooth of the driven gear rotating at frequency F_{r2}, we observe an increase in vibration amplitudes compared to the case without gear faults in both the signals and their spectra.

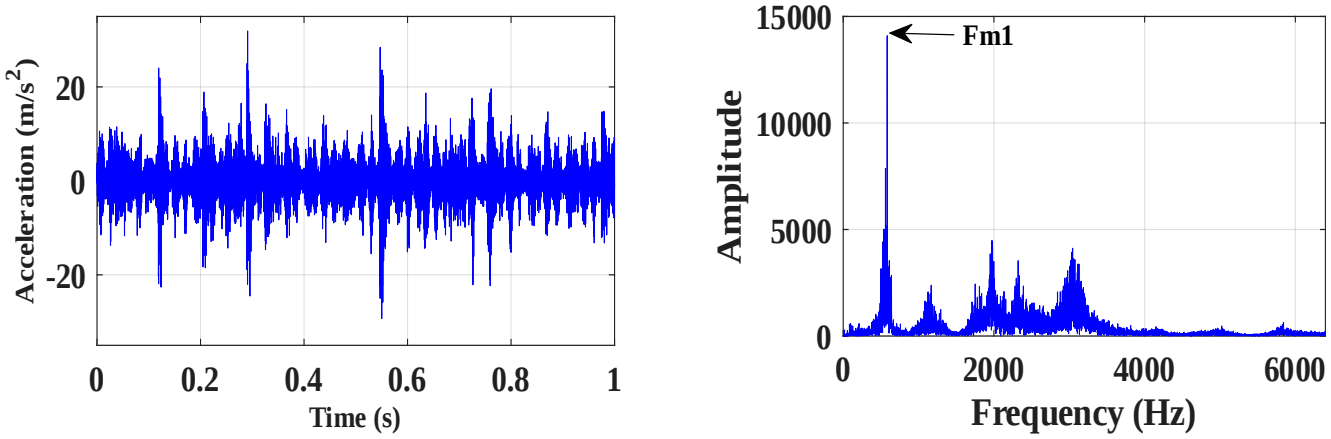

a.

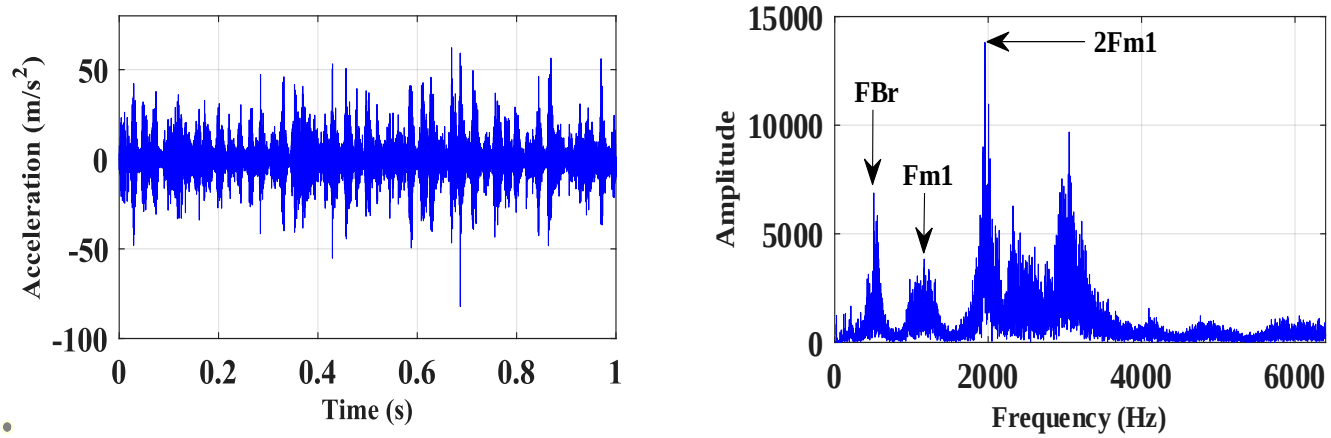

b.

Figure 3.20. Signals with gear faults and their corresponding spectra:

a. *S3* with $F_{r1} = 14\ Hz$, b. *S4* with $F_{r1} = 23\ Hz$.

The signal *S3*, shown in Figure 3.20(a), exhibits high-amplitude shocks compared to *S1*, and the corresponding spectrum still shows the dominance of the meshing frequency F_{m1}. The spectrum of *S4*, shown in Figure 3.20(b), reveals that the presence of a fault on the gear rotating at *23 Hz* has exacerbated the insufficient backlash fault, as the amplitude of $2F_{m1}$ exceeds that of F_{m1} by approximately 3.5 times. We also observe a sevenfold increase in the amplitude of F_{Br} compared to *S2*, with a frequency shift up to *502 Hz*. This frequency shift is due to the increase in belt tension *T* resulting from the worsening of the insufficient backlash fault and the misalignment on the various shafts.

6.2.1. Results obtained by WMRA

In the envelope spectra obtained by processing the two signals using WMRA, as shown in Figure 3.21, we observe the absence of harmonics of F_{r2} for both rotational speeds of *14 Hz* and *23 Hz*. Therefore, we can conclude that WMRA alone does not allow for the localization of the gear fault on the driven gear.

It turns out that during the disassembly and reassembly of gear Z_2 to create a fault on the flank of a tooth, misalignment was introduced on the intermediate shaft. This latter fault is represented by the presence of a peak at $2F_{r2}$, as well as the confirmation of input shaft misalignment by a peak at $3F_{r1}$, as shown in Figure 3.21(a). On the other hand, for *S4*, shown in Figure 3.21(b), we observe a significant increase in vibration amplitudes, approximately 20 times, due to: on one hand, the increase in rotational speed in the presence of faults and, on the other hand, the belt resonance, which allows the appearance of the third harmonic of the belt fault at $3F_B$ and misalignment faults on both shafts.

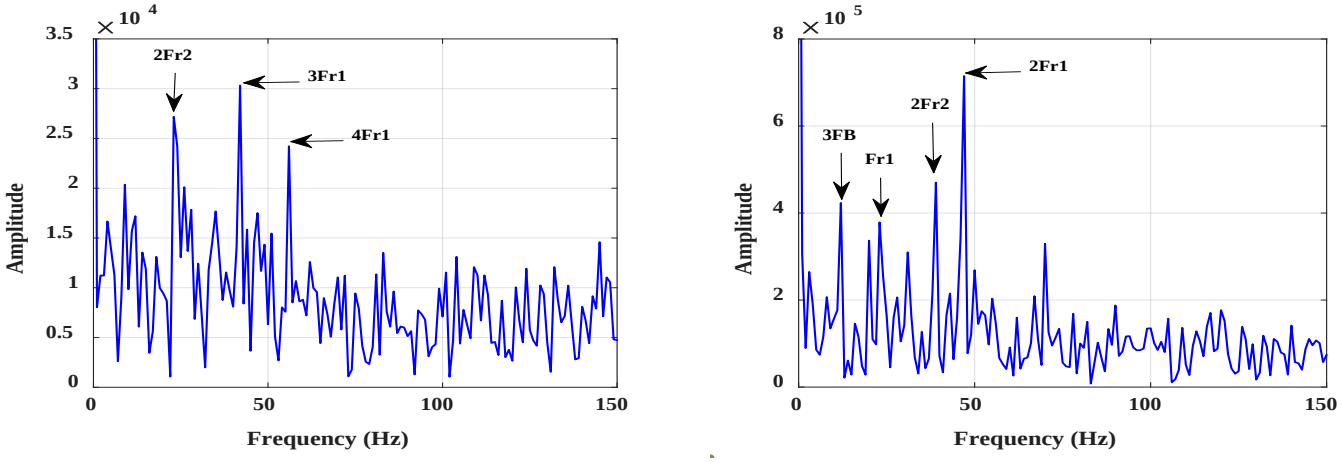

a. b.

Figure 3.21. Envelope spectra obtained by WMRA:

a. *S3* with $F_{r1} = 14\ Hz$, b. *S4* with $F_{r1} = 23\ Hz$.

6.2.2. Results obtained by VMD-WMRA combination.

Figure 3.22 presents the IMFs and their spectra obtained by VMD using the proposed criterion for the two signals *S3* and *S4*. We observe that the IMFs perfectly isolate the different frequencies (belt resonance frequency, meshing frequency, and its harmonics). Figure 3.22(a) shows the isolation of F_{m1} and some of its harmonics ($3F_{m1}$, $4F_{m1}$, $5F_{m1}$, $10F_{m1}$), while Figure 3.22(b) shows the appearance of the belt resonance frequency F_{Br} and some of the harmonics of the meshing frequency ($2F_{m1}$, $3F_{m1}$, $5F_{m1}$).

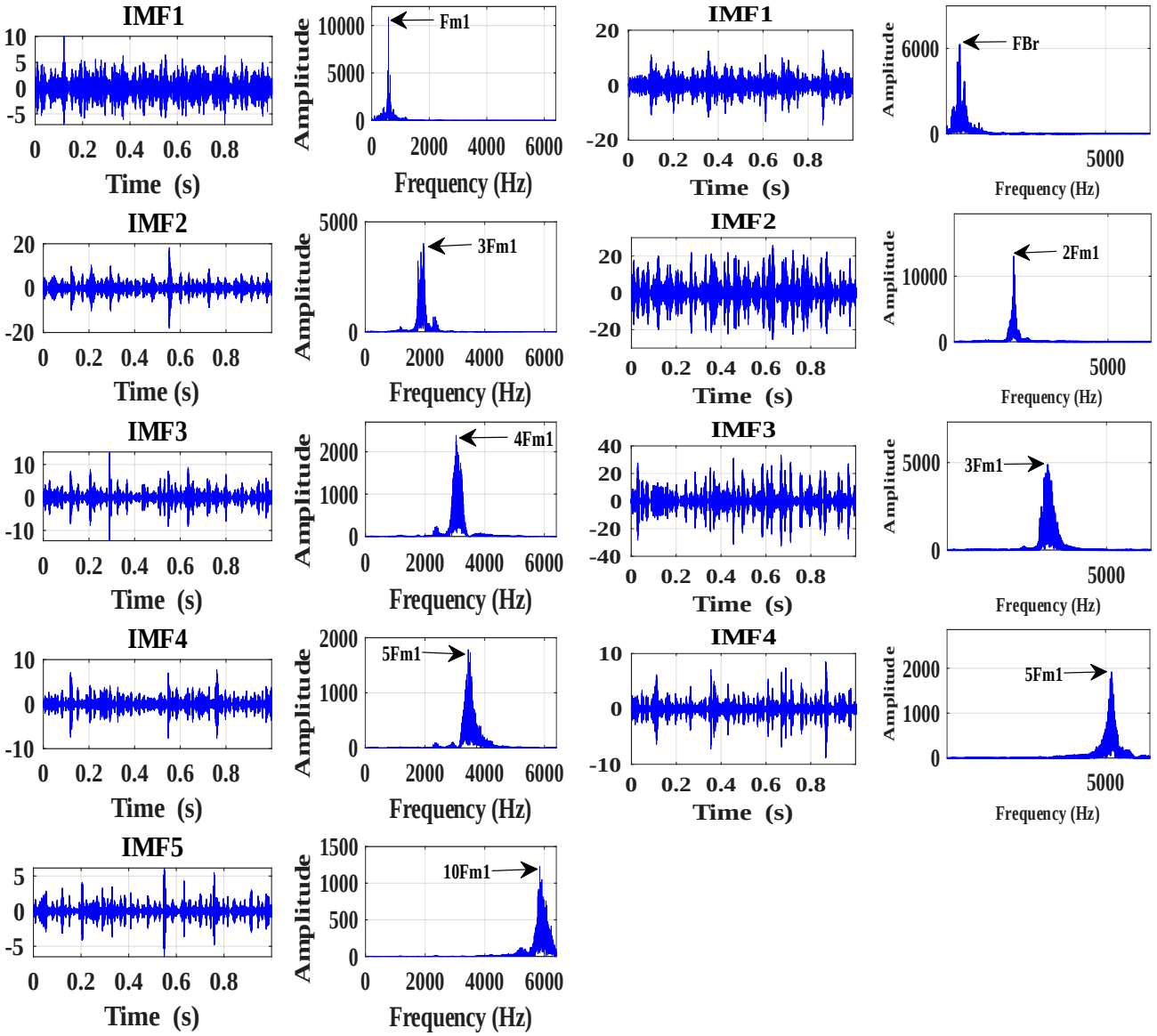

Figure 3.22. The IMFs obtained by VMD and the corresponding spectra:

a. *S3* with $F_{r1} = 14\ Hz$, b. *S4* with $F_{r1} = 23\ Hz$.

The envelope spectra of each IMF for the rotational frequency of *14 Hz*, obtained by applying WMRA, are presented in Figure 3.23. In the envelope spectra of IMF1, IMF2, and IMF3, we clearly observe the modulation of F_{m1} by the rotational frequency of the intermediate shaft F_{r2}, on which the gear with the tooth fault is mounted. This result was not achievable using WMRA alone.

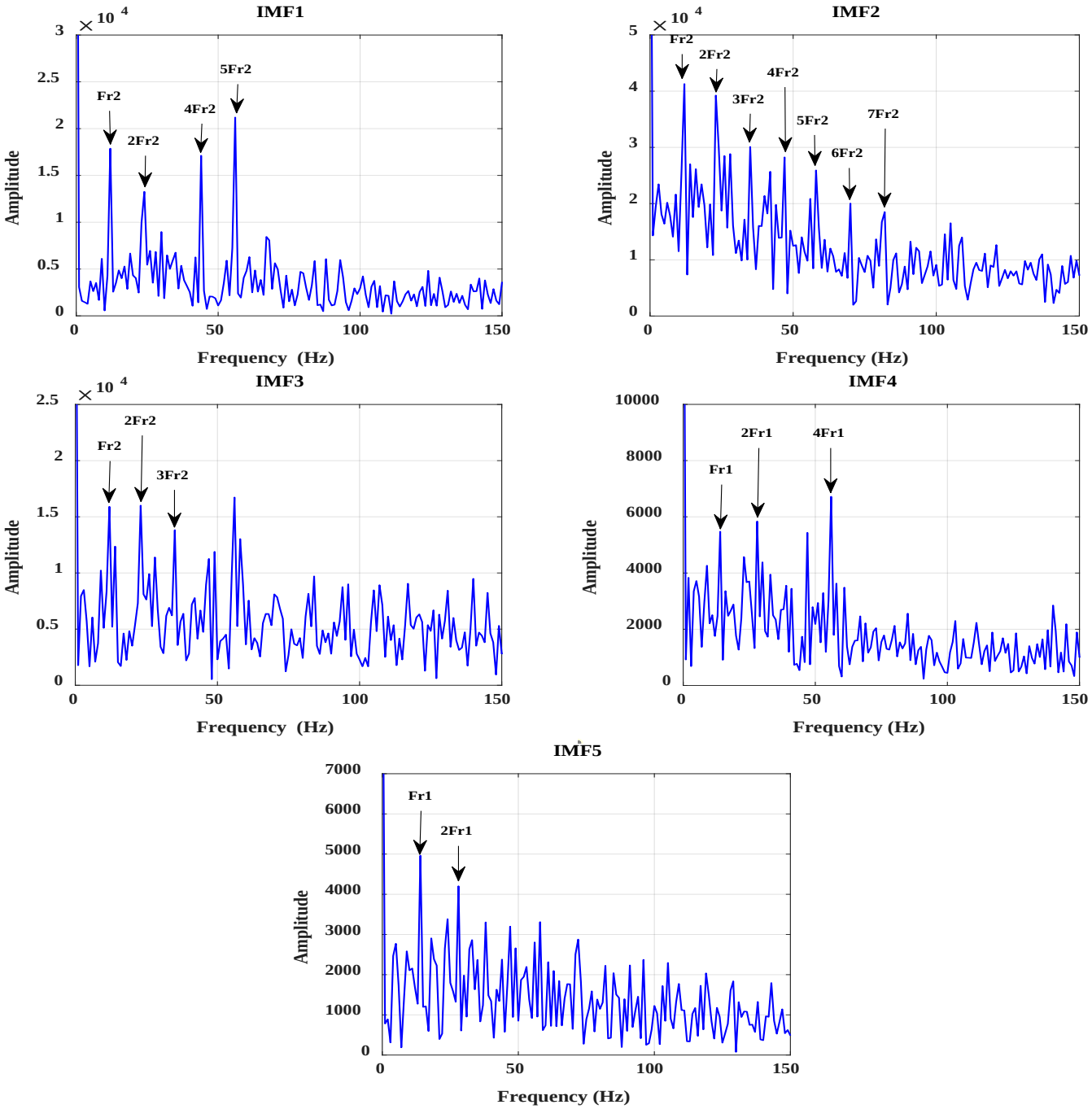

Figure 3.23. Envelope spectra obtained by the WMRA for each IMF of *S3*.

Figure 3.24 presents the envelope spectra obtained by combining VMD and WMRA. In the envelope spectrum of IMF1, we observe the presence of a large number of harmonics of F_B , with amplitudes lower than F_B . This indicates the presence of a belt fault, as previously illustrated in Figure 3.19. In the envelope spectrum of IMF2, we observe the modulation of F_{m1} by the rotational frequency of the driven shaft F_{r2}. Unlike the case of *S3*, the diagnosis of the gear fault is less evident due to the presence of major misalignment on the input shaft, represented by a peak at $2F_{r1}$, which dominates the harmonics of F_{r2}. The envelope spectrum

of IMF3 shows the presence of harmonics of F_{r1}, which is explained by insufficient backlash. Additionally, IMF4 confirms the presence of belt faults through the appearance of multiple harmonics of F_B.

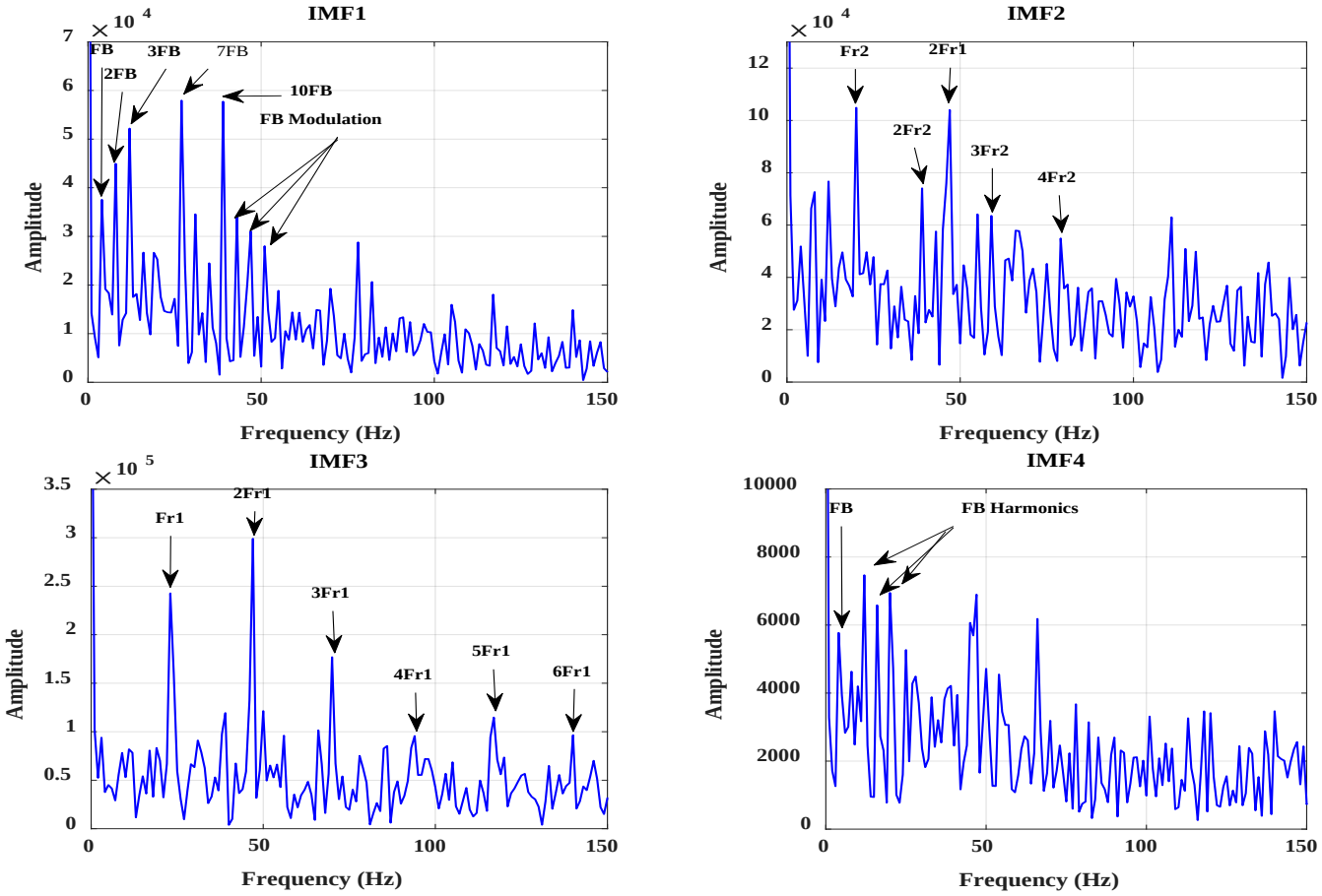

Figure 3.24. Envelope spectra obtained by the WMRA for each IMF of *S4*.

7. Conclusions

In this chapter, we proposed a combined approach based on VMD and WMRA for fault detection in gearboxes. The primary objective was to develop a robust and efficient method for diagnosing faults, even in the presence of noise or disturbances in the measured vibration signals.

We highlighted the advantages of our approach through both numerical simulations and experimental measurements. The obtained results demonstrate that VMD is a powerful tool for decomposing complex signals into Intrinsic Mode Functions (IMFs). Also, the use of SE enabled the determination of the optimal number of IMFs for each decomposition.

The analysis of IMFs obtained via VMD was further enhanced using WMRA, which helped isolate resonance frequencies and identify specific gearbox fault characteristics, even in noisy signals. We illustrated the effectiveness of our approach by processing both simulated signals and real signals measured on a test bench.

In conclusion, our proposed method offers a promising approach for fault detection in gearboxes, effectively addressing the challenges posed by noise and signal disturbances. The encouraging results obtained through both simulations and experimental validation demonstrate the potential of this approach to improve the reliability and accuracy of gear fault diagnostics. This could have significant implications for preventive maintenance in mechanical systems, contributing to enhanced operational efficiency and extended service life of industrial equipment.

Chapter 04

Automated diagnosis of rotating machine faults using the VMD-LSTM approach

In this chapter, we present a new approach combining VMD with Long Short-Term Memory (LSTM) networks for fault diagnosis in rotating machinery. Our method surpasses traditional vibration analysis techniques by offering enhanced accuracy in identifying fault types and severity levels across various datasets. The results from our research demonstrate the robustness and effectiveness of the VMD-LSTM approach, which provides a reliable framework for proactive maintenance and real-time monitoring of industrial systems.

1. Introduction

In the current industrial context, the early detection of rotating machinery failures represents a major challenge for optimizing performance and reducing maintenance costs. Although conventional vibration analysis techniques have proven effective, they show limitations when faced with the increasing complexity of mechanical faults. This evolution has led to the development of innovative approaches combining advanced signal processing and artificial intelligence.

This chapter explores a novel methodology that integrates VMD with Long Short-Term Memory (LSTM) neural networks. This synergy between signal processing and deep learning aims to create a more robust and adaptable fault detection system. Our study first presents the theoretical foundations of LSTM networks, detailing their architecture and mathematical formulations, before demonstrating their practical application to mechanical fault detection. Experimental results obtained on various datasets demonstrate the relevance of this hybrid approach for monitoring rotating machinery under demanding industrial conditions.

This research contributes to the evolution of predictive maintenance strategies by proposing a methodological framework capable of identifying and characterizing complex faults, paving the way for more efficient management of industrial equipment.

2. Proposed approach

Traditional vibration analysis is widely used to detect faults in rotating machinery but struggles with complex fault patterns in signals and a wide range of fault types. On the other hand, researchers have used raw signals to train fault classification networks. Improved signal decomposition techniques are introduced to address these issues by breaking down signals into simpler components and revealing hidden fault signatures. The integration of artificial intelligence enables smarter learning from these signal features. This paper proposes a method that combines fault revelation through VMD and sequential learning through LSTM to enhance fault detection in machinery, overcoming the limitations of traditional analysis through intelligent signal decomposition for more accurate results.

Figure 4.1 outlines the steps of the proposed approach:

- Data Acquisition: This is the simplest and most straightforward step. It involves repeatedly measuring vibration signals on the machine for different fault scenarios.
- Application of VMD: The signals measured in the first step are decomposed using the VMD method. The number of IMFs, denoted as KK, is chosen by taking the average number of IMFs for each signal using the previously proposed criterion.

- Data Splitting: At this stage, the dataset is divided into three subsets: training (80%), validation (10%), and testing (10%). Each signal is defined by its IMFs.
- Feature Extraction: Scalar indicators are the most important features in detecting faults in rotating machinery. Therefore, scalar indicators are calculated for all IMFs obtained in the three subsets.
- Training and Classification: The features from the training and validation subsets are used to train the LSTM network to obtain a reliable classification model. Once the model is trained, it is used to classify the test set defined by the calculated features.

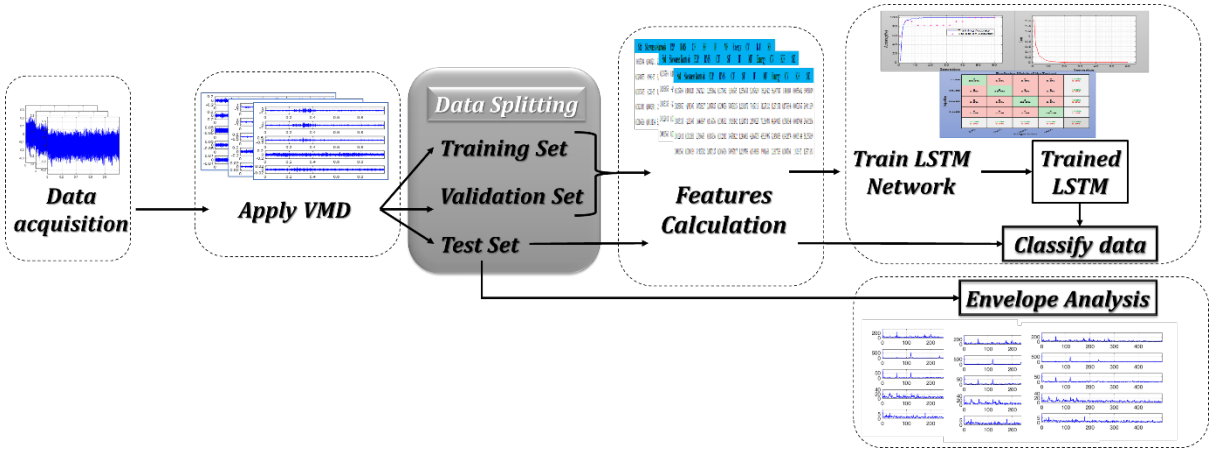

Figure 4.1. Flow chart of the proposed VMD-LSTM fault detection approach.

Finally, to confirm the superiority of the proposed approach over conventional vibration analysis, envelope analysis is performed on the IMFs of the test set to obtain envelope spectra and verify the potential detection of faults in these signals.

3. Theoretical context

Understanding the theoretical foundations is essential to grasp the proposed approach for fault detection. This section briefly describes the basic principles of LSTM networks, while VMD and scalar indicators have been thoroughly explained in the previous chapters.

LSTM networks are a type of Recurrent Neural Network (RNN) architecture designed to capture long-term dependencies in sequential data. An LSTM unit consists of different gates (input, forget, and output gates) that regulate the flow of information within the network. Mathematically, an LSTM unit for a given input sequence $X = \{x_1, x_2, ..., x_T\}$ of length T can be defined through the following computational steps [105]:

- Compute the Input, Forget, and Output Gates:

$$\begin{aligned} i_t &= \sigma\left(W_i \cdot \left[h_{t-1}, x_t\right] + b_i\right) \\ f_t &= \sigma\left(W_f \cdot \left[h_{t-1}, x_t\right] + b_f\right) \\ o_t &= \sigma\left(W_o \cdot \left[h_{t-1}, x_t\right] + b_o\right) \end{aligned} \tag{4.1}$$

- Update the Cell State C_t and Hidden State h_t:

$$\begin{aligned} \tilde{C}_t &= \tanh\left(W_C \cdot \left[h_{t-1}, x_t\right] + b_C\right) \\ C_t &= f_t * C_{t-1} + i_t * \tilde{C}_t \\ h_t &= o_t * \tanh\left(C_t\right) \end{aligned} \tag{4.2}$$

Where: i_t, f_t and o_t are the input, forget, and output gate vectors at time step t,

W_i, W_f, W_o and W_C are the weight matrices,

b_i, b_f, b_o and b_C are the bias terms,

σ represents the sigmoid activation function,

tanh is the hyperbolic tangent function,

4. Experimentations

In the experimental phase, the proposed approach was validated using two distinct datasets. The first dataset, LMSDS (Laboratory of Mechanics and Structures Dataset), was developed at the Laboratory of Mechanics and Structures at the University of Guelma, Algeria. This dataset provides an extensive collection of vibration signals, including gear and bearing faults under various operating conditions. The test bench used to generate this data is described in detail in Chapter 3 and illustrated in Figure 3.12. The data was sampled at a frequency of 16,384 Hz with a recording duration of one second.

The second dataset, CWRUDS (Case Western Reserve University Dataset), was obtained from the Case Western Reserve University Bearing Data Center [132]. This dataset includes a wide range of vibration signals from bearings operating under various conditions, covering both normal and faulty states. The data was collected using a dedicated test bench designed to simulate typical bearing faults, including ball, inner race, and outer race faults. The test bench, shown in Figure 4.2, consists of a motor, a coupling with a transducer/encoder, and a dynamometer. The signals were recorded at a sampling frequency of 48 kHz, with each case comprising 10-second recordings, subsequently segmented into one-second samples. This dataset enables an in-depth analysis of bearing behavior across a wide range of operating conditions, providing a solid foundation for the analysis and validation of the proposed approach.

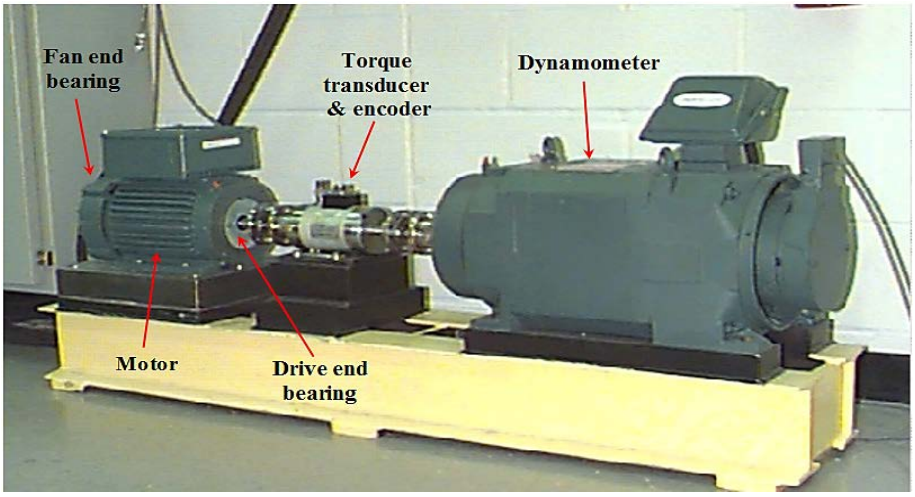

Figure 4.2. Case Western Reserve University's test bench.

This strategy of using two datasets ensures that the effectiveness of the proposed method can be demonstrated for both gear and bearing faults, regardless of the type or severity of the fault.

Table 4.1 presents the frequency characteristics necessary for fault detection, including the rotational frequencies F_r and the calculated bearing fault frequencies (*BPFO*, *BPFI*, *BPF*, and *CF*).

Table 4.1. Frequency characteristics of the defects for both sets.

LMSDS				CWRUDS				
F(Hz)	**Shaft 1**	**Shaft 2**	**Shaft 3**	***Fr* (Hz)**	***BPFI***	***BPFO***	***BPF***	***CF***
F_r	*14*	*11.76*	*16.93*	*28.66* to *29.95*	*155.19* to *162.18*	*102.74* to *107.36*	*135.08* to *141.16*	*10.68* to *11.16*
BPFO	*42.88*	*36.02*	*51.86*					
BPFI	*69.10*	*58.04*	*83.56*					
BPF	*56.50*	*47.46*	*68.32*					
CF	*5.34*	*4.49*	*6.46*					

Table 4.2 provides the complete compositions of the samples in the two datasets: SD (Small Defect), AD (Average Defect), and CD (Critical Defect). Each severity level in the dataset includes 30 samples, each one second long, divided into 24 for training, 3 for validation, and 3 for testing.

Table 4.2. Total compositions of the datasets used (CWRUDS on the left and LMSDS on the right).

Data Set	Defect Type	Defect Severity	Data Set	Defect Type	Defect Severity
CWRUDS	Without Defect	/	LMSDS	Without Defects	/
	Ball Defect	SD		Bearings Defects	SD
		AD			AD
		CD			CD
	Inner Ring Defect	SD		Gears Defects	SD
		AD			AD
		CD			CD
	Outer Ring Defect	SD			CD + SD
		AD			CD + AD
		CD			CD + CD
				Combined Gears and Bearings Defects	SD Bearing + SD gear
					SD Bearing + AD Gear
					SD Bearing + CD Gear
					AD Bearing + SD Gear
					AD Bearing + AD Gear
					AD Bearing + CD Gear
					CD Bearing + SD Gear
					CD Bearing + AD Gear
					CD Bearing + CD Gear

5. Results and discussions

5.1. Vibratory analysis

This section presents a conventional vibration analysis of the test datasets. The VMD decomposition parameters (K, α) were defined based on [88, 129, 133], resulting in an average number of IMFs equal to $K = 5$. Among the large number of processed samples, the ball bearing faults from the CWRUDS dataset and the gear faults from the LMSDS dataset are presented below.

Figure 4.3 describes the analysis procedure, with Figure 4.3(a) showing the time-domain representation of three signals with small ball defects, Figure 4.3(b) presenting the resulting IMFs for each signal, and Figure 4.3(c) displaying the envelope spectrum of the signals. Analyzing the envelope spectrum in Figure 4.3(c), we can clearly see that there is no fault characteristics related to BPF. Despite the presence of some peaks in IMFs 2 and 3 of the first signal and IMF 3 of the second signal, these peaks correspond to the rotational frequency F_r and do not provide a diagnostic of the bearing's condition.

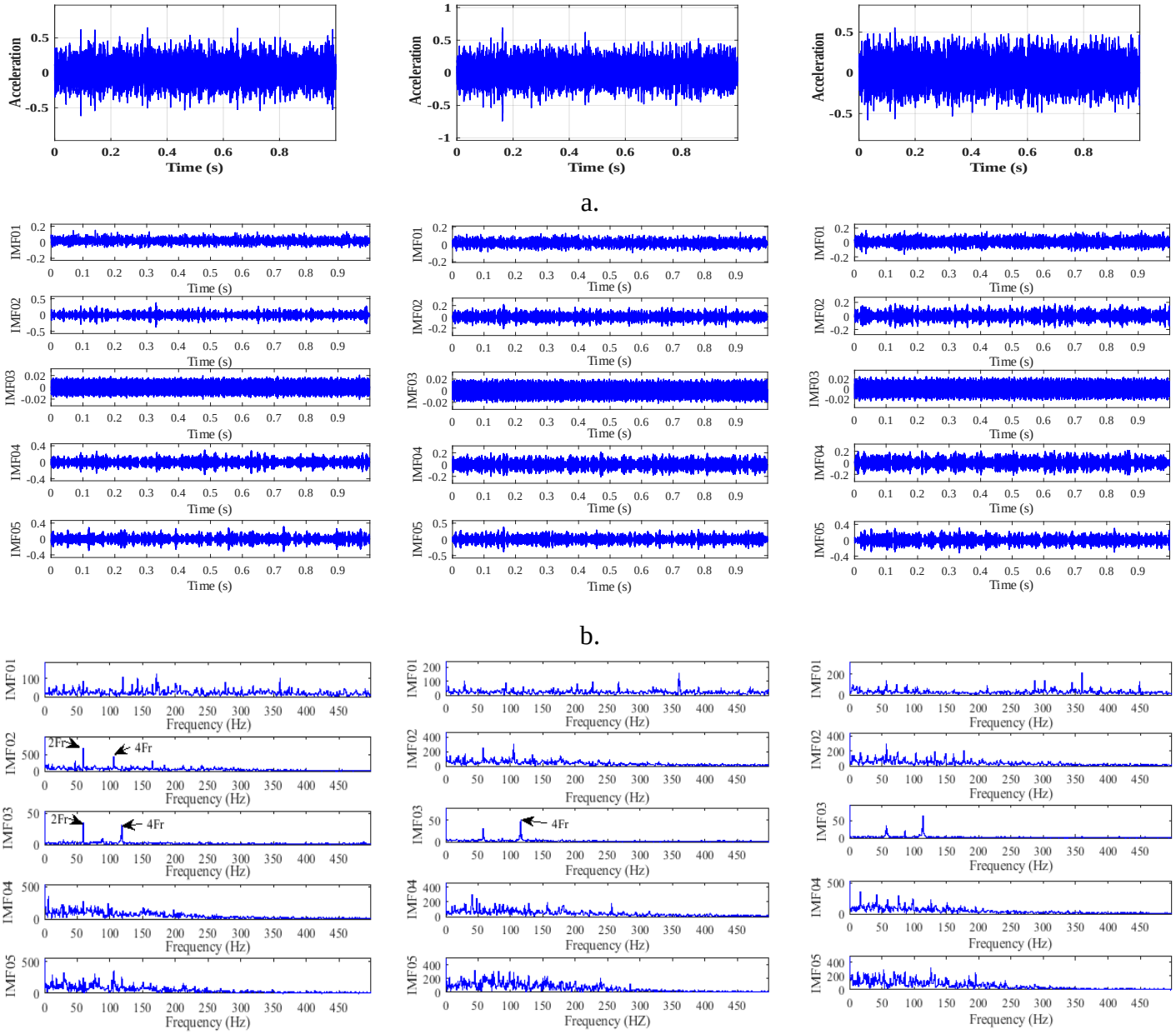

Figure 4.3. Vibratory analysis of small ball defect of CWRUDS:

a. Time domain representation, b. Resulting IMFs and c. Envelope spectrum of the IMFs.

Figure 4.4 shows the envelope spectra for other severity levels of the ball defect. Figure 4.4(a) represents different samples of the average defect, while Figure 4.4(b) examines the critical defect. The absence of BPF is also evident in these envelope spectra. Despite the robustness of VMD for fault detection, which enabled it to detect both inner and outer race faults in the same dataset, diagnosing the ball defect across all three severity levels proved impossible in this case. These results are highly consistent and confirm the findings of [134, 135].

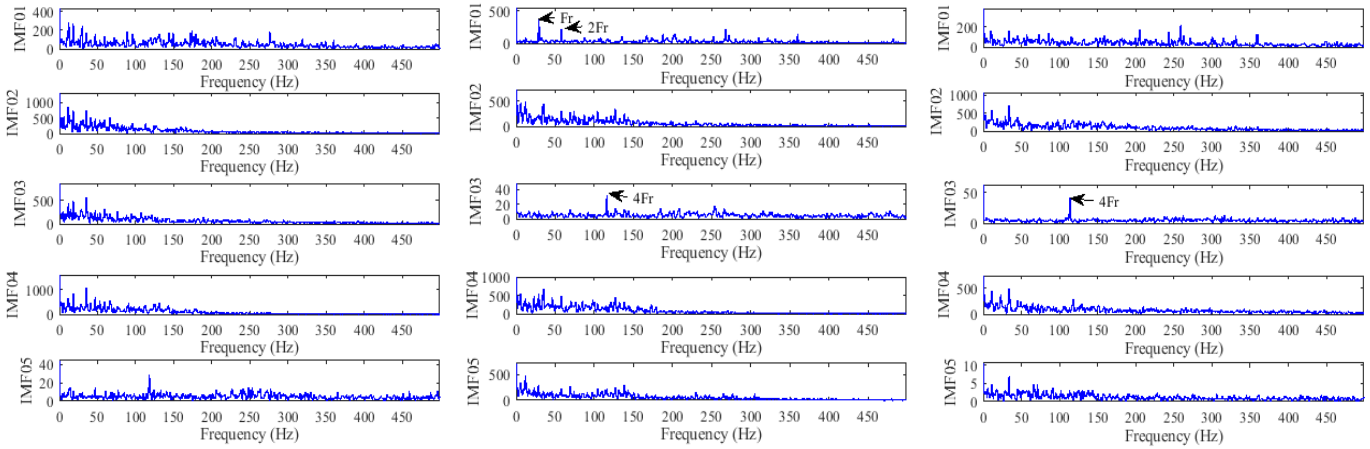

a.

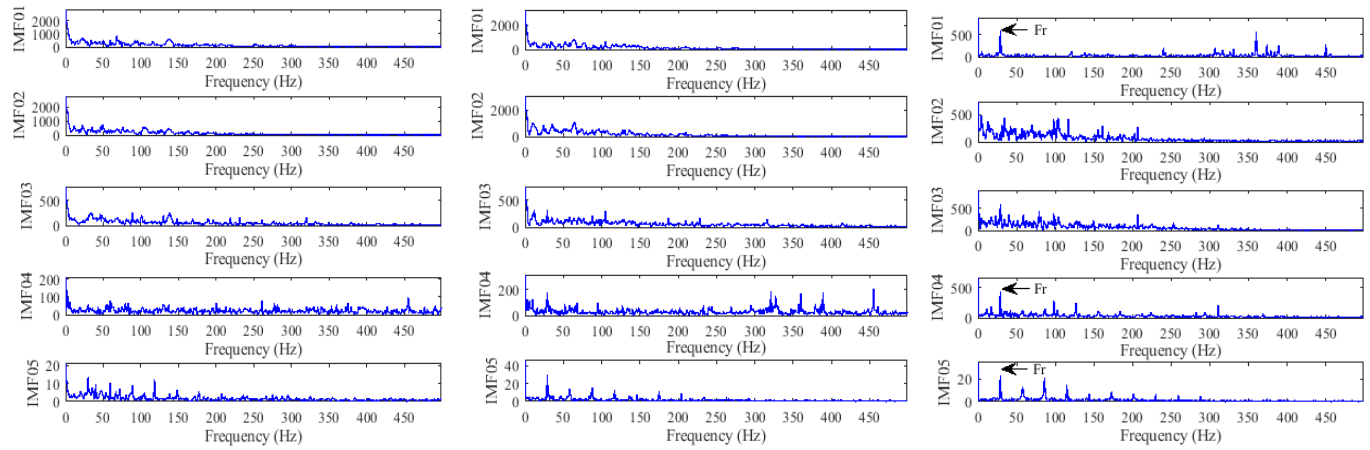

b.

Figure 4.4. IMFs' envelope spectrum of ball bearing defect signals from CWRUDS:

a. Average ball defect and b. Critical ball defect.

The LMSDS signals contain noise, making detection more challenging. It was impossible to detect faults in all cases. While VMD is an effective signal processing tool, the measured signals in this case posed a significant challenge. For gear faults, the analysis of the small defect signals presented in Figure 4.5 yielded no results. Figure 4.5(a) shows the time-domain representation of the three signals, and it is clear that the signals are corrupted with high levels of noise. The resulting IMFs in Figure 4.5(b) are analyzed using envelope analysis to produce the spectrum in Figure 4.5(c). The analysis of these spectra reveals the presence of some peaks corresponding to F_{r1} and its harmonics ($\times 2$, $\times 3$, ...), which are related to the first shaft, suggesting the presence of misalignment on the input shaft. However, the spectrum in Figure 4.5(c) reveals the absence of F_{r2}, which is linked to the faulty gear.

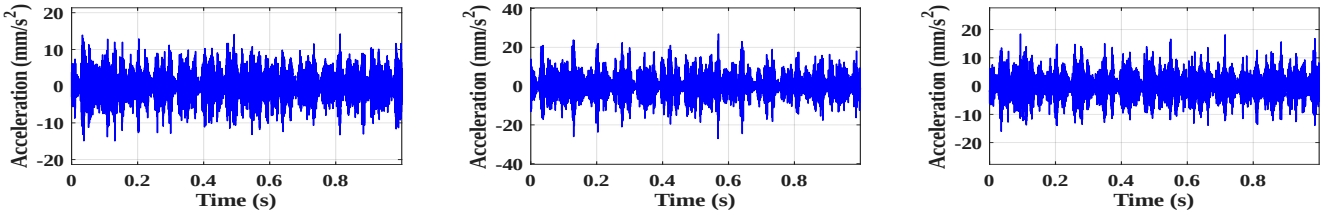

a.

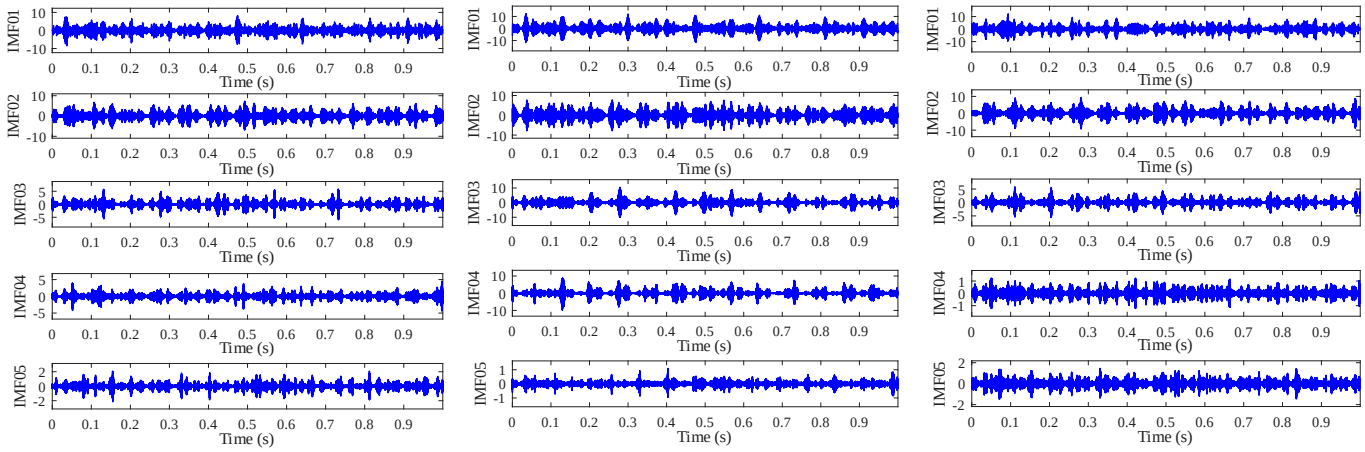

b.

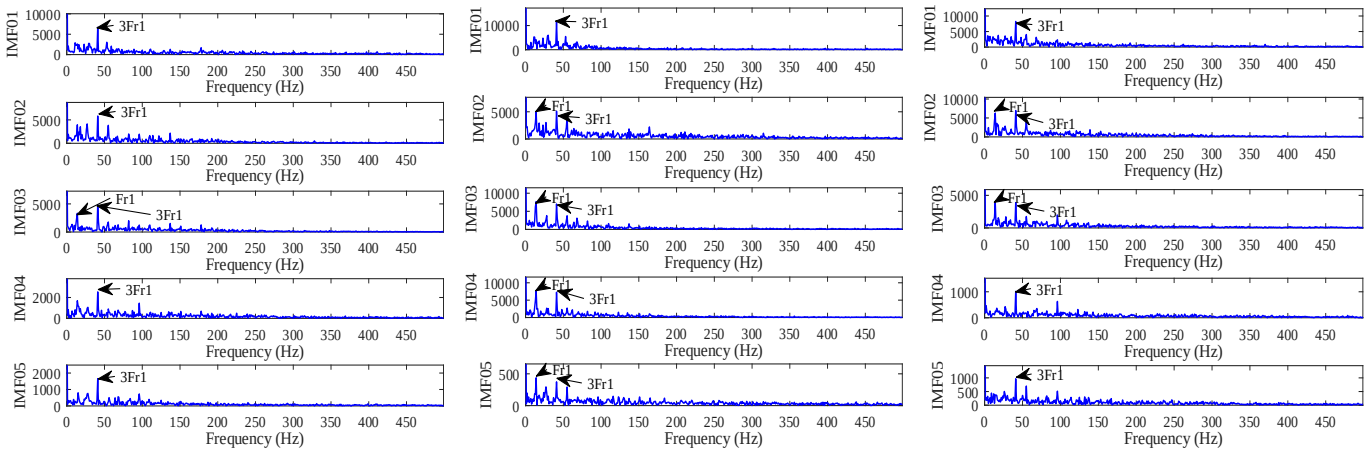

c.

Figure 4.5. Vibratory Analysis of small gear defect of LMSDS:

a. time domain representation, b. Resulting IMFs, and c. Envelope spectrum of the IMFs.

The analysis of residual gear faults in Figure 4.6 continues without providing clear indications of faults. In Figures 4.6(a) and 4.6(b), the presence of F_{r1} and its harmonics confirms the diagnosis of misalignment for the average and critical gear faults, where the amplitude of the harmonics exceeds that of the rotational frequency.

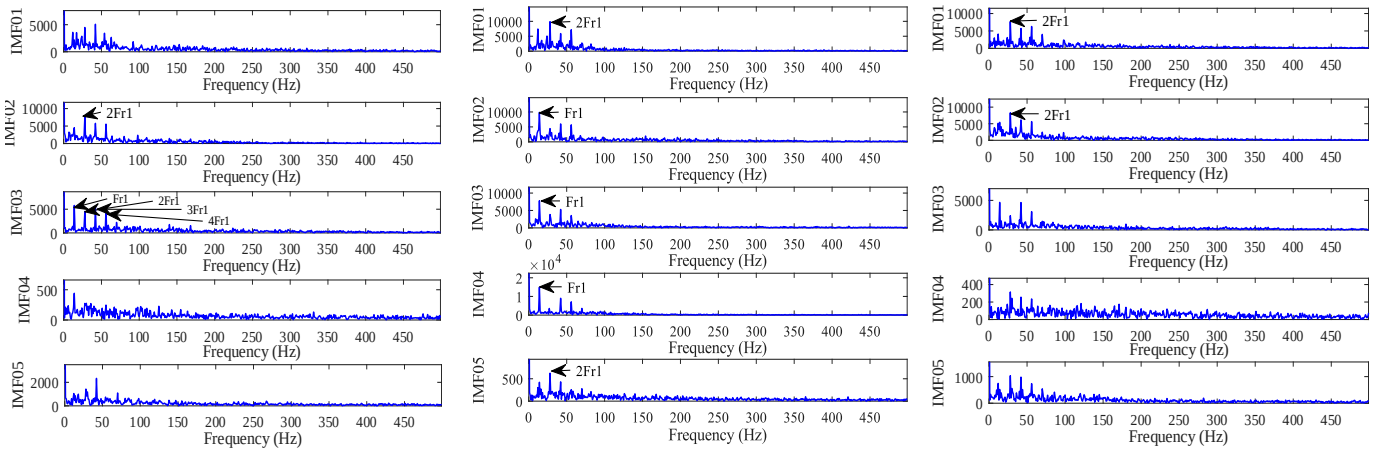

a.

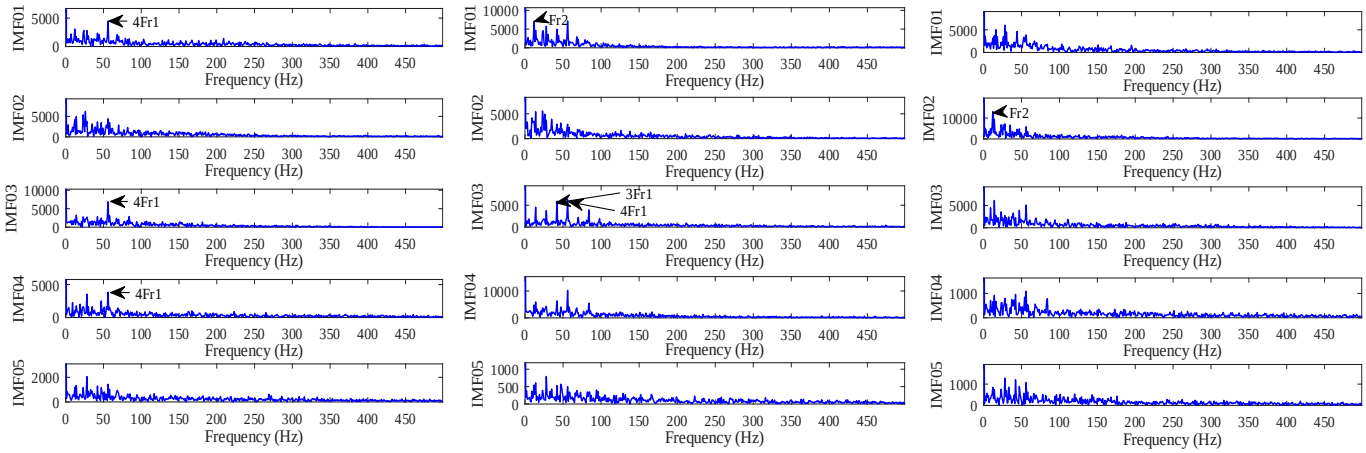

b.

Figure 4.6. IMFs' envelope spectrum of gear defect signals from LMSDS:

a. Average gear defect, b. Critical gear defect.

Figures 4.7(a) to 4.7(c) present the analysis of combined gear faults, corresponding to critical and small, critical and average, and critical and critical defects, respectively. Some peaks of F_{r2} are visible, but there are no harmonics, and F_{r3} is completely absent, making the detection of gear faults impossible.

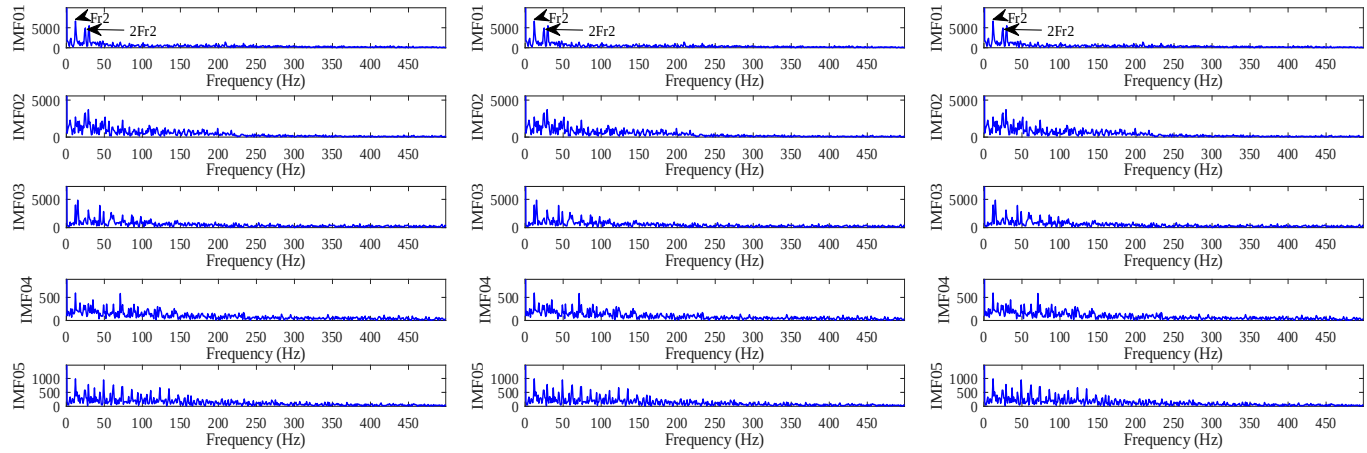

a.

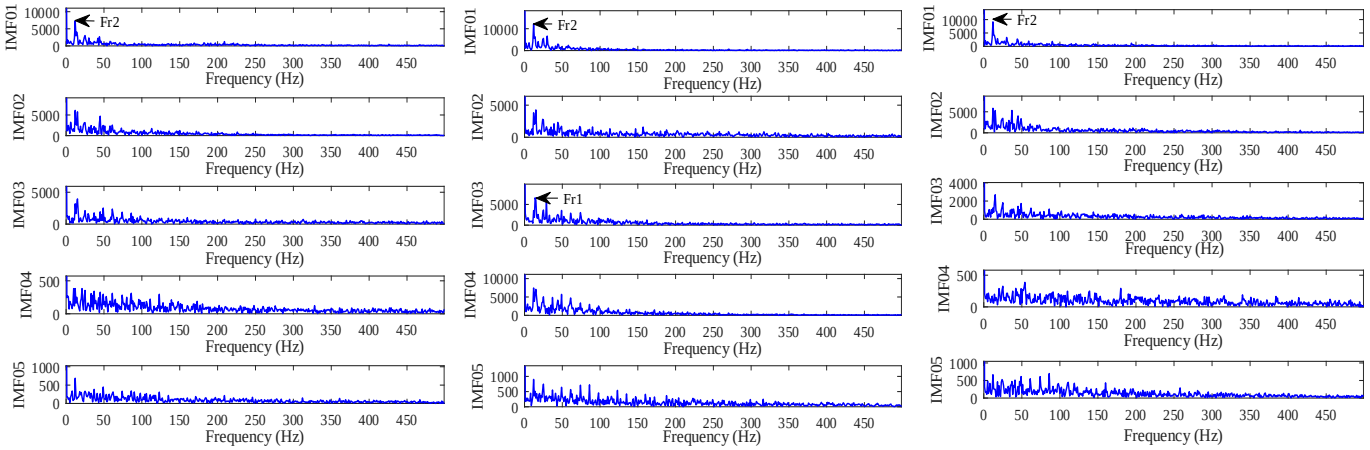

b.

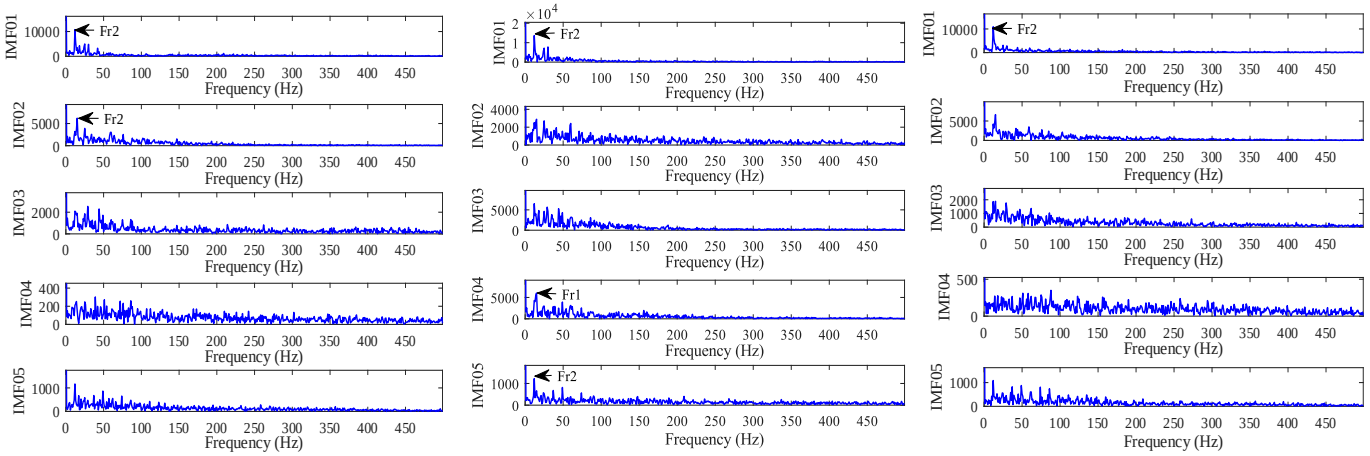

c.

Figure 4.7. IMFs' envelope spectrum of combined gear defect signals from LMSDS:

a. Critical and small defects, b. Critical and average defects, c. Critical and critical defects.

The diagnostic process for the two datasets containing gear and bearing faults revealed that traditional VMD analysis struggled to accurately detect the majority of fault types, with the exception of inner and outer race faults. While acknowledging these limitations, it is important to highlight the inherent complexity and variability of fault signatures, which can render traditional methods ineffective in certain scenarios.

5.2. Application of the VMD-LSTM combination

This section presents the results of the classification and diagnosis of gear and bearing faults found in the two datasets. This manuscript provides a comprehensive investigation of the datasets using several Recurrent Neural Networks (RNNs) to accurately detect faults. The RNNs are created by feeding the feature matrix obtained from the calculation of scalar indicators of the IMFs produced by VMD decomposition into LSTM networks.

Table 4.3 provides a complete overview of the feature matrix extracted from the signals. The feature matrix includes a wide range of parameters derived from the signal, providing valuable information about the machine's condition. The feature matrix captures a broad spectrum of parameters, enabling the LSTM network to learn complex relationships and temporal dependencies in the data. Each element of the feature matrix adds valuable information about the underlying vibrational characteristics of the machine. Using Table 5.3 as the input feature matrix allows the LSTM network to learn and adapt effectively to the complexities of the data, resulting in robust fault detection capabilities. The predictive accuracy of the model can be refined through iterative training and validation processes, providing actionable insights for proactive maintenance and condition monitoring of rotating machinery.

Table 4.3. Feature matrix of a signal without defect from the CWRUDS.

Scalar Indicator	Signal without defect				
	IMF1	IMF2	IMF3	IMF4	IMF5
STD	*0.03958896*	*0.0368447*	*0.02334455*	*0.00817395*	*0.00174969*
Skewness	*0.05681834*	*-0.00012252*	*-1.85E-05*	*0.00533201*	*4.48E-05*
Kurtosis	*2.71165859*	*2.89355662*	*1.57581672*	*3.15807748*	*3.13994139*
Peak to Peak	*0.25788425*	*0.24297596*	*0.09014244*	*0.08313773*	*0.01543696*
RMS	*0.04057073*	*0.03684446*	*0.02334432*	*0.00817412*	*0.00174968*
Crest Factor	*3.35643633*	*3.32929993*	*1.91088351*	*4.96755348*	*4.41690562*
Shape Factor	*1.24073652*	*1.26023958*	*1.11796921*	*1.25710614*	*1.2617955*
Impulse Factor	*4.16445314*	*4.19571555*	*2.13630892*	*6.24474199*	*5.57323165*
Margin Factor	*127.357565*	*143.51159*	*102.308736*	*960.385072*	*4019.17476*
Energy	*79.0072305*	*65.1606772*	*26.1579428*	*3.20717998*	*0.14694662*
Crest Value	*0.13617307*	*0.12266625*	*0.04553417*	*0.04253234*	*0.00772818*
K Factor	*0.00552464*	*0.00451957*	*0.00106296*	*0.00034766*	*1.35E-05*
Entropy	*451.797539*	*382.196711*	*187.878762*	*28.4404843*	*1.75466756*

5.2.1. Case of CWRUBDS

Figure 4.8 shows the RNNs trained for the CWRUDS dataset. The process begins with the classification of the fault type (RNN1), followed by the classification of the severity of each fault type (RNN2, RNN3, RNN4). Finally, to further test the proposed approach, a classification of all classes in this dataset was performed (RNN5). This last step includes the procedure used by the previous RNNs (RNN1, RNN2, and RNN3) to provide a direct fault type and its corresponding severity.

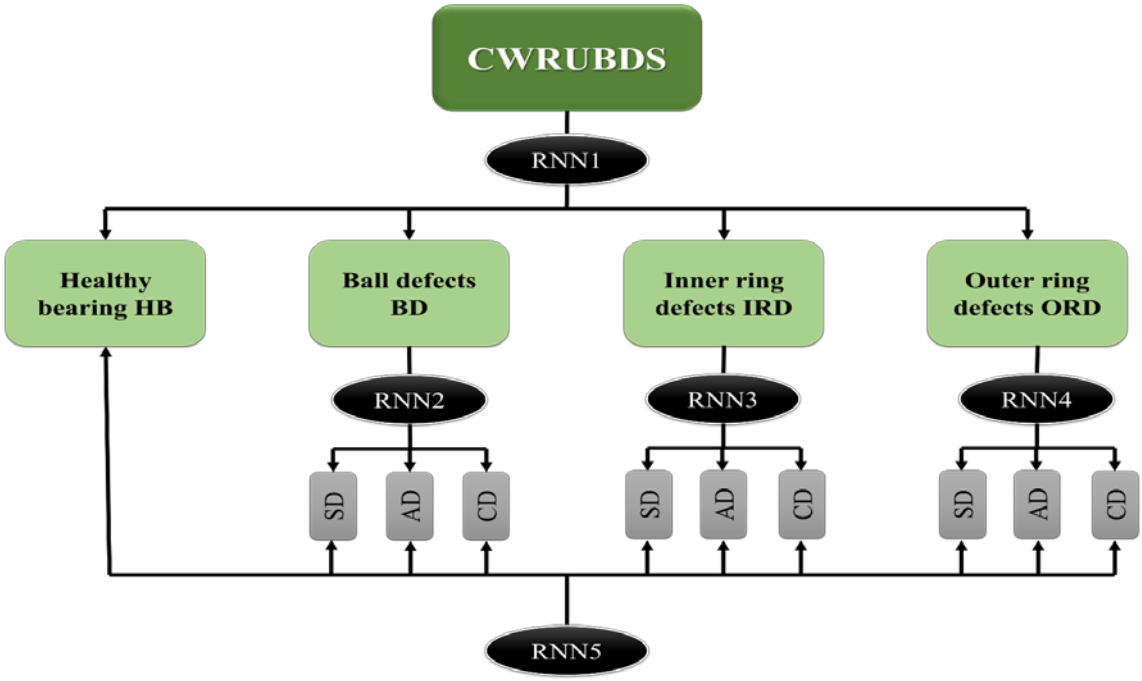

Figure 4.8. Trained RNNs for fault detection of CWRUDS.

Figure 4.9 shows the training progress of RNN1. The total number of iterations was set to 60, and the training accuracy reached 100% before the end of the process, despite some disturbances at the beginning of the training process, as shown in Figure 4.10. The model initially had high variance, but as progress was made and the performance of the LSTM networks in sequential training improved, the RNN converged, and both the training and validation accuracy (Figure 4.10(a)) reached 100% and stabilized before the end of training. The loss function in Figure 4.10(b) confirms the model's convergence, as we can see good alignment with the training process and lower loss values.

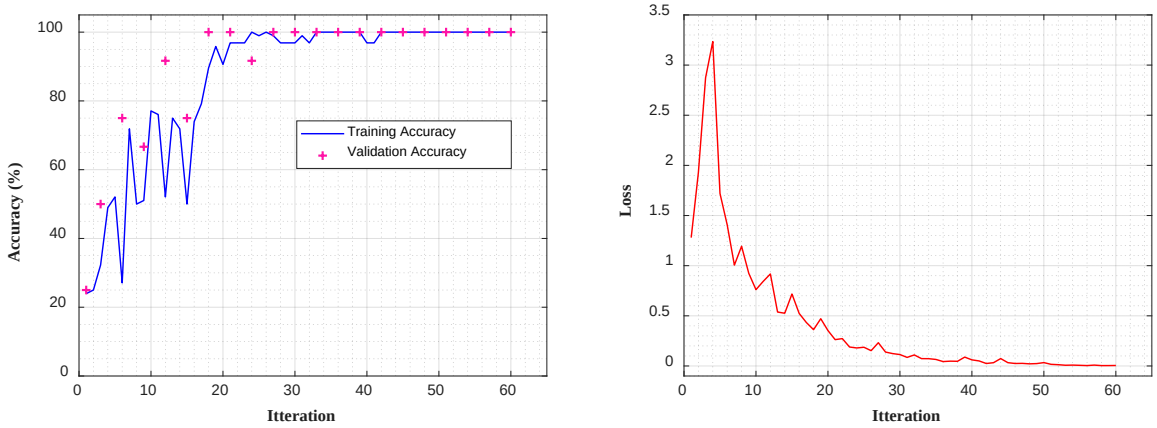

a. b.

Figure 4.9. Training progress of RNN1: a. Training accuracy and b. Loss.

Figure 4.10 represents the confusion matrix of RNN1 trained to detect fault types in the CWRUDS dataset. The strong diagonal concentration demonstrates the performance of RNN1 in identifying different machine health states. Even with multiple states, the trained network correctly predicted each target class. Despite the limitations of traditional vibration analysis using VMD, the proposed approach accurately diagnosed the health state, offering an intelligent fault detection method for bearing faults.

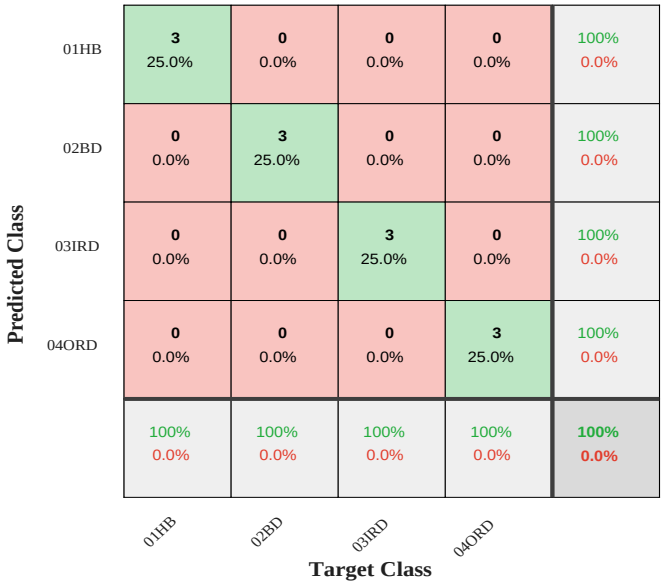

Figure 4.10. The confusion matrix resulted from the trained RNN1 for defect type classification of CWRUDS.

Figure 4.11 presents the performance of the other RNNs trained for the CWRUDS dataset. Figures 4.11(a), 4.11(b), and 4.11(c) show the classification results for detecting the severity of different bearing faults found in CWRUDS, complementing the results of RNN1. Figure 4.11(a) represents the confusion matrix for detecting ball faults using RNN2. The classification accuracy was 100%, demonstrating the proposed approach's ability to accurately detect ball faults, even at early stages such as small defects. Figures 4.11(b) and 4.11(c) show the results of RNN3 and RNN4, with classification accuracy also at 100%. These results confirm those obtained from classical vibration analysis, where VMD was able to detect faults in both inner and outer races. Figure 4.11(d), on the other hand, shows the classification results using RNN4, where the proposed approach performed admirably in detecting bearing faults in CWRUDS. The classification was performed on all ten data cases, and the accuracy was 100%, demonstrating the proposed approach's ability to monitor machine condition and diagnose faults. The output class correctly classified each target class, from healthy bearings to various faults (ball, inner race, outer race), as well as the three fault severities (small, average, critical).

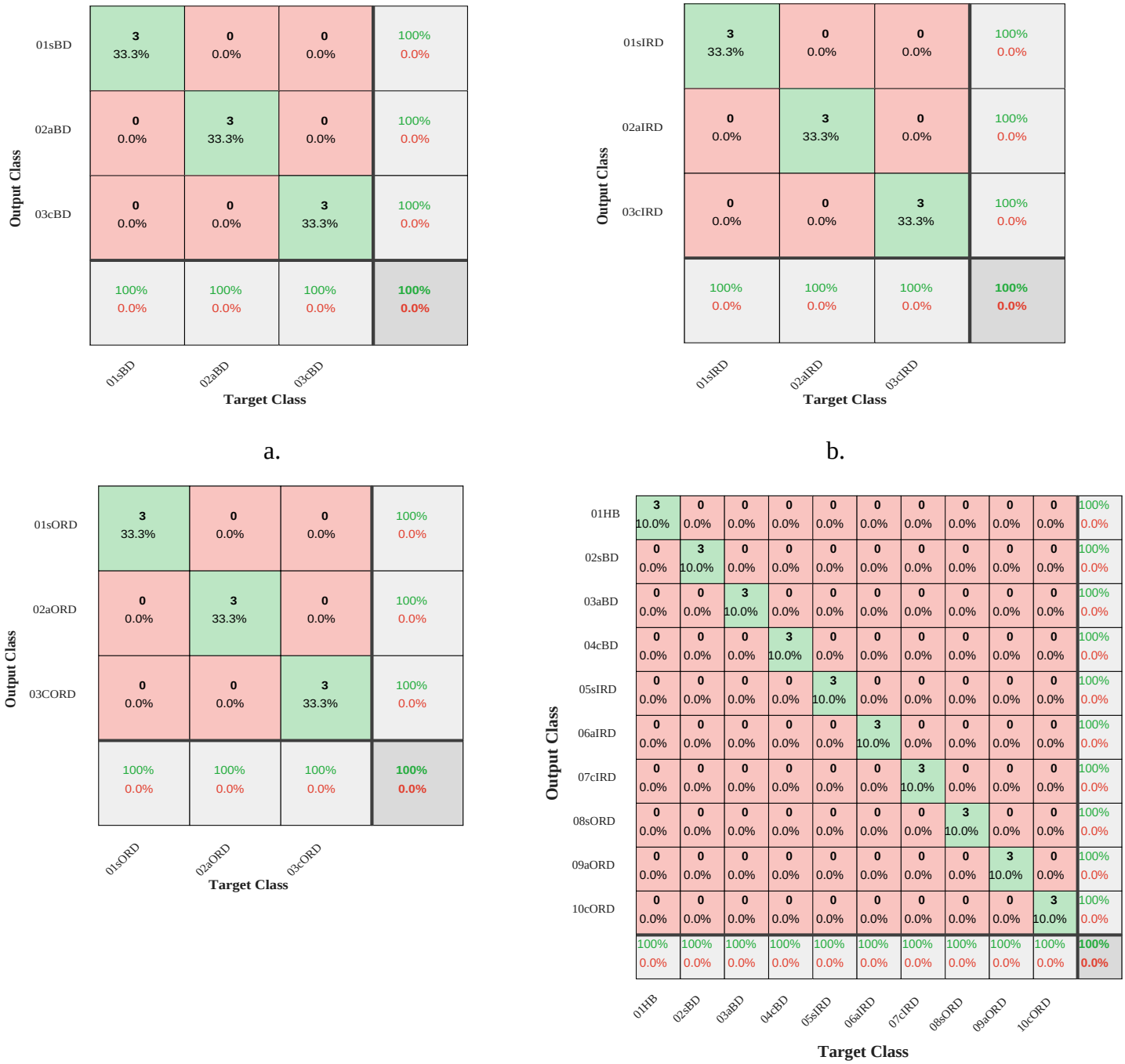

Figure 4.11. Confusion matrix resulted from the classification of CWRUDS:

a. RNN2, b. RNN3, c. RNN3 and d. RNN4.

5.2.2. Case of LMSDS

The RNNs trained for the LMSDS dataset, presented in Figure 4.12, were constructed using the same concept as the previous ones. The first step is to determine the fault type (RNN6). The next step was to determine the severity of bearing and gear faults (RNN7, RNN8). Finally, a classification of the combination of both faults was performed (RNN9) to obtain a comprehensive diagnosis.

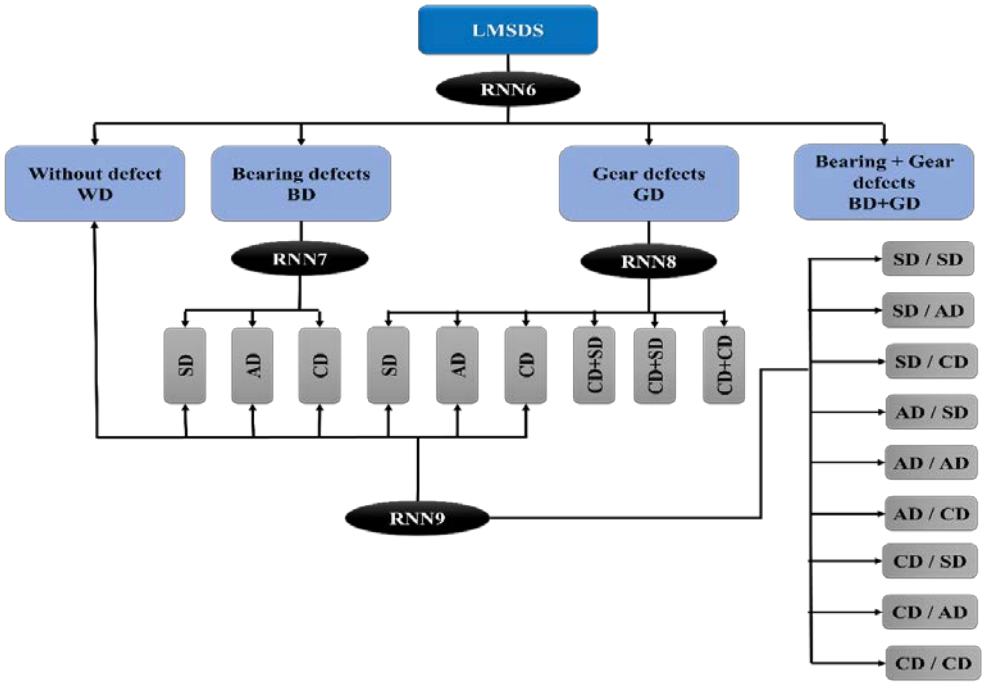

Figure 4.12. Trained RNNs for fault detection of LMSDS.

Figure 4.13 shows the training progress of RNN6 for classifying fault types in the LMSDS dataset. The training accuracy reached 100% before the end of the iterations, consistent with the validation accuracy shown in Figure 4.13(a). Both the training and validation results indicate that the trained RNN6 learned the features effectively. The loss presented in Figure 4.13(b) also aligns with these results, as we can see that the loss dropped to nearly zero.

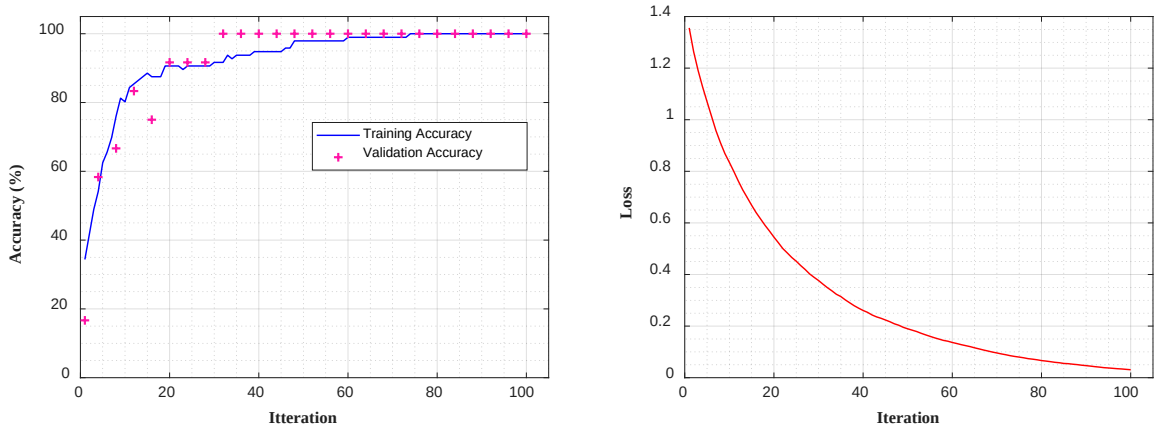

a. b

Figure 4.13. Training progress of RNN6: a. Training accuracy and b. Loss.

Figure 4.14 shows the classification results for RNN6. The confusion matrix shows complete concentration on the diagonal, with all target classes correctly predicted. The proposed approach was able to identify and classify different machine cases, even in the presence of gear and bearing faults.

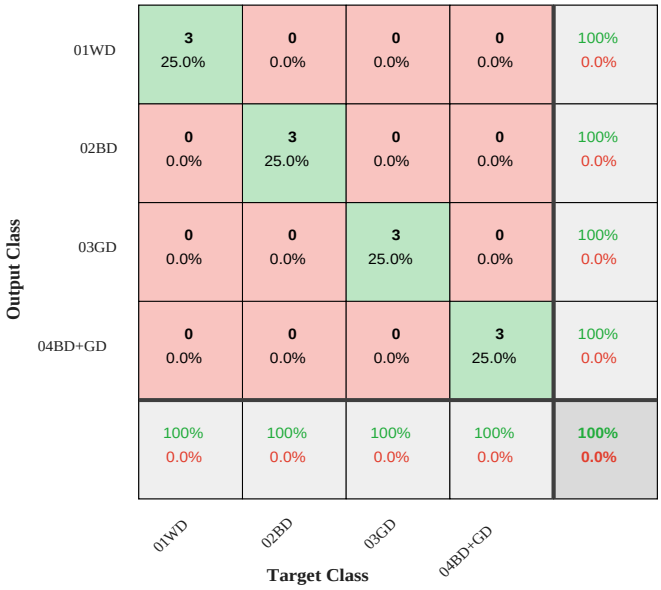

Figure 4.14. The confusion matrix resulted from the trained RNN6 for defect type classification of LMSDS.

Figure 4.15 illustrates the performance evaluation of LMSDS using confusion matrices generated from three different fault severity categorization scenarios. First, Figure 4.15(a) represents the confusion matrix for bearing fault severity classification generated by RNN7, demonstrating an impressive accuracy of 100%.

This shows the effectiveness of combining VMD and LSTM in accurately classifying bearing fault severity levels. Similarly, Figure 4.15(b) represents the confusion matrix of RNN8 for gear fault severity classification, achieving a remarkable accuracy of 100% and detecting all gear faults. Even in the presence of combined faults, the proposed approach is able to correctly classify gear fault severity levels. However, when faced with the challenge of classifying mixed gear and bearing faults, as shown in Figure 4.15(c), RNN9 exhibits a slight drop in accuracy to 83.3%. This decrease in accuracy is due to the inherent complexity associated with the combined nature of gear and bearing faults.

Overall, the use of VMD-LSTM as a combined approach is robust and reliable for detecting fault types and classifying severity in rotating machinery. Its ability to accurately identify fault types and severity levels, even in the presence of multiple faults, demonstrates its potential as a powerful tool for proactive maintenance and condition monitoring in industrial applications.

a.

b.

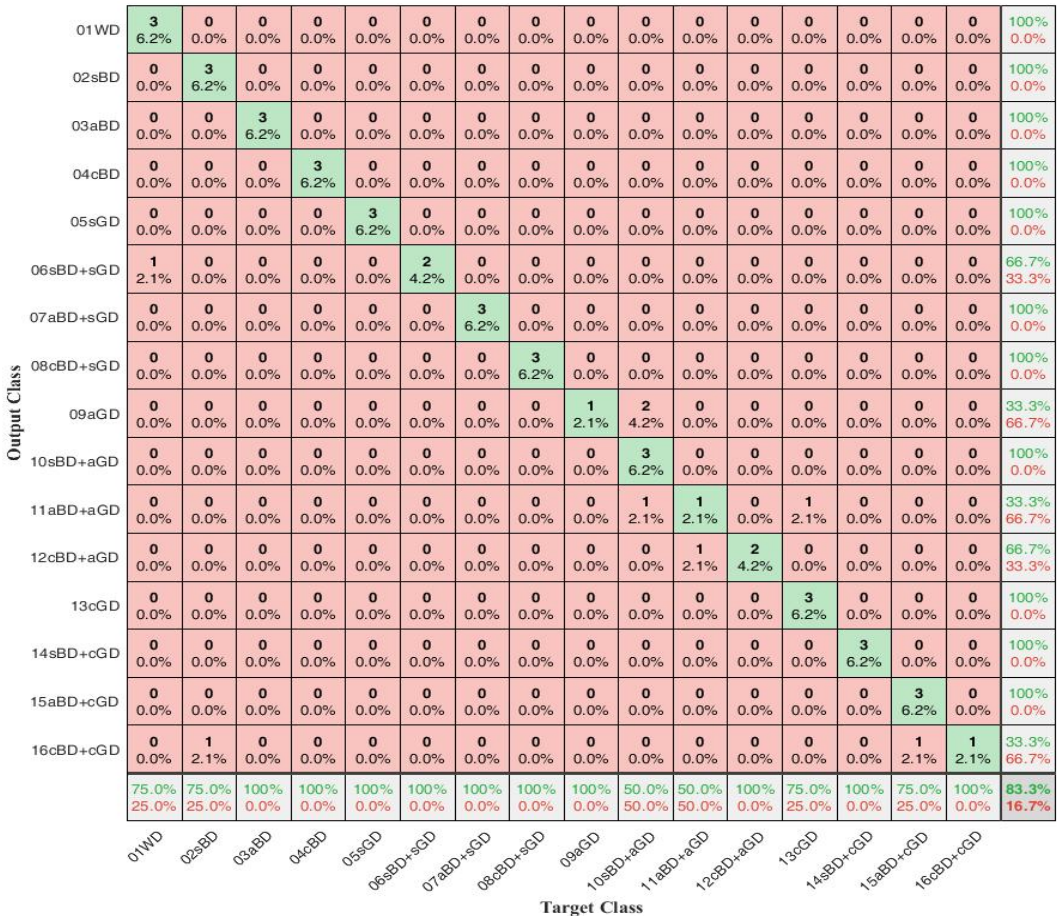

c.

Figure 4.15. Confusion matrix resulted from the classification of LMSDS:

a. results of RNN7, b. results of RNN8 and c. results of RNN9.

The main novelty of this approach lies in its ability to achieve high accuracy in fault detection using a small dataset for training, thereby reducing the need for large datasets typically required by conventional deep learning models. Thanks to VMD's ability to extract meaningful features from signals, LSTM can effectively classify fault types and their severity levels, even with a limited dataset. This method proves particularly useful in industrial applications where obtaining large labeled datasets is impractical. The method's ability to handle small datasets is demonstrated by its high classification accuracy, validated using two distinct datasets: bearing faults from CWRUDS and combined gear and bearing faults from LMSDS.

6. Performance evaluation of the proposed approach

Table 4.4 summarizes the results of vibration analysis and the VMD-LSTM method for fault detection across two different datasets: CWRUDS and LMSDS. In the case of vibration analysis with VMD, it is evident that while the method was effective in detecting inner and outer race faults in the CWRUDS dataset, it showed limitations in diagnosing other types of faults.

Table 4.4. Results of vibratory analysis and VMD-LSTM approach.

Dataset	Vibratory analysis		VMD-LSTM approach	
	Defect	**Detection**	**RNNs**	**Test accuracy**
CWRUDS			RNN1	*100%*
	Ball defects	No detection	RNN2	*100%*
	Inner ring defects	Fault detected	RNN3	*100%*
	Outer ring defects	Fault detected	RNN4	*100%*
			RNN5	*100%*
LMSDS			RNN6	*100%*
	Bearing defects	No detection	RNN7	*100%*
	Gear defects	No detection	RNN8	*100%*
	Bearing + Gear defects	No detection	RNN9	*83.3%*

In particular, VMD failed to diagnose ball faults in the CWRUDS dataset, as these faults are challenging to detect, and it provided no diagnosis for fault cases in the LMSDS dataset, where the signals were corrupted by noise. In contrast, the proposed VMD-LSTM approach proved to be a robust alternative, outperforming the results for both datasets. The VMD-LSTM method surpassed traditional vibration analysis by detecting all fault types in the CWRUDS dataset with 100% accuracy, including ball faults that classical VMD analysis could not detect.

Furthermore, the VMD-LSTM approach maintained strong fault detection performance in the LMSDS dataset, achieving 100% accuracy for all fault types except for combined gear and bearing faults, where it still achieved an accuracy of 83.3%. Gear faults are generally more frequent than bearing faults.

Using a small set of training samples, the proposed VMD-LSTM approach is compared to several other methods, such as Long Short-Term Memory (LSTM), Multi-Layer Perceptron (MLP), one-dimensional Convolutional Neural Networks (1D-CNN), and two-dimensional Convolutional Neural Networks (2D-CNN). This comparison highlights the effectiveness of the VMD-LSTM approach for fault detection and severity classification, particularly in scenarios where data is limited.

Table 4.5 summarizes the performance of each classifier on the CWRUDS dataset for different fault types, showing that the VMD-LSTM model outperforms other classifiers by achieving 100% accuracy for all fault types and for the entire dataset. Although MLP and 1D-CNN exhibit relatively low overall accuracies (46.66% and 53.33%), with particular difficulties in detecting inner race faults, 2D-CNN and LSTM offer better performance, with overall accuracies of 75.00% and 73.33%, respectively. However, none of them achieve the perfect classification obtained by VMD-LSTM, demonstrating its effectiveness for fault detection in rotating machinery.

Table 4.5. Results for the classification models of the CWRUDS.

Classifier	**CWRUDS' test accuracy**				
	Defect type	**Ball defect**	**Inner ring defects**	**Outer ring defect**	**All dataset**
MLP	41.66%	33.33%	58.33%	66.66%	46.66%
1D-CNN	50.00%	40.66%	58.33%	58.33%	53.33%
2D-CNN	66.66%	41.66%	80.00%	83.33%	75.00%
LSTM	58.33%	50.00%	66.66%	66.66%	73.33%
VMD-LSTM	100%	100%	100%	100%	100%

Table 4.6 compares the classification performance of various models on the LMSDS dataset for bearing faults, gear faults, and combined gear and bearing faults. The VMD-LSTM method achieves 100% accuracy for bearing and gear faults and 83.3% for combined faults, demonstrating its robustness. In contrast, MLP shows the weakest overall performance, particularly for detecting bearing faults (55.56%) and combined faults (60.41%). 1D-CNN and LSTM offer moderate performance, with accuracies ranging from 66.70% to 77.77% for bearing and gear faults but lower for combined faults. 2D-CNN shows high accuracy, especially for gear faults (94.44%) and bearing faults (88.88%), but still falls short of VMD-LSTM's performance. Overall, VMD-LSTM stands out as the most effective model for fault detection in this dataset.

Table 4.6. Results for the classification models of the LMSDS.

Classifier	LMSDS' test accuracy			
	Defect type	**Bearing defects**	**Gear defects**	**Combined gears and bearings defects**
MLP	58.33%	55.56%	66.66%	60.41%
1D-CNN	75.00%	66.70%	77.77%	68.75%
2D-CNN	91.66%	88.88%	94.44%	79.16%
LSTM	83.34%	77.77%	83.33%	72.91%
VMD-LSTM	100%	100%	100%	83.3%

The VMD-LSTM approach combines the strengths of VMD's signal decomposition and LSTM's sequential learning capabilities to provide a powerful and reliable framework for identifying fault patterns and assessing their severity. This method not only overcomes the limitations of traditional vibration analysis techniques but also excels in managing complex fault scenarios. Moreover, it demonstrates consistent and superior diagnostic performance for a wide range of fault types, even with a reduced training dataset, making it particularly useful in real-world industrial applications where data is often limited.

7. Conclusions

In this chapter, we developed an innovative method combining VMD and LSTM networks for fault detection in gears and bearings of rotating machinery. Tested on two datasets (CWRUDS and LMSDS), our approach outperformed classical vibration methods and traditional classifiers, particularly for complex fault signatures. It combines the adaptive decomposition capabilities of VMD and the sequential learning of LSTM, enabling precise detection and effective classification of fault types and severity levels. This work opens perspectives for future improvements and applications to larger datasets in industrial contexts.

General Conclusion

The primary objective of this thesis was to develop and implement advanced diagnostic techniques for fault detection in rotating machinery. Specifically, we explored methods of signal analysis techniques (VMD, WMRA) and artificial intelligence approaches (LSTM) to propose robust and accurate solutions for industrial environments. This research was supported by a series of experimental studies aimed at optimizing fault detection in gears and bearings, overcoming the challenges posed by the complexity of vibration signals, which are often nonlinear and noisy.

Fault diagnosis in rotating machinery presents major challenges, including the variability of real-world machines and the difficulty in isolating a specific fault when multiple anomalies coexist. While traditional approaches have proven effective, they exhibit limitations in detecting combined or low-amplitude faults. In this context, our research focused on enhancing signal processing techniques and integrating machine learning methods to improve fault detection sensitivity and accuracy.

First, a literature review was conducted on condition-based maintenance and vibration-based fault diagnosis techniques. Then, different signal decomposition methods (EMD and VMD) were analyzed in the context of vibration signals, demonstrating the relevance of VMD for better separation of signal components.

For gear fault diagnosis, the VMD-WMRA approach was implemented to optimize the isolation of significant frequency components, particularly by introducing a Shannon entropy-based criterion. This method demonstrated notable efficiency in detecting gear defects, even in high-noise environments. The main findings of this study indicate that:

- The VMD-WMRA combination provides a more precise separation of frequency components, thus facilitating the detection of subtle anomalies.
- The proposed criterion optimizes the number of required modes for effective signal decomposition, improving the robustness of fault detection.

Finally, to meet the need for automated fault diagnosis, the VMD-LSTM approach was developed, combining the advantages of VMD decomposition with deep learning for automatic and accurate fault detection in bearings and gears. Experimental tests on multiple datasets demonstrated that:

- The classification of faults was significantly improved, with high accuracy across various types and severity levels of defects.
- This approach proved to be robust for predictive maintenance of rotating machinery under challenging industrial conditions.

Future Perspectives

This work opens new research directions, including:

- The development of additional indicators for multi-fault diagnostics in high-noise environments.
- The optimization of decomposition techniques using hybrid approaches to maximize the accuracy of vibration-based monitoring techniques.
- The expansion of experimental tests to include signals simulating various degradation levels, ensuring the practical applicability of the proposed diagnostic models in industrial settings.

In conclusion, this thesis demonstrated the effectiveness of combined diagnostic approaches for improving fault detection and providing advanced tools for proactive maintenance in industrial systems. The results contribute to enhancing vibration-based machine monitoring and aligning maintenance practices with the growing demands of modern industrial environments, particularly in Algeria.

References

1. JARDINE, A. K. S., LIN, D., & BANJEVIC, D. (2006). A Review on Machinery Diagnostics and Prognostics Implementing Condition-Based Maintenance. *Mechanical Systems and Signal Processing*.

2. HUANG, N., SHEN, Z., LONG, S., WU, M., SHIH, H., ZHENG, Q., … LIU, H. (1998). The Empirical Mode Decomposition and the Hilbert Spectrum for Nonlinear and Non-Stationary Time Series Analysis. *Proceedings: Mathematical, Physical and Engineering Sciences*.

3. DRAGOMIRETSKIY, K., & Zosso, D. (2014). Variational Mode Decomposition. *IEEE Transactions on Signal Processing*.

4. YOUNES, R. (2015). *Perception Sonore au Service de l'Optimisation du Diagnostic des Défauts Mécaniques de Machines Tournantes* (Doctorate thesis). Université 08 MAI 1945, Guelma, Algerie.

5. DJEBALA, A. (2008). *Application de la Transformée par Ondelettes à l'Etude et l'Analyse Vibratoire des Systèmes Mécaniques* (Doctorate thesis). Université Badji Mokhtar, Annaba, Algerie.

6. TAHI, M. (2019). *Développement d'un Système d'Aide au Diagnostic des Machines Tournantes par Utilisation de l'Arbre de Décesion* (Doctorate thesis). Université Houari Boumediene, Alger, Algerie.

7. OUELAA, Z. (2024). *Application of Objective and Subjective Methods for the Diagnosis of Rotating Machine Faults* (Doctorate thesis). Université 08 MAI 1945, Guelma, Algerie.

8. MATANIA, O., BACHAR, L., BECHHOEFER, E., & BORTMAN, J. (2024). Signal Processing for the Condition-Based Maintenance of Rotating Machines via Vibration Analysis: A Tutorial. *Sensors*.

9. CHAABI, L. (2021). *Conception d'un Système Expert pour le Diagnostic des Roulements dans les Machines Tournantes Fonctionnant en Régime Variable* (Doctorate thesis). Université 08 MAI 1945, Guelma, Algerie.

10. ESTOCQ, P. (2004). *Une Approche Méthodologique Numérique et Expérimentale d'Aide à la Détection et au Suivi Vibratoire de Défauts d'Ecaillage de Roulements à Billes* (Doctorate thesis). Université de Champagne Ardenne, Reims, France.

11. BRENEUR, C. (2002). *Eléments de Maintenance Préventive de Machines Tournantes dans le Cas de Défauts Combines d'Engrenages et de Roulements* (Doctorate thesis). Institut National des sciences appliquées, Lyon, France.

12. FELDMAN, M. (2011). Hilbert Transform in Vibration Analysis. *Mechanical Systems and Signal Processing*.

13. ARABACI, H., & BILGIN, O. (2007). The Detection of Rotor Faults By Using Short Time Fourier Transform. In *IEEE 15th Signal Processing and Communications Applications*. Eskisehir, Turkey: IEEE.

14. BABOURI, M. K., OUELAA, N., KEBABSA, T., & DJEBALA, A. (2021). Diagnosis of Mechanical Defects Using a Hybrid Method Based on Complete Ensemble Empirical Mode Decomposition with Adaptive Noise (CEEMDAN) and Optimized Wavelet Multi-Resolution

Analysis (OWMRA): Experimental Study. *The International Journal of Advanced Manufacturing Technology*.

15. KEBABSA, T. (2016). *Eude des Aspects de Défaillances et Techniques de Maintenance Préventive Conditionnelle Appliquées aux Turbomachines* (Doctorate thesis). Université Badji Mokhtar, Annaba, Algerie.

16. BRÜEL & KJÆR VIBRO. (2005). Analyse des vibrations : Maintenance conditionnelle des machines tournantes. Retrieved from https://drive.google.com/file/d/1LTkKSjRM_yqKjEIkuNeZ3byEaOlB16EB/view?usp=sharing

17. YANG, H., MATHEW, J., & MA, L. (2003). Vibration Feature Extraction Techniques for Fault Diagnosis of Rotating Machinery : a Literature Survey. In *QUT*. Presented at the Asia-Pacific Vibration Conference, Australia.

18. MCFADDEN, P., & TOOZHY, M. M. (2000). Application Of Synchronous Averaging to Vibration Monitoring of Rolling Element Bearings. *Mechanical Systems and Signal Processing*.

19. MCCLINTIC, K., LEBOLD, M., MAYNARD, K., BYINGTON, C., & CAMPBELL, R. (2001). Residual And Difference Feature Analysis With Transitional Gearbox Data. Presented at the The 54th Meeting of the Society for Machinery Failure Prevention Technology, Virginia, USA.

20. HOWARD, I. (1994). A Review of Rolling Element Bearing Vibration : Detection, Diagnosis and Prognosis. *DSTO Aeronautical and Maritime Research Laboratory*. Australia.

21. SHARMA, V., & PAREY, A. (2016). A Review of Gear Fault Diagnosis Using Various Condition Indicators. *Procedia Engineering*.

22. MCFADDEN, P. (2000). Detection of Gear Faults by Decomposition of Matched Differences of Vibration Signals. *Mechanical Systems and Signal Processing*.

23. Ma, H., PANG, X., FENG, R., SONG, R., & WEN, B. (2015). Fault Features Analysis of Cracked Gear Considering the Effects of the Extended Tooth Contact. *Engineering Failure Analysis*.

24. HONG, L., & DHUPIA, J. S. (2014). A Time Domain Approach to Diagnose Gearbox Fault Based on Measured Vibration Signals. *Journal of Sound and Vibration*.

25. DECKER, H. (2002). Crack Detection for Aerospace Quality Spur Gears. Presented at the International 58th Annual Forum and Technology Display, Montreal, Quebec, Canada.

26. GANGSAR, P., & TIWARI, R. (2014). Multiclass Fault Taxonomy in Rolling Bearings at Interpolated and Extrapolated Speeds Based on Time Domain Vibration Data by SVM Algorithms. *Journal of Failure Analysis and Prevention*.

27. SHIRVASTAVA, A., & WADHWANI, S. (2014). An Approach for Fault Detection and Diagnosis of Rotating Electrical Machine Using Vibration Signal Analysis. Presented at the International Conference on Recent Advances and Innovations in Engineering, Jaipur, India.

28. BENCHAABANE, C., DJEBALA, A., OUELAA, N., & GUENFOUD, S. (2009). Diagnostic Vibratoire des Défauts d'Engrenages Basé sur les Indicateurs Scalaires. Presented at the Congrés Algérien de Mécanique CAM, Biskra, Algerie.

29. RGEAI, M., GU, F., BALL, A., ELHAJ, M., & GHERTILI, M. (2010). Gearbox Fault Detection Using Spectrum Analysis of the Drive Motor Current Signal. Presented at the Engineering Asset Lifecycle Management, London, UK.

30. HAMEED, Z., HONG, Y., CHO, Y., AHN, S., & SONG, C. (2009). Condition Monitoring and Fault Detection of Wind Turbines and Related Algorithms: a Review. *Renewable and Sustainable Energy Reviews*.

31. BAYDAR, N., & BALL, A. (2000). Detection of Gear Deterioration Under Varying Load Conditions by Using the Instantaneous Power Spectrum. *Mechanical Systems and Signal Processing*.

32. LI, C. J., MA, J., & HWANG, B. (1996). Bearing Condition Monitoring by Pattern Recognition Based on Bicoherence Analysis of Vibrations. *Proceedings of the Institution of Mechanical Engineers, Part C: Journal of Mechanical Engineering Science*.

33. RANDALL, R. (1982). A New Method of Modeling Gear Faults. *Journal of Mechanical Design*.

34. NACIB, L., MIDZODZI KOMI, P., & SAKHARA, S. (2013). Detecting Gear Tooth Cracks Using Cepstral Analysis in Gearbox of Helicopters. *International Journal of Advances in Engineering & Technology*.

35. AMEID, T., MENACER, A., TALHAOUI, H., & HARZELLI, I. (2017). Broken Rotor Bar Fault Diagnosis Using Fast Fourier Transform Applied to Field-Oriented Control Induction Machine: Simulation and Experimental Study. *The International Journal of Advanced Manufacturing Technology*.

36. VERNEKAR, K., HEMANTHA, K., & K. V., G. (2015). Fault Detection of Gear Using Spectrum and Cepstrum Analysis. *Proceedings of the Indian National Science Academy*.

37. EL MORSY, M., & ACHETENOVA, G. (2014). Vehicle Gearbox Fault Diagnosis Based On Cepstrum Analysis. *International Journal of Computer and Information Engineering*.

38. AYON-SICAEROS, R., CABAL-YEPEZ, E., LEDESMA-CARRILLO, L., & HERNANDEZ-GOMEZ, G. (2019). Broken-Rotor-Bar Detection Through STFT and Windowing Functions. Presented at the IEEE Sensors Applications Symposium (SAS), Sophia Antipolis, France.

39. ELBOUCHIKHI, E., AMIRAT, Y., FELD, G., & BENBOUZID, M. (2018). Diagnostic et Détection des Défauts dans les Machines Asynchrones par des Méthodes Avancées de Traitement du Signal. *Sûreté de fonctionnement et diagnostic*.

40. JEROME, A. (2010). Apports de la Cyclostationnarite a l'Analyse des Signaux Mecaniques. *Mécanique & Industries*.

41. CHUI, C. (1992). *An Introduction to Wavelets* (Academic press.).

42. XUAN, Z. Y., & GE, M. (2012). Application of the Hilbert – Huang Transform for Machine Fault Diagnostics. *Applied Mechanics and Materials*.

43. CUISDO, J., ROMERAL, L., ORTEGA, J., ROSERO, J., & GARCIA ESPINOSA, A. (2008). Fault Detection in Induction Machines Using Power Spectral Density in Wavelet Decomposition. *IEEE Transactions on Industrial Electronics*.

44. BENDJAMA, H., GHERFI, K., IDIOU, D., & BOUCHERIT, M. S. (2014). Condition Monitoring of Rotating Machinery by Vibration Signal Processing Methods. Presented at the International Conference on Industrial Engineering and Manufacturing, Batna, Algerie.

45. DJEBALA, A., OUELAA, N., HAMZAOUI, N., & CHAABI, L. (2006). Detecting Mechanical Failures Inducing Periodical Shocks by Wavelet Multiresolution Analysis. Application to Rolling Bearings Faults Diagnosis. *Mechanika*.

46. ZHENG, H., LI, Z., & CHEN, X. (2002). Gear Fault Diagnosis Based on Continious Wavelet Transform. *Mechanical Systems and Signal Processing*.

47. WU, J.-D., HSU, C.-C., & WU, G.-Z. (2009). Fault Gear Identification and Classification Using Discrete Wavelet Transform and Adaptive Neuro-Fuzzy Inference. *Expert Systems with Applications*.

48. WANG, W., & MCFADDEN, P. (1996). Application of Wavelets to Gearbox Vibration Signals for Fault Detection. *Journal of Sound and Vibration*.

49. NIKOLAOU, N. G., & ANTONIADIS, I. A. (2002). Rolling Element Bearing Fault Diagnosis Using Wavelet Packets. *NDT & E International*.

50. SUNG, C., TAI, H., & CHEN, C. (2000). Locating Defects of a Gear System by the Technique of Wavelet Transform. *Mechanism and Machine Theory*.

51. YOSHIDA, A., OHUE, Y., & ISHIKAWA, H. (2000). Diagnosis of Tooth Surface Failure by Wavelet Transform of Dynamic Characteristics. *Tribology International*.

52. MELTZER, G., & DIEN, N. P. (2004). Fault Diagnosis in Gears Operating Under Non-Stationary Rotational Speed Using Polar Wavelet Amplitude Maps. *Mechanical Systems and Signal Processing*.

53. DJEBALA, A., OUELAA, N., & HAMZAOUI, N. (2007). Optimisation de l'Analyse Multirésolution en Ondelettes des Signaux de Choc. Application aux Signaux Engendrés par des Roulements Défectueux. *Mécanique & Industries*.

54. DJEBALA, A., OUELAA, N., & HAMZAOUI, N. (2008). Detection of Rolling Bearing Defects Using Discrete Wavelet Analysis. *Meccanica*.

55. DJEBALA, A., BABOURI, M. K., & OUELAA, N. (2015). Rolling Bearing Fault Detection Using a Hybrid Method Based on Empirical Mode Decomposition and Optimized Wavelet Multi-Resolution Analysis. *The International Journal of Advanced Manufacturing Technology*.

56. MOUMENE, I., & OUELAA, N. (2016). Application of the Wavelets Multiresolution Analysis and the High-Frequency Resonance Technique for Gears and Bearings Faults Diagnosis. *The International Journal of Advanced Manufacturing Technology*.

57. BOUHALAIS, M. L., DJEBALA, A., OUELAA, N., & BABOURI, M. K. (2018). CEEMDAN and OWMRA as a Hybrid Method for Rolling Bearing Fault Diagnosis Under Variable Speed. *The International Journal of Advanced Manufacturing Technology*.

58. CHAABI, L., LEMZADMI, A., DJEBALA, A., BOUHALAIS, M. L., & OUELAA, N. (2020). Fault Diagnosis of Rolling Bearings in Non-Stationary Running Conditions Using Improved CEEMDAN and Multivariate Denoising Based on Wavelet and Principal Component Analyses. *The International Journal of Advanced Manufacturing Technology*.

59. DU, Q., & YANG, S. (2007). Application of the EMD Method in the Vibration Analysis of Ball Bearings. *Mechanical Systems and Signal Processing*.

60. GAO, Q., DUAN, C., FAN, H., & MENG, Q. (2008). Rotating Machine Fault Diagnosis Using Empirical Mode Decomposition. *Mechanical Systems and Signal Processing*.

61. LOUTRIDIS, S. (2004). Damage Detection in Gear Systems Using Empirical Mode Decomposition. *Engineering Structures*.

62. SHUFENG, A., & HUI, L. (2008). Gear Fault Detection Based on Ensemble Empirical Mode Decomposition and Hilbert-Huang Transform. Presented at the Fifth International Conference on Fuzzy Systems and Knowledge Discovery, Jinan, China.

63. JIANG, Y., TANG, C., ZHANG, X., JIAO, W., LI, G., & HUANG, T. (2020). A Novel Rolling Bearing Defect Detection Method Based on Bispectrum Analysis and Cloud Model-Improved EEMD. *IEEE Access*.

64. YANG, J., HUANG, D., ZHOU, D., & LIU, H. (2020). Optimal IMF Selection and Unknown Fault Feature Extraction for Rolling Bearings with Different Defect Modes. *Measurement*.

65. MAHGOUN, H., CHAARI, F., FELKAOUI, A., & HADDAR, M. (2017). Early Detection of Gear Faults in Variable Load and Local Defect Size Using Ensemble Empirical Mode Decomposition (EEMD). In *Applied Condition Monitoring*. Presented at the Advances in Acoustics and Vibration, Springer International Publishing.

66. CHEN, H., CHEN, P., Chen, W., WU, C., LI, J., & WU, J. (2017). Wind Turbine Gearbox Fault Diagnosis Based on Improved EEMD and Hilbert Square Demodulation. *Applied Sciences*.

67. TORRES, M. E., COLOMINAS, M. A., SCHLOTTHAUER, G., & FLANDRIN, P. (2011). A Complete Ensemble Empirical Mode Decomposition With Adaptive Noise. Presented at the IEEE International Conference on Acoustics, Speech and Signal Processing, Prague, Czech Republic: IEEE.

68. VANRAJ, DHAMI, S. S., & PABLA, B. (2017). Non-Contact Incipient Fault Diagnosis Method of Fixed-Axis Gearbox Based on CEEMDAN. *Royal Society Open Science*.

69. LEI, Y., LIU, Z., OUAZRI, J., & LIN, J. (2017). A Fault Diagnosis Method of Rolling Element Bearings Based on CEEMDAN. *Proceedings of the Institution of Mechanical Engineers, Part C: Journal of Mechanical Engineering Science*.

70. LINGLI, J., LIMAN, C., HONGCHUANG, T., & XUEJUN, L. (2020). Fault Diagnosis of Spiral Bevel Gears Based on CEEMDAN Permutation Entropy. Presented at the Advances in Asset Management and Condition Monitoring, Springer International Publishing.

71. COLOMINAS, M. A., SCHLOTTHAUER, G., & TORRES, M. E. (2014). Improved Complete Ensemble EMD: A Suitable Tool for Biomedical Signal Processing. *Biomedical Signal Processing and Control*.

72. DING, F., LI, X., & QU, J. (2017). Fault Diagnosis of Rolling Bearing Based on Improved CEEMDAN and Distance Evaluation Technique. *Journal of Vibroengineering*.

73. JEROME, A. (2009). Cyclostationarity by Examples. *Mechanical Systems and Signal Processing*.

74. URBANEK, J., BARSZCZ, T., & JEROME, A. (2013). A Two-Step Procedure for Estimation of Instantaneous Rotational Speed with Large Fluctuations. *Mechanical Systems and Signal Processing*.

75. URBANEK, J., BARSZCZ, T., & JEROME, A. (2014). Integrated Modulation Intensity Distribution as a Practical Tool for Condition Monitoring. *Applied Acoustics*.

76. KEBABSA, T., OUELAA, N., JEROME, A., DJAMAA, M. C., KHETTABI, R., & DJEBALA, A. (2015). Experimental Study of a Turbo-Alternator in Industrial Environment Using Cyclostationarity. *The International Journal of Advanced Manufacturing Technology*.

77. KEBABSA, T., OUELAA, N., JEROME, A., DJAMAA, M. C., KHETTABI, R., & DJEBALA, A. (2017). Fault Diagnosis Through the Application of Cyclostationarity to Signals Measured. Presented at the Applied Mechanics, Behavior of Materials, and Engineering Systems, Springer International Publishing.

78. BABOURI, M. K., OUELAA, N., KEBABSA, T., & DJEBALA, A. (2019). Application of the Cyclostationarity Analysis in the Detection of Mechanical Defects: Comparative Study. *The International Journal of Advanced Manufacturing Technology*.

79. ASSAD, B., ELTABACH, M., & JEROME, A. (2014). Vibration Based Condition Monitoring of a Multistage Epicyclic Gearbox in Lifting Cranes. *Mechanical Systems and Signal Processing*.

80. ISHAM, F., LEONG, S., LIM, M. H., & M. K, Z. (2018). A Review on Variational Mode Decomposition for Rotating Machinery Diagnosis. In *MATEC Web Conf*. Presented at the Engineering Application of Artificial Intelligence Conference, EDP Sciences.

81. MOHANTY, GUPTA, K. K., & RAJU, K. S. (2014). Bearing Fault Analysis Using Variational Mode Decomposition. Presented at the International Conference on Industrial and Information Systems, Gwalior, India: IEEE.

82. AN, X., ZENG, H., & LI, C. (2016). Envelope Demodulation Based on Variational Mode Decomposition for Gear Fault Diagnosis. *Proceedings of the Institution of Mechanical Engineers, Part E: Journal of Process Mechanical Engineering*.

83. MAHGOUN, H., CHAARI, F., & FELKAOUI, A. (2016). Detection of Gear Faults in Variable Rotating Speed Using Variational Mode Decomposition (VMD). *Mechanics & Industry*.

84. WANG, YINGJIE, WENTAO, Y., & JIANYI, Q. (2018). Gear Fault Diagnosis based on Variational Mode Decomposition and Envelope Spectrum. *Journal of Engineering Science & Technology Review*.

85. LIQUAN, C., LIANSHENG, L., MIN, H., & DATONG, L. (2019). Gearbox Fault Diagnosis Based on VMD and Acoustic Emission Technology. Presented at the International Instrumentation and Measurement Technology Conference, Auckland, New Zealand: IEEE.

86. LIN, Y., XIAO, M., Liu, H., LI, Z., ZHOU, S., XU, X., & Wang, D. (2022). Gear Fault Diagnosis Based on CS-Improved Variational Mode Decomposition and Probabilistic Neural Network. *Measurement*.

87. LI, Z., CHEN, J., Zi, Y., & PAN, J. (2017). Independence-Oriented VMD to Identify Fault Feature for Wheel Set Bearing Fault Diagnosis of High Speed Locomotive. *Mechanical Systems and Signal Processing*.

88. FENG, Z., ZHANG, D., & ZUO, M. J. (2017). Planetary Gearbox Fault diagnosis via Joint Amplitude and Frequency Demodulation Analysis Based on Variational Mode Decomposition. *Applied Sciences*.

89. ZHANG, M., JIANG, Z., & FENG, K. (2017). Research on Variational Mode Decomposition in Rolling Bearings Fault Diagnosis of the Multistage Centrifugal Pump. *Mechanical Systems and Signal Processing*.

90. JIANG, X., SHEN, C., SHI, J., & ZHU, Z. (2018). Initial Center Frequency-Guided VMD for Fault Diagnosis of Rotating Machines. *Journal of Sound and Vibration*.

91. JIANG, X., WANG, J., SHI, J., SHEN, C., HUANG, W., & ZHU, Z. (2019). A Coarse-to-Fine Decomposing Strategy of VMD for Extraction of Weak Repetitive Transients in Fault Diagnosis of Rotating Machines. *Mechanical Systems and Signal Processing*.

92. SHI, R., WANG, B., Liu, J., FENG, X., & DONG, L. (2022). Research on Fault Diagnosis of Rolling Bearings Based on Variational Mode Decomposition Improved by the Niche Genetic Algorithm. *Entropy*.

93. GUO, Y., YANG, Y., JIANG, S., & WEI, Y. (2022). Rolling Bearing Fault Diagnosis Based on Successive Variational Mode Decomposition and the EP Index. *Sensors*.

94. CHEN, Q., CHEN, J., LANG, X., REHMAN, N. ur, & Su, H. (2021). Self-Tuning Variational Mode Decomposition. *Journal of the Franklin Institute*.

95. Li, H., Liu, T., Wu, X., & Chen, Q. (2020). An optimized VMD method and its applications in bearing fault diagnosis. *Measurement*, *166*, 108185. https://doi.org/10.1016/j.measurement.2020.108185

96. LIAN, J., Liu, Z., WANG, H., & DONG, X. (2018). Adaptive Variational Mode Decomposition Method for Signal Processing Based on Mode Characteristic. *Mechanical Systems and Signal Processing*.

97. DIKE, H. U., Zhou, Y., DEVEERASETTY, K. K., & WU, Q. (2018). Unsupervised Learning Based On Artificial Neural Network: A Review. Presented at the International Conference on Cyborg and Bionic Systems, Shenzhen, China: IEEE.

98. MNASSRI, B., ELADEL, E. M., ANANOU, B., & OULADSINE, M. (2009). Fault Detection and Diagnosis Based on PCA and a New Contribution Plot. *IFAC Proceedings Volumes*.

99. ASHISH, B., & VASSILIS, S. (2007). Data Driven Approach for Fault Detection and Identification Using Competitive Learning techniques. Presented at the European Control Conference, Kos, Greece: IEEE.

100. SAUCEDO-DORANTES, J. J., DELGADO-PRIETO, M., ROMERO-TRONCOSO, R. D. J., & OSORNIO-RIOS, R. A. (2019). Multiple-Fault Detection and Identification Scheme Based on Hierarchical Self-Organizing Maps Applied to an Electric Machine. *Applied Soft Computing*.

101. RAJAKARUNAKARAN, S., VENKUMAR, P., DEVARAJ, D., & SURYAPRAKASA RAO, K. S. (2008). Artificial Neural Network Approach for Fault Detection in Rotary System. *Applied Soft Computing*.

102. WIDODO, A., & YANG, B.-S. (2007). Support Vector Machine in Machine Condition Monitoring and Fault Diagnosis. *Mechanical Systems and Signal Processing*.

103. JANSSENS, O., SLAVKOVIKJ, V., VERVISCH, B., STOCKMAN, K., LOCCUUFIER, M., VERSTOCKT, S., … VAN HOECKE, S. (2016). Convolutional Neural Network Based Fault Detection for Rotating Machinery. *Journal of Sound and Vibration*.

104. LU, J., QIAN, W., LI, S., & CUI, R. (2021). Enhanced K-Nearest Neighbor for Intelligent Fault Diagnosis of Rotating Machinery. *Applied Sciences*.

105. YANG, R., HUANG, M., LU, Q., & ZHONG, M. (2018). Rotating Machinery Fault Diagnosis Using Long-short-term Memory Recurrent Neural Network. *IFAC-PapersOnLine*.

106. YUAN, X., & TAO, Z. (2018). A Long Short Term Memory Recurrent Neural Network Approach for Rotating Machinery Fault Prognosis. Presented at the CSAA Guidance, Navigation and Control Conference, Xiamen, China: IEEE.

107. ANWARSHA, A., & NARENDIRANATH BABU, T. (2023). Intelligent Fault Detection of Rotating Machinery Using Long-Short-Term Memory (LSTM) Network. Presented at the The 2nd International Conference on Emerging Technologies and Intelligent Systems, Springer International Publishing.

108. CAO, L., ZHANG, J., WANG, J.-Y., & QIAN, Z. (2019). Intelligent Fault Diagnosis of Wind Turbine Gearbox Based on Long Short-Term Memory Networks. Presented at the 28th International Symposium on Industrial Electronics, Vancouver, BC, Canada: IEEE.

109. MASRI, A., & AL-JABI, M. (2022). LSTM Neural Network Techniques-Based Analytical Predictive Models for Wind Energy and Mechanical Power. *Advances in Mechanical Engineering*.

110. DAMOU, A., RATNI, A., & BENAZZOUZ, D. (2024). Intelligent Multi-Fault Identification and Classification of Defective Bearings in Gearbox. *Advances in Mechanical Engineering*.

111. MOUMENE, I., & OUELAA, N. (2022). Gears and Bearings Combined Faults Detection Using Optimized Wavelet Packet Transform and Pattern Recognition Neural Networks. *The International Journal of Advanced Manufacturing Technology*.

112. GU, J., PENG, Y., LU, H., CHANG, X., & CHEN, G. (2022). A Novel Fault Diagnosis Method of Rotating Machinery Via VMD, CWT and Improved CNN. *Measurement*.

113. ALMUTAIRI, K., & Jyoti, S. (2023). Experimental Vibration Data in Fault Diagnosis: A Machine Learning Approach to Robust Classification of Rotor and Bearing Defects in Rotating Machines. *Machines*.

114. TONG, Q., CAO, J., HAN, B., WANG, D., LIN, Y., ZHANG, W., & WANG, J. (2017). A Fault Diagnosis Approach for Rolling Element Bearings Based on Dual-Tree Complex Wavelet Packet Transform-Improved Intrinsic Time-Scale Decomposition, Singular Value Decomposition, and Online Sequential Extreme Learning Machine. *Advances in Mechanical Engineering*.

115. DELECHELLE, E., LEMOINE, J., & NIANG, O. (2005). Empirical Mode Decomposition: An Analytical Approach for Sifting Process. *Signal Processing Letters*.

116. DEJIE, Y., JUNSHENG, C., & YANG, Y. (2005). Application of EMD Method and Hilbert Spectrum to the Fault Diagnosis of Roller Bearings. *Mechanical Systems and Signal Processing*.

117. HE, X., ZHOU, X., YU, W., HOU, Y., & MECHEFSKE, C. K. (2021). Adaptive Variational Mode Decomposition and its Application to Multi-Fault Detection Using Mechanical Vibration Signals. *ISA Transactions*.

118. UZUNOGLU, C. (2018). A Comparative Study of Empirical and Variational Mode Decomposition on High Voltage Discharges. *Electrica*.

119. SATISH, M., KARUNESH KUMAR, G., & KOTA SOLOMON, R. (2014). Comparative Study Between VMD and EMD in Bearing Fault Diagnosis. Presented at the 9th International Conference on Industrial and Information Systems, Gwalior, India: IEEE.

120. KUMAR, P. S., KUMARASWAIDHAS, & LAHA, S. K. (2019). Selecting Effective Intrinsic Mode Functions of Empirical Mode Decomposition and Variational Mode Decomposition Using

Dynamic Time Warping Algorithm for Rolling Rlement Bearing Fault Diagnosis. *Transactions of the Institute of Measurement and Control*.

121. ZHU, J., WANG, C., HU, Z., KONG, F., & LIU, X. (2017). Adaptive Variational Mode Decomposition Based on Artificial Fish Swarm Algorithm For Fault Diagnosis of Rolling Bearings. *Proceedings of the Institution of Mechanical Engineers, Part C: Journal of Mechanical Engineering Science*.

122. WANG, J., LI, J., WANG, H., & GUO, L. (2021). Composite Fault Diagnosis of Gearbox Based on Empirical Mode Decomposition and Improved Variational Mode Decomposition. *Journal of Low Frequency Noise, Vibration and Active Control*.

123. JUNSHENG, C., DEJIE, Y., & YU, Y. (2007). The Application of Energy Operator Demodulation Approach Based on EMD in Machinery Fault Diagnosis. *Mechanical Systems and Signal Processing*.

124. LEI, Y., LIN, J., HE, Z., & ZUO, M. J. (2013). A Review on Empirical Mode Decomposition in Fault Diagnosis of Rotating Machinery. *Mechanical Systems and Signal Processing*.

125. OUELAA, Z., YOUNES, R., DJEBALA, A., HAMZAOUI, N., & OUELAA, N. (2022). Comparative Study Between Objective and Subjective Methods for Identifying the Gravity of Single and Multiple Gear Defects in Case of Noisy Signals. *Applied Acoustics*.

126. MALLAT, S. (1989). A Theory for Multiresolution Signal Decomposition: the Wavelet Representation. *Transactions on Pattern Analysis and Machine Intelligence*.

127. SHANNON, C. E. (1948). A Mathematical Theory of Communication. *The Bell System Technical Journal*.

128. HEIDARI BAFRAOUI, H., & OHAIDI, A. (2014). Application of Wavelet Energy and Shannon Entropy for Feature Extraction in Gearbox Fault Detection Under Varying Speed Conditions. *Neurocomputing*.

129. ISHAM, F., LEONG, S., LIM, H., & AHMAD, A. (2018). Variational Mode Decomposition: Mode Determination Method for Rotating Machinery Diagnosis. *Journal of Vibroengineering*.

130. CECILE, C., & MENAD, S. (1991). Analyse des Vibrations d'un Engrenage : Cepstre, Corrélation, Spectre. *Traitement Du Signal*.

131. BOUYER, J. (2003). *Thermoelastohydrodynamic Study of the Performance of a Journal Bearing Sujected to Severe Operating Conditions* (Doctorate thesis). Université de Poitiers, France.

132. Case Western Reserve University (CWRU) Bearing Data Center. (2023, April).

133. MRABTI, A., OUELAA, N., YOUNES, R., DJAMAA, M. C., & OUELAA, Z. (2024). Diagnosis of Faults Using a New VMD-WMRA Approach, Optimized by a New Criterion: Industrial Application. *Advances in Mechanical Engineering*.

134. SMITH, W., & RANDALL, R. (2015). Rolling Element Bearing Diagnostics Using the Case Western Reserve University Data: A Benchmark Study. *Mechanical Systems and Signal Processing*.

135. NOUIOUA, I., YOUNES, R., MRABTI, A., MEDDOUR, I., & ALIA, S. (2023). Self-Organizing Maps and VMD for Accurate Diagnosis of Bearing Defects. *Journal of Vibration Engineering & Technologies*.